

**-Development of somatic modified mouse models of Non-Small cell
lung cancer-**

**-Entwicklung von somatisch veränderten Mausmodellen für nicht-
kleinzelligen Lungenkrebs-**



Doctoral thesis for a doctoral degree
at the Graduate School of Life Sciences,
Julius-Maximilians-Universität Würzburg,
Section Biomedicine
submitted by

Oliver Hartmann

from

Hagenow

Würzburg, **2023**

Submitted on:

.....

Office stamp

Members of the Thesis Committee

Chairperson: Prof. Dr. Alexander Buchberger

.....

Primary Supervisor: Dr. Markus E. Diefenbacher

Supervisor (Second): Prof. Dr. Stefan Müller

Supervisor (Third): Prof. Dr. Martin Eilers

Supervisor (Fourth): Prof. Dr. Emma Rawlins

.....

(If applicable)

Date of Public Defence:

Date of Receipt of Certificates:

.....

Für Ann-Marie 

Abstract

Abstract

In 2020, cancer was the leading cause of death worldwide, accounting for nearly 10 million deaths. Lung cancer was the most common cancer, with 2.21 million cases per year in both sexes. This non-homogeneous disease is further subdivided into small cell lung cancer (SCLC, 15%) and non-small cell lung cancer (NSCLC, 85%). By 2023, the American Cancer Society estimates that NSCLC will account for 13% of all new cancer cases and 21% of all estimated cancer deaths.

In recent years, the treatment of patients with NSCLC has improved with the development of new therapeutic interventions and the advent of targeted and personalised therapies. However, these advances have only marginally improved the five-year survival rate, which remains alarmingly low for patients with NSCLC.

This observation highlights the importance of having more appropriate experimental and preclinical models to recapitulate, identify and test novel susceptibilities in NSCLC. In recent years, the Trp53^{fl/fl} KRas^{Isl-G12D/wt} mouse model developed by Tuveson, Jacks and Berns has been the main in vivo model used to study NSCLC. This model mimics ADC and SCC to a certain extent. However, it is limited in its ability to reflect the genetic complexity of NSCLC.

In this work, we use CRISPR/Cas9 genome editing with targeted mutagenesis and gene deletions to recapitulate the conditional model. By comparing the Trp53^{fl/fl} KRas^{Isl-G12D/wt} with the CRISPR-mediated Trp53^{mut} KRas^{G12D}, we demonstrated that both showed no differences in histopathological features, morphology, and marker expression. Furthermore, next-generation sequencing revealed a very high similarity in their transcriptional profile.

Adeno-associated virus-mediated tumour induction and the modular design of the viral vector allow us to introduce additional mutations in a timely manner. CRISPR-mediated mutation of commonly mutated tumour suppressors in NSCLC reliably recapitulated the phenotypes described in patients in the animal model.

Lastly, the dual viral approach could induce the formation of lung tumours not only in constitutive Cas9 expressing animals, but also in wildtype animals. Thus, the implementation of CRISPR genome editing can rapidly advance the repertoire of in vivo models for NSCLC research. Furthermore, it can reduce the necessity of extensive breeding.

Zusammenfassung

Zusammenfassung

Krebs war mit fast 10 Millionen Todesfällen weltweit die häufigste Todesursache in 2020. Mit 2,21 Millionen Fällen pro Jahr in beiden Geschlechtern kombiniert war Lungenkrebs die häufigste Unterart. Auszeichnend für diese Krankheit ist die hohe Komplexität und Heterogenität. Daher wird diese weiter in kleinzelligen Lungenkrebs (SCLC, 15 %) und nicht-kleinzelligen Lungenkrebs (NSCLC, 85 %) unterteilt. Die American Cancer Society schätzt, dass bis 2023 13 % aller neuen Krebsfälle und 21 % aller geschätzten Krebstodesfälle auf das nicht-kleinzellige Lungenkarzinom entfallen werden.

In den letzten Jahren hat sich die Behandlung von Patienten mit nicht-kleinzelligem Lungenkarzinom durch die Entwicklung neuer therapeutischer Maßnahmen und das Anwenden personalisierter Therapien verbessert. Allerdings haben diese Fortschritte die Fünfjahresüberlebensrate nur geringfügig verbessert, die für Patienten mit NSCLC nach wie vor alarmierend niedrig ist.

Diese macht deutlich, wie wichtig es ist, über geeignetere experimentelle und präklinische Modelle zu verfügen, um neue Therapieansätze beim NSCLC zu rekapitulieren, zu identifizieren und zu testen.

In der letzten Dekade war das von Tuveson, Jacks und Berns entwickelte $\text{Trp53}^{\text{fl/fl}}$ $\text{KRas}^{\text{Isl-G12D/wt}}$ -Mausmodell das wichtigste In-vivo-Modell zur Untersuchung von NSCLC. Dieses kann grundlegend das Krankheitsbild von NSCLC widerspiegeln. Es ist jedoch nur begrenzt in der Lage, die genetische Komplexität von NSCLC im vollen Umfang zu reflektieren.

In dieser Arbeit verwenden wir CRISPR/Cas9 Genome Editing mit gezielter Mutagenese und Gendeletionen, um das konditionale Modell zu rekapitulieren. Durch den Vergleich des $\text{Trp53}^{\text{fl/fl}}$ $\text{KRas}^{\text{Isl-G12D/wt}}$ mit dem CRISPR-vermittelten $\text{Trp53}^{\text{mut}}$ $\text{KRas}^{\text{G12D}}$ konnten wir zeigen, dass beide keine Unterschiede in Bezug auf histopathologische Merkmale, Morphologie und Markerexpression aufweisen. Darüber hinaus ergab die Analyse mittels Next Generation Sequencing (Hochdurchsatz-Sequenzierung) eine sehr große Ähnlichkeit in ihrem Transkriptionsprofil.

Die Adeno-assoziierte Virus-vermittelte Tumorinduktion und der modulare Aufbau des viralen Vektors ermöglichen es uns, zusätzliche Mutationen zeitnah einzuführen. Die

Zusammenfassung

CRISPR-vermittelte Mutation von häufig mutierten Tumorsuppressoren bei NSCLC rekapitulierte zuverlässig die bei Patienten beschriebenen Phänotypen im Tiermodell. Schließlich konnte der duale virale Ansatz die Bildung von Lungentumoren nicht nur in konstitutiv Cas9 exprimierenden Tieren, sondern auch in Wildtyp-Tieren induzieren. Somit kann die Anwendung von CRISPR-Genome Editing das Repertoire an In-vivo-Modellen für die NSCLC-Forschung rasch erweitern. Darüber hinaus kann es die Notwendigkeit umfangreicher Züchtungen verringern.

Table of Contents

Table of Contents

<i>Abstract</i>	<i>III</i>
<i>Zusammenfassung</i>	<i>IV</i>
<i>Table of Contents</i>	<i>VI</i>
1 Introduction	- 1 -
1.1 Non-Small Cell Lung Cancer	- 2 -
1.2 Genetic complexity in NSCLC	- 5 -
1.3 Current Therapeutic Intervention	- 12 -
1.3.1. Treatment modalities for early-stage disease:	- 13 -
1.3.2. Treatment of progressed disease:	- 14 -
1.3.3. Beyond pathway interference: Immuno-modulatory interventions:	- 16 -
-	
1.4 Animal models in NSCLC research	- 17 -
1.5 Aim of the thesis	- 21 -
2 Materials and Method	- 22 -
2.1 Materials	- 22 -
2.1.1. Buffers and Solutions	- 22 -
2.1.2. Chemicals	- 24 -
2.1.3. Consumables	- 27 -
2.1.4. Bacterial culture media	- 27 -
2.1.5. Bacterial strains	- 28 -
2.1.6. Cell culture media, supplements, and antibiotics	- 28 -
2.1.7. Cell lines	- 28 -
2.1.8. Antibodies	- 29 -
2.1.9. Enzymes and corresponding buffers	- 33 -
2.1.10. Oligonucleotides	- 34 -
2.1.11. Plasmids	- 34 -
2.1.12. Commercial kits	- 36 -
2.1.13. Software/Websites	- 38 -
2.1.14. Instruments	- 39 -

Table of Contents

2.2	Methods	- 41 -
2.2.1.	Molecular biology methods	- 41 -
2.2.1.1	Restriction Digest	- 41 -
2.2.1.2	Polymerase Chain Reaction	- 41 -
2.2.1.3	T4 Ligation	- 42 -
2.2.1.4	Oligo cloning	- 42 -
2.2.1.5	Agarose gel electrophoresis	- 42 -
2.2.1.6	Heat Shock Transformation	- 42 -
2.2.1.7	DNA Purification	- 43 -
2.2.1.8	DNA Isolation (MidiPrep)	- 43 -
2.2.1.9	DNA Quantification	- 43 -
2.2.1.10	DNA Sequencing	- 43 -
2.2.1.11	RNA Isolation	- 43 -
2.2.1.12	cDNA synthesis	- 43 -
2.2.1.13	Quantitative real-time PCR (qPCR)	- 44 -
2.2.1.14	AAV titration	- 45 -
2.2.1.15	RNA sequencing	- 45 -
2.2.2.	Biochemical methods	- 45 -
2.2.2.1	Protein Isolation	- 45 -
2.2.2.2	SDS-PAGE	- 46 -
2.2.2.3	Immunoblot	- 46 -
2.2.2.4	Immunoprecipitation	- 47 -
2.2.2.5	Tandem Ubiquitin Binding Entities (TUBE)	- 47 -
2.2.2.6	Warhead assay	- 47 -
2.2.3.	Cell biology methods	- 48 -
2.2.3.1	Cultivation of cells	- 48 -
2.2.3.2	Establishment of primary tumour cell lines	- 48 -
2.2.3.3	Transfection of cells	- 49 -
2.2.3.4	Lentivirus production	- 49 -
2.2.3.5	Adeno-associated virus production	- 49 -
2.2.3.6	Infection of cells	- 50 -
2.2.3.7	Immunofluorescence	- 50 -
2.2.4.	Animal models	- 50 -

Table of Contents

2.2.4.1	Licences	- 50 -
2.2.4.2	Animal welfare	- 51 -
2.2.4.3	AAV induced lung tumours	- 51 -
2.2.4.4	Orthotropic transplantation of lung tumour cell lines	- 51 -
2.2.4.5	Mice euthanasia	- 51 -
2.2.5.	Immunohistochemistry	- 52 -
2.2.5.1	Formalin-fixated and paraffin embedded tissue	- 52 -
2.2.5.2	Immunohistochemistry (IHC)	- 52 -
3	Results	- 53 -
3.1	CRISPR/Cas9 mediated genome editing to generate murine <i>KRas</i>^{G12D}/<i>Trp53</i>^{mut} driven lung cancer	- 53 -
3.1.1.	TP53 and KRAS are frequently altered in ADC and SCC NSCLC subtypes	- 53 -
3.1.2.	Intratracheal installation of AAV-DJ in KP ^{GEMM} shows the highest efficacy	- 55 -
3.1.3.	Crispr/Cas9 mediated editing of <i>Trp53</i> and <i>KRas</i> ^{G12D} induces formation of NSCLC morphological indistinguishible from the classical model	- 59 -
3.1.4.	KP ^{GEMM} and KP ^{CRISPR} demonstrate a similar upregulation of NSCLC oncogenic transcription factors	- 64 -
3.1.5.	CRISPR/Cas9-mediated NSCLC formation has similar transcriptional profile adaptations to the classical model	- 69 -
3.2	CRISPR/Cas9 mediated genome editing to generate murine NSCLC models reflecting patient relevant <i>loss-of-function</i> mutations.	- 75 -
3.2.1.	<i>APC</i> , <i>KEAP1</i> , <i>STK11/LKB1</i> and <i>PTEN</i> are frequently altered and thus negatively impact patient survival	- 76 -
3.2.2.	Modular AAV-vector enables successful targeting of commonly mutated tumour suppressor in mice	- 79 -
3.2.3.	Dual viral approaches enhance applicability of CRISPR for translational research, irrespective of the mouse strain	- 87 -
4	Discussion	- 96 -

Table of Contents

4.1	CRISPR/Cas9-mediated editing induces formation of NSCLC morphologically and molecularly indistinguishable from the classical model	- 96 -
4.2	Modular AAV-vector enables successful targeting of commonly mutated tumour suppressor in mice with simple modifications	- 105 -
4.3	Dual viral approach allows to reduce and refine animal testing	- 108 -
4.4	Conclusion	- 110 -
5	<i>Bibliography</i>	- 112 -
6	<i>Appendix</i>	- 136 -
6.1	Supplementary Figure	- 136 -
6.2	List of abbreviations	- 137 -
6.3	List of Figures	- 140 -
7	<i>Acknowledgments</i>	- 142 -
8	<i>Publications</i>	- 144 -
9	<i>Affidavit</i>	- 146 -
10	<i>Curriculum Vitae</i>	- 147 -

Introduction

1 Introduction

The term cancer refers to a large and heterogeneous group of roughly around 277 diseases that are primarily characterised by uncontrolled growth and spread of abnormal cells [Hassanpour and Dehghani 2017] [American Cancer Society]. The development of cancer is characterized by a multi-stage process, referred to as oncogenesis. Due to changes in the DNA of normal cells, successive mutations accumulate and transform them into tumour cells. Certain risk factors such as chemical compounds, smoking, radiation and contact with viruses and bacteria can increase the risk of developing cancer [Parkin 2006, Poon et al. 2014, Antwi et al. 2015]. In addition, age and genetic factors have a pivotal role in the development of certain cancer types, such as FAP.

In 2020, cancer was the leading cause of death worldwide, accounting for almost 10 million deaths, surpassing cardiovascular disease [Ferlay, Ervik et al. 2020]. Next to breast cancer (2.26 million cases and 685 000 deaths) is lung cancer the most common cancer type with 2.21 million cases among both sexes per annum. [WHO]

Lung cancer was first recognised and described as a disease by Isaac Adler more than 100 years ago, in 1912. For his study, he reported all known cases of lung cancer in the world, which at the time were only 374 patients [Adler 1912]. Since then, lung cancer has become the leading cause of cancer-related death with over 1.8 million victims. [Siegel et al. 2022][WHO] For the coming years, the WHO predicts an increase in lung cancer cases as the 'tobacco epidemic' continues to grow, particularly in low- and middle-income countries smoking was identified as the main cause of lung cancer as early as 1950, with an estimated 80% of lung cancer deaths caused by tobacco consumption [Zappa and Mousa 2016, Sung et al. 2021].

It is worth noting that lung cancer is not a homogenous disease but, according to histology and molecular analysis, is subdivided into two major groups: small cell lung carcinoma (SCLC, 15%) and Non-SCLC (NSCLC, 85%) [Travis et al. 2015]. The majority of patients with lung cancer are diagnosed with Non-small cell lung cancer (85 %) and in 2023, the American Cancer Society estimated that 13% of all new cancer cases relate to NSCLC and cause a total of 21% estimated cancer deaths are NSCLC, thereby making this cancer type the variant with the highest mortality rate in both sexes. In the latter and specifically within this thesis, NSCLC is discussed.

Introduction

1.1 Non-Small Cell Lung Cancer

In order to undergo oncogenic transformation of lung epithelium, these somatic cells have to accumulate changes in their own DNA, which not only affects the cell but also alters the microenvironment. These changes, so-called mutations, can be induced either by exposure to carcinogens, such as tobacco smoke, can be triggered by tissue damage and/or chronic inflammation. Subsequently, the development of tumours can occur via a well characterised progress, encompassing basal cell hyperplasia to metaplasia, severe dysplasia to carcinoma *in situ* and carcinoma, or by the transition of less well-characterized premalignant lesions called atypical adenomatous hyperplasia (AAH). [Colby et al. 1998, Travis et al. 2015]

Furthermore, patients are frequently diagnosed with progressed ,late-stage NSCLC. In this patient cohort overall the 5 year survival rate drops to just 2-13 % [Moldaver et al. 2020]. Not only the late diagnosis but also the complexity and heterogeneity of this disease presents a major challenge for targeted treatment of patients [Cancer Genome Atlas Research 2014]. Furthermore, for a long time, NSCLC was considered as one disease and a "one size fits all" approach for therapeutic intervention to therapy was taken. Treatment strategies for NSCLC were based on disease stage and a platinum-based dual chemo-/- radiotherapy as first-line treatment was predominantly used. [Schiller et al. 2002]. With Next-Generation Sequencing (NGS), a deepened understanding on the molecular complexity of NSCLC could be established, allowing for an improved, personalised therapeutic approach. However, despite the advent of therapeutic strategies based on genetic profiling, such as checkpoint inhibition and epidermal growth factor receptor tyrosine kinase inhibitors (EGFR-TKIs), the majority of NSCLC patients and, hence, overall survival of NSCLC has only marginally increased [Asao et al. 2019, Lim and Ma 2019]. As a consequence, and to further refine treatment options, large databases and NGS is used to re-define and identify NSCLC subsets and patient stratification accordingly. Currently, NSCLC is classified into two

Introduction

major subtypes based on the tumours histopathological features: Adenocarcinoma (ADC) and Squamous Cell Carcinoma (SCC) [Mengoli et al. 2018] (Figure 1-1).

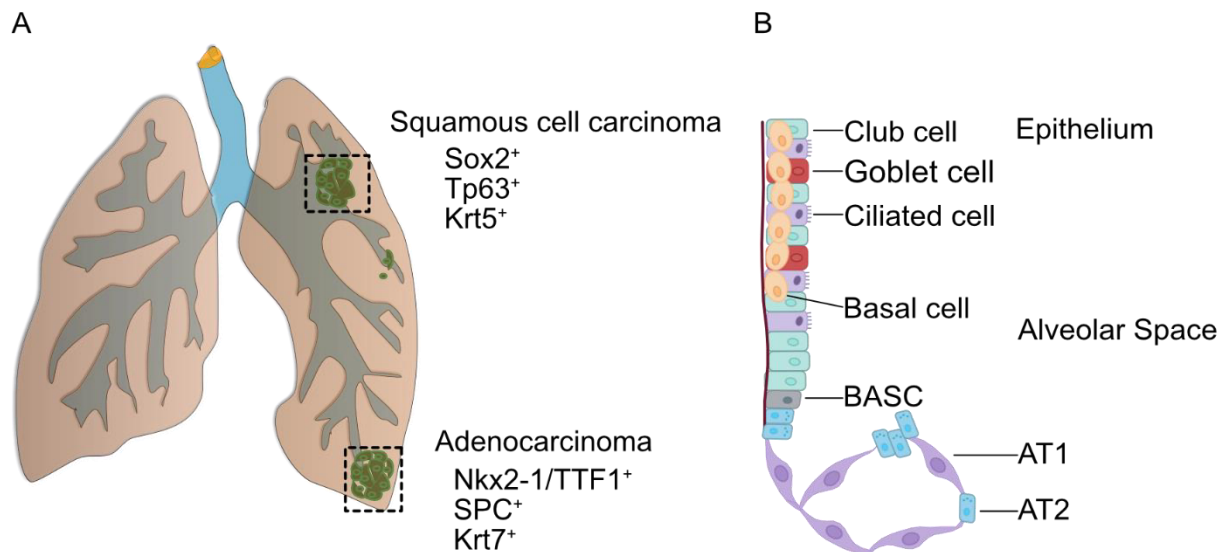


Figure 1-1: A diagram of a lung with the regions for SCC and ADC

A An schematic overview of a lung with the distal region of origin for Adenocarcinomas (ADC) and the more proximal region for Squamous cell carcinoma (SCC). Below each tumour entity are the typical histological marker listed.

B Schematic overview of a lung epithelium and the alveolar space with the cell population. The basal cells are considered as putative cell of origin for SCC, since they express the common marker p63 and Sox2 and Krt5 of this cancer subtype. The bronchioalveolar duct junction with the bronchioalveolar stem cells (BASCs) follows the epithelium. The alveolar space is composed of fully differentiated AT1 cells and the alveolar stem cells AT2. The alveolar epithelial type 2 cells are positive for thyroid transcription factor 1 (Nkx2-1/TTF1), surfactant protein C (SPC) and Krt7 expression and the cell of origin for ADC.

(Modified from [Chen et al. 2014])

ADC is the dominant subtype, accounting for 50% of all diagnosed NSCLC cases, followed by SCC at 40%. The remaining 10 % of NSCLC cases are classified as large cell carcinoma due to the lack of a defined marker expression and morphological features. [Langer et al. 2010, Davidson et al. 2013]

Adenocarcinomas are malignant epithelial tumours that usually derive from alveolar and bronchioalveolar epithelia cells. They represent the most common lung cancer type in non-smokers [Davidson et al. 2013]. According to their morphology, they can be classified as epidic, acinar, papillary, micropapillary or solid. In addition, a classification system has been introduced by IASLC/ATS/ERS to improve resection surgery: Adenocarcinoma in situ (AIS), minimally invasive adenocarcinoma (MIA) and solid adenocarcinoma with mucin production.[Travis et al. 2011]. However, in most patients a mix of ADC-types is very common. [Travis et al. 2015] The majority of ADCs is positive for the expression of the thyroid transcription factor 1 (Nkx2-1/TTF1), with

Introduction

the exception of a minor AIS portion, which are TTF1 negative. Furthermore, ADC is characterised by the expression of surfactant protein C (SPC) and Krt7, in rare cases also Krt20 [Lau et al. 2002].

As a cell of origin, the TTF1 expressing alveolar epithelial type 2 (AT2) has been identified [Xu et al. 2014]. However, this understanding prior to 2014 was based on the genetically engineered mouse model (GEMM) and was controversial. Due to the genetic approaches chosen for tumour induction, bronchioalveolar stem cells (BASC) and Clara cells were also considered as putative 'cells of origin' of ADC. [Kim et al. 2005, Ventura et al. 2007]. However, with the use of more complex *in vivo* model systems, BASC and Clara cells could be excluded and AT2 cells as *cell of origin* of ADC experimentally confirmed. [Rawlins et al. 2009, Xu et al. 2012, Xu et al. 2014].

Squamous cell carcinoma is the second largest subgroup of patients diagnosed with non-small cell lung cancer (NSCLC) and is predominantly located in the central areas of the lung in proximity to airways [Giangreco et al. 2012]. Common morphologies for SCC include the eponymous squamous differentiation, intercellular bridges, keratinisation of single cells and squamous formation [Kumar V et al. 2013]. SCC, like ADC, is also subclassified according to the current WHO classification, including papillary, clear cell, small cell, and basaloid subtypes of SCC. However, they have no clinical nor prognostic value, with the exception of basaloid SCC [Travis et al. 2015].

The very characteristic squamous differentiation, the proximity to airways and the expression of p63, Krt5 and SRY-box 2 (SOX2) in SCC, points towards tracheal basal cell progenitors as cell of origin [Langer et al. 2010, Lu et al. 2010, Giangreco et al. 2012]. However, extensive *in vivo* studies could not clearly identify the cell of origin nor the mechanism for the development of squamous cell carcinoma. BASC-specific overexpression of Sox2 leads to the development of morphological ADC with the expression of SCC markers such as p63. Knockout of the tumour suppressor liver kinase B1 (LKB1) in combination with a Kras^{G12D} mutation also led to a mixture of ADC and SCC. Only the simultaneous loss of PTEN and LKB1 could lead to SCC, but without clearly indicating a cell of origin. [Ji et al. 2007, Lu et al. 2010, Malkoski et al. 2014, Xu et al. 2014].

Unlike ADC, squamous cell carcinoma is often associated with chronic inflammation and smoking. Due to changes in smoking behaviour, the overall diagnosis of SCC was declining [Langer et al. 2010, Davidson et al. 2013].

Introduction

The last subgroup of NSCLC is the large cell carcinoma (LCC). Unlike the former two, LCC is a diagnosis of exclusion [Travis et al. 2015]. Thus, the tumours do not have morphological features or cellular characteristics that unambiguously associate them with ADC or SCC. The expression of markers for several subtypes, or the lack of clear marker expression is possible. Therefore, non-invasive methods such as biopsy or ultrasound are not suitable for the correct identification of LCC. Surgical excision is required for a complete histological examination and exclusion of local differentiation of other lung cancer types. [Travis et al. 2011, Travis et al. 2015]

Since 2004 the WHO differentiates between several subtypes of LCC, including large cell neuroendocrine cancer (LCNEC), basaloid carcinoma, lymphoepithelial-like carcinoma, and clear cell carcinoma [Travis et al. 2015]

1.2 Genetic complexity in NSCLC

To date NSCLC subtypes are still distinguished by histopathological approaches, but advances in NGS have improved insight into the mutational burden and differences between adenocarcinomas and squamous cell carcinomas. Two major studies from The Cancer Genome Atlas Research Network in 2012 and 2014 analysed 230 untreated ADC and 178 untreated SCC patient samples according to copy number alterations, exonic mutations and genomic rearrangements [Cancer Genome Atlas Research 2012, Cancer Genome Atlas Research 2014]. In these studies, as well as in subsequent analyses, a mean somatic alteration rate of more than 8.5 to 10 mutations per megabase were identified in both tumour types, making ADC and SCC one of the most somatically mutated tumour types, trailing only melanoma. [Lawrence et al. 2014]. Comparison of the two tumour entities with regard to common somatic (driving) mutations revealed both, similarities, and differences, between ADC and SCC (Figure 1-2).

Introduction

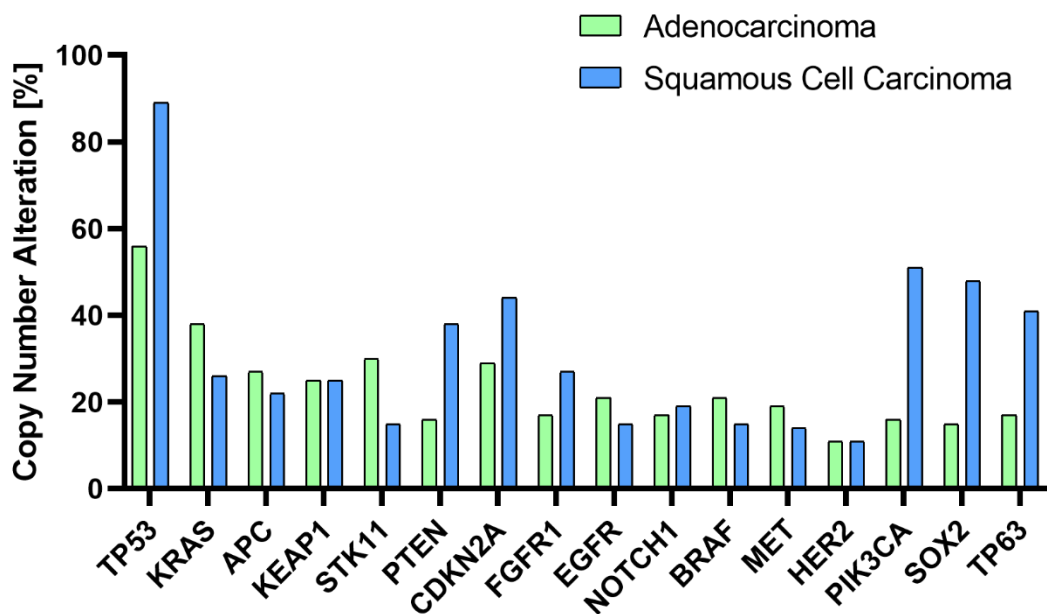


Figure 1-2: Most common genetic alterations in Adenocarcinoma and Squamous Cell Carcinoma

A snapshot of common genetic alterations in % according to NSCLC histological subtypes: Adenocarcinoma (green) and Squamous Cell Carcinoma (blue). Shown are combined alterations of tumour suppressors and oncogenes, including mutations, amplifications and up- or downregulation on mRNA level. (adapted from [Gridelli et al. 2015] and Cbioportal.org)

Although genetic analysis of ADC and SCC has shown that alterations in the same genes can be found in both subtypes, they differ at the molecular level. Mutations in the Epidermal growth factor receptor (EGFR) as well as in BRAF are predominantly found in ADC whereas SCC rather shows amplifications of those genes [Paez et al. 2004] [cbioportal.org]. Furthermore, alterations in SOX2, TP63 and PI3KCA are significantly more prominent in squamous cell carcinomas these genes are present on chromosome 3q, a region frequently amplified in SCC (~65%) [cBioportal.org].

More than half of all ADC patients and over 85% of all SCC patients had alterations in the tumour suppressor gene TP53, making this the most commonly altered tumour suppressor in NSCLC. TP53 was first discovered in 1979 and later characterised as a tumour suppressor in 1989 [Lane and Crawford 1979, Linzer and Levine 1979, Baker et al. 1989]. Referred to as the “guardian of the genome”, it plays an important role in the response to DNA damage and a plethora of cellular stressors and is stabilised in response to stress signals [Lane 1992]. This is a prerequisite to fulfil its biological function. Subsequently, TP53 transcriptionally regulates target genes involved in cell cycle arrest, senescence, DNA repair, cell metabolism and apoptosis [Aubrey et al. 2016]. The majority of identified *TP53* mutations are missense mutations, which is in

Introduction

contrast to other tumour suppressors, such as APC or RB, which frequently harbour nonsense or frameshift alterations [Soussi 2005]. Loss of TP53 function in lung cancer is associated with poor survival and therapy resistance. Furthermore, studies reported that mutations and LOH of *TP53* occur already at early tumour onset and contribute to metastasis. These observations imply that loss of TP53 function is contributing to tumour initiation, progression, maintenance and metastatic spread [Mogi and Kuwano 2011].

The second most frequent alteration and the most mutated oncogenes in human cancer are the Rat sarcoma family members (RAS) [Soh et al. 2009]. The small membrane bound proteins are GTPases and switch between an active guanosine triphosphate (GTP)-bound and inactive guanosine diphosphate (GDP)-bound state [Cherfils and Zeghouf 2013]. Thus, they transmit extracellular signals, which subsequently activate important downstream pathways and thereby control cell proliferation, cell cycle regulation, differentiation, survival, and metabolism. Among those signalling cascades are mitogen-activated protein kinase (MAPK) and phosphatidylinositol-3-kinase (PI3K) [Stokoe et al. 1994, Malumbres and Barbacid 2003] (Figure 1-3).

Among the RAS family, the Kirsten rat sarcoma (KRAS) accounts for 85 % of all observed mutations within the RAS family and is altered in approximately 30 - 35 % of all NSCLC cases [Simanshu et al. 2017, Prior et al. 2020], but also found as a major oncogenic driver in various solid tumours. Clinically, dysregulated KRAS signalling is associated with increased expression of programmed cell death–ligand 1 (PD-L1) and an immunosuppressive tumour microenvironment [Dias Carvalho et al. 2019].

Most common are gain-of-function point mutations at codon 12 (90 %), resulting in a constant active state and promoting the oncogenic features [Karachaliou et al. 2013].

Introduction

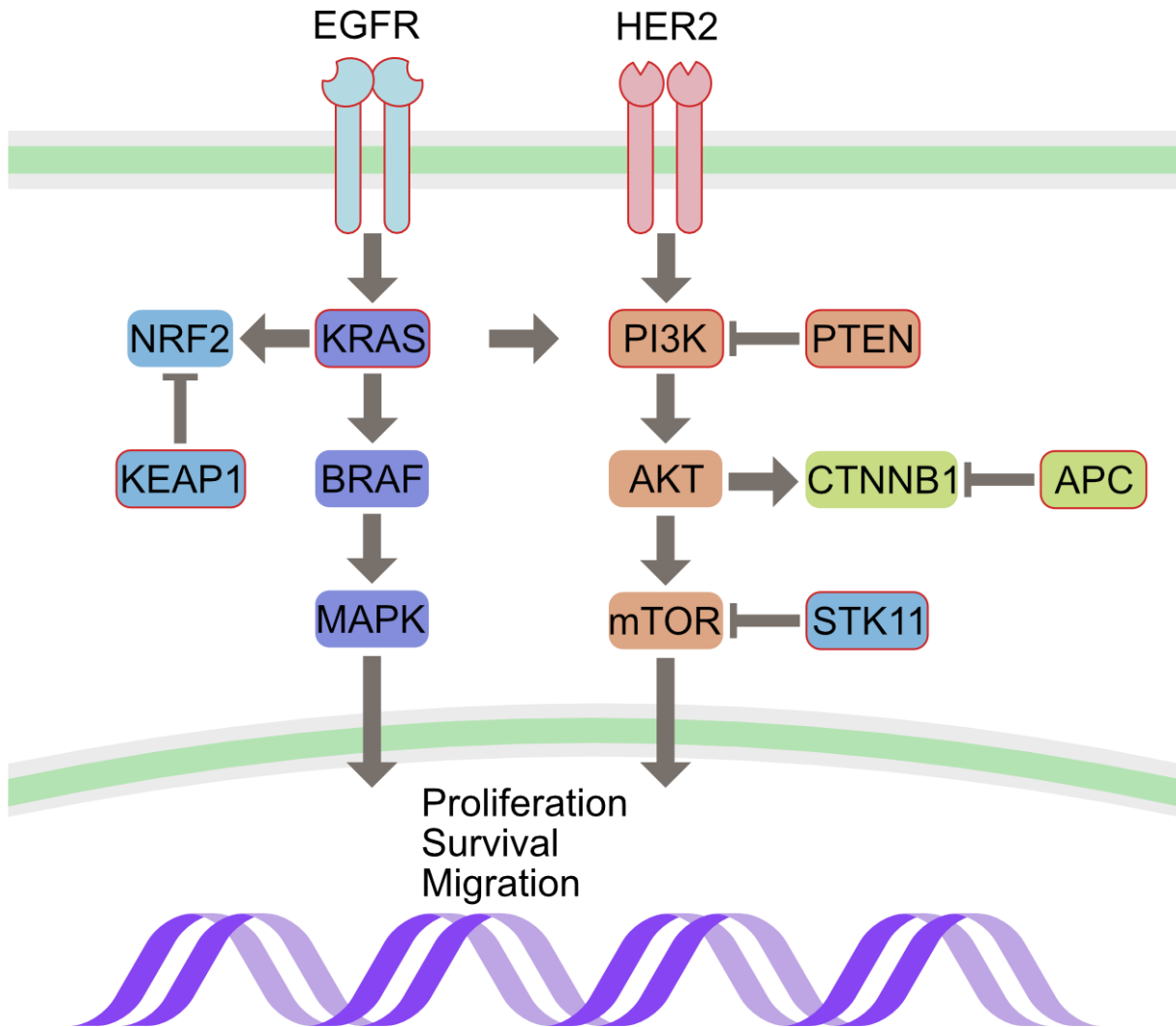


Figure 1-3: A simplified overview of the impact of commonly altered genes in NSCLC

Significantly altered signalling pathways in non-small cell lung cancer in a simplified overview. Arrows indicate a downstream activating effect; boxed connections describe an inhibitory effector. Frequently mutated or altered genes are highlighted by a red outline. (cbioportal.org 2023)

The most common point mutation in non-smokers is the substitution of glycine (Gly) for asparagine (Asp) at codon 12 (G12D), accounting for 56% of all cases. Interestingly, smoking behaviour changes this observation. Former and current smokers have predominantly a G12C and G12V mutation [Dogan et al. 2012].

Although all three mutations lead to a constitutively active state, an *in vitro* study showed that different substitutions alter the affinity of downstream effectors, such that G12D leads to increased PI3K-AKT activation, while G12C/V has higher RAL-NFκB activation [Ihle et al. 2012]. Likewise, the different point mutations not only influence subsequent oncogenic pathways, but also have an impact on metastasis and the overall survival rate of patients with NSCLC. Patient studies have shown that metastases arise significantly more frequently in the lung with KRAS G12C compared

Introduction

to the other point mutations in codon 12. However, metastases in the lymphatic system and pleura were diagnosed more frequently in non-G12C mutants [Wu et al. 2021]

Of note, apart from smoking does ethnical background (Caucasian vs Asian population 26 % to 11 %) as well as sex (female vs male 31.25 % to 23.7 %) and tumour type (ADC vs SCC 37.2 % to 4.4 %) affect the ratio of KRAS mutations as well as the characteristics of single KRAS point mutations [Cascetta et al. 2022]. For example, a low mutational burden of KRAS in squamous cell carcinoma compared to adenocarcinoma is reported. However, in 26 % percent of all patients, alterations in KRAS were found in SCC (Figure 1-2) which are predominantly upregulation on mRNA level [cbioportal.org] [Cancer Genome Atlas Research 2012].

Although there are significant and tumour type discreet differences in the individual point mutations of KRAS, the prognostic value and clinical applicability of genetic information regarding KRas status is controversial. A meta-analysis of 43 studies could demonstrate that the overall survival (OS) and the progression-free survival (PFS) is impaired for KRAS mutant tumours, however, this finding could not be confirmed in clinical studies [Goulding et al. 2020, Cascetta et al. 2022]

Not only does the different point mutations in KRAS add to the heterogeneity of both NSCLC subtypes. The largest cohort study published by Riely et al. reported that KRAS mutations frequently occur together with loss-of-function mutations in various tumour suppressors such as TP53, STK11/LKB1 and KEAP1. [Arbour et al. 2018]. Co-mutation of TP53 and KRAS are predominantly found in ADC and range between 31 % to 45 % [Lei et al. 2020]. Interestingly, single KRAS or TP53 mutations have an overall worse prognosis than co-occurring mutations in both genes. The cause was predicted to be the better response to targeted immunotherapy of KRAS/TP53 mutant patients [Assoun et al. 2019]. This observation highlights the importance to use suitable in vivo and ex vivo model systems to study the disease, NSCLC, in greater detail.

The liver kinase B1 (LKB1) is encoded by the serine/threonine kinase 11 (STK11) gene and is an additional known tumour suppressor, which is frequently mutated in KRas/TP53 driven NSCLC, predominantly in ADC [Ding et al. 2008, Cancer Genome Atlas Research 2014]. In its unperturbed status LKB1 regulates cell growth and metabolism by regulating the activity of adenosine monophosphate-activated protein kinase (AMPK) cascade. By phosphorylation of AMPK, LKB1 regulates the energy homeostasis and suppresses cell growth [Shackelford and Shaw 2009]. The loss of

Introduction

LKB1 function, due to downregulation or mutation, is associated with highly aggressive tumours and an increased resistance to standard treatment [Skoulidis et al. 2015].

Co-occurring genomic alterations in STK11/LKB1 together with KRAS range between 8 % to 31 % [Gu et al. 2021], depending on tumour type and study group. An additional loss of TP53 defines even a distinct subset of KRAS driven ADC [Skoulidis et al. 2015]. Loss of LKB1 and KRAS is characterised by an immunosuppressive tumour environment and an associated poor prognosis for patients. Furthermore, the tumours demonstrate a dysregulated energy metabolism and a decreased survivability [Galan-Cobo et al. 2019].

In addition to KRAS and TP53, the Kelch-like ECH-associated protein 1 (KEAP1) has been identified as a frequent co-mutated tumour suppressor by Skoulidis et al [Cancer Genome Atlas Research 2014, Skoulidis et al. 2015]. In its normal function as an E3 ligase, it regulates the protein stability of NRF2 (nuclear factor erythroid 2-related factor 2). The KEAP1-NRF2 axis is thereby regulating and coping with oxidative stress and a crucial factor in the regulation of the antioxidant transcription factor. Furthermore, KEAP1 has been described as a tumour suppressor and its loss is associated with resistance to checkpoint inhibition, establishment of immune cold tumours and driver of tumour progression [Romero et al. 2017, Lignitto et al. 2019]. Intriguingly, previous work identified that mutations in KRAS are causative to increased Nrf2 levels. Here, the additional loss of KEAP1 further stabilizes Nrf2 and lead to a strong activation of the oxidative stress response in cells, leading to an increased chemoresistance [Romero et al. 2017].

It is also noteworthy that in addition to the co-occurring mutations of KRAS with KEAP1 or STK11, a simultaneous loss of KEAP1 and STK11 can occur. The reason for this is the proximity of both genes on chromosome 19 [Skoulidis et al. 2015]. Studies could show that the loss of Lkb1 sensitizes KRAS mutant NSCLC to glucose starvation. The additional loss of KEAP1 lead either to a metabolic reprogramming or an upregulation of NRF2 and thus could further accelerate the proliferation [Caiola et al. 2018].

The aforementioned tumour suppressors are predominantly altered in lung adenocarcinoma. One of the major dysregulated pathways in lung squamous cell carcinoma is the PI3K/Akt/mTOR pathway (Figure 1-2, Figure 1-3). In its crucial function, this signalling pathway regulates cell growth and cell metabolism in an important signalling cascade. As early as 1985, the role of abnormal PI3K signalling

Introduction

was described in connection with cancer and its role in tumour proliferation [Whitman et al. 1985]. In brief, PI3K are intracellular lipid kinases that phosphorylate the 3'-hydroxyl group of phosphatidylinositol and phosphoinositides. Thus a signalling cascade involving mTOR and AKT is activated, leading to proliferation, survival and cell growth [Engelman et al. 2006].

Amplifications or mutations in the pathway member PIK3CA have been linked to tumorigenesis and progression of NSCLC [Scheffler et al. 2015]. Furthermore, these studies could demonstrate, that alterations in PIK3CA co-occur with mutations in KRAS or EGFR and are not mutual exclusive [Okudela et al. 2007, Ji et al. 2011]. In addition to amplifications or activating mutations in PIK3CA loss of Phosphatase and tensin homolog deleted on chromosome 10 (PTEN) function was observed in 44 % of SCC patients (Figure 1-2). The tumour suppressor is the main negative regulator of the PI3K signalling pathway and as an important role to maintain homeostasis, cell growth, survival and metabolism [Stiles 2009]. Alterations in PTEN are associated with resistance to standard of care therapy and increased resistance to chemotherapy or immunotherapy. [Gkoutakos et al. 2019, Fischer et al. 2022].

The most common somatic alteration in the PI3K pathway are loss-of function mutations in the catalytic phosphatase domain of PTEN. In SCC patients up to 10 % demonstrate mutations in PTEN, in ADC only 2 % [Liaw et al. 1997]. In addition to mutations, loss of heterozygosity (LOH) of PTEN as well as epigenetic downregulation has been described as reason for loss of gene expression [Marsit et al. 2005]. Lastly, PTEN abundance can be decreased by a PI3K driven feedback loop. The activation of mTOR and AKT subsequently leads to an increased NF κ B transcriptional activity, that results in a downregulation of PTEN transcription [Perez-Ramirez et al. 2015]. In addition to changes in PTEN, up to 10% somatic mutations and 35% amplifications in SCC have been described for PI3KCA. Most prominent are point mutations in exon 9 and 20 which either render the intra-molecular inhibitory effect inactive or lead to constitutive active state [Perez-Ramirez et al. 2015].

In addition to the regulation of TP53 stability via MDM2 and the inhibition of apoptosis via the PI3K downstream effector AKT, other pathways are also regulated indirectly via the PI3K axis. For example, the WNT pathway is activated via the inactivation of the kinase GSK3 [Rubinfeld et al. 1996, Zhou et al. 2001].

Introduction

In NSCLC subtypes the Wingless-type protein (Wnt) signalling has been proposed to play a role in cancer stemness, decreased apoptotic behaviour and an increase in the abundance of other oncogenic transcription factors such as cMyc [Nakashima et al. 2008, Huang 2010]. In vivo studies in mice could link activated Wnt signalling to the development of NSCLC and recapitulate the activation in the context of KRAS mutant mice [Pacheco-Pinedo et al. 2011, Vaughan et al. 2012].

As mentioned above, increased Wnt activity can be observed in lung cancer with deregulated PI3K/AKT pathway. In addition, changes in Adenomatous polyposis coli (APC) and CTNNB1 were also found in NSCLC patients. APC has been described as a tumour suppressor and is notorious for its importance in the development of colorectal cancer. In its function, APC is part of the destruction complex that binds the WNT pathway signal protein β -Catenin. This facilitates the phosphorylation and subsequently the proteasomal degradation, leading to a WNT signal off state [Ikeda 1998]. Mutations on APC or β -Catenin prevent degradation and can increase β -Catenin abundance. However, changes, especially mutations, are rarely found in lung cancer [Kinzler et al. 1991]. More common are the loss of heterozygosity on chromosome 5q, which is the APC locus [Ohgaki et al. 2004]. In addition to the loss of APC, overexpression of β -Catenin can be observed rather than mutations [Nakayama et al. 2014].

Furthermore, the prognostic role of accumulated β -Catenin is still controversial. Expression of the transcription factor was observed in over 90 % of all SCC and in 51 % of all ADC patients [Choi et al. 2003]. On the one hand, studies have shown that the loss of β -catenin has a negative impact on the prognosis and that the overexpression had beneficial effects [Hommura et al. 2002]. On the other hand studies could link aberrant WNT signalling to poor prognosis as well as a dedifferentiation state of early and late stage non-small-cell lung cancer [Shapiro et al. 2013].

1.3 Current Therapeutic Intervention

The high mortality of lung cancer (18% in 2020) is predominantly associated with the late diagnosis in advanced stages or distant metastasis. A reason for the delayed recognition is the lack of clear symptoms in an early stage [Henschke et al. 1999].

Introduction

However, studies have shown that, in addition to prevention, early detection can greatly increase the chance of disease-free survival and cure [Ganti et al. 2021].

In order to reduce mortality and improve the treatment of NSCLC, the diagnostic, treatment, and classification of lung cancer has been constantly modernised and revised with the latest addition in 2015 by the World Health Organisation (WHO) [Travis et al. 2015].

The next step in further refining the treatment of patients diagnosed with lung cancer is to determine the tumour stage. The American Joint Committee on Cancer (AJCC) TNM (tumour-lymph node-metastasis) system is used to grade tumours based on key information. The decisive factors are the size of the tumour, the proximity to neighbouring organs, the spread to nearby lymph nodes and the metastasis to distant organs. For lung cancer the stages can range from **0**, where the tumours have not invaded the lung tissue, are smaller than 3 cm and have not spread to lymph nodes or metastasised to distant organs, up to stage **IV**. A tumour at this late stage has metastasised to distant organs or lymph nodes outside the chest. [AmericanCancerSociety 2019].

1.3.1. Treatment modalities for early-stage disease:

The treatment options for lung cancer have been established over 50 years ago and have not changed much since. The standard of care includes chemotherapy, radiotherapy and surgery, either as single or combinational treatment strategies [Spiro and Silvestri 2005].

The oldest treatment for lung tumours is surgical removal of the tumour. This standard of care is predominantly applied for patients in early-stage disease, stage I or II. In addition, for a small group of patients with stage IIIA, where the tumour is smaller than 3 cm, surgical removal is also applicable as first line treatment. [Ettinger et al. 2021] Despite having a curative attempt, patients suffer from lung cancer relapse after full resection of the primary tumours. Reasons are unclear, however, the co-existence of further tumour nodules deriving from additional oncogenic events or as part of intra-organ metastasis, is likely the cause. In order to improve the 5-year survival rate, neoadjuvant and adjuvant chemotherapy is provided to patients before and after surgery [Pignon et al. 2008].

Introduction

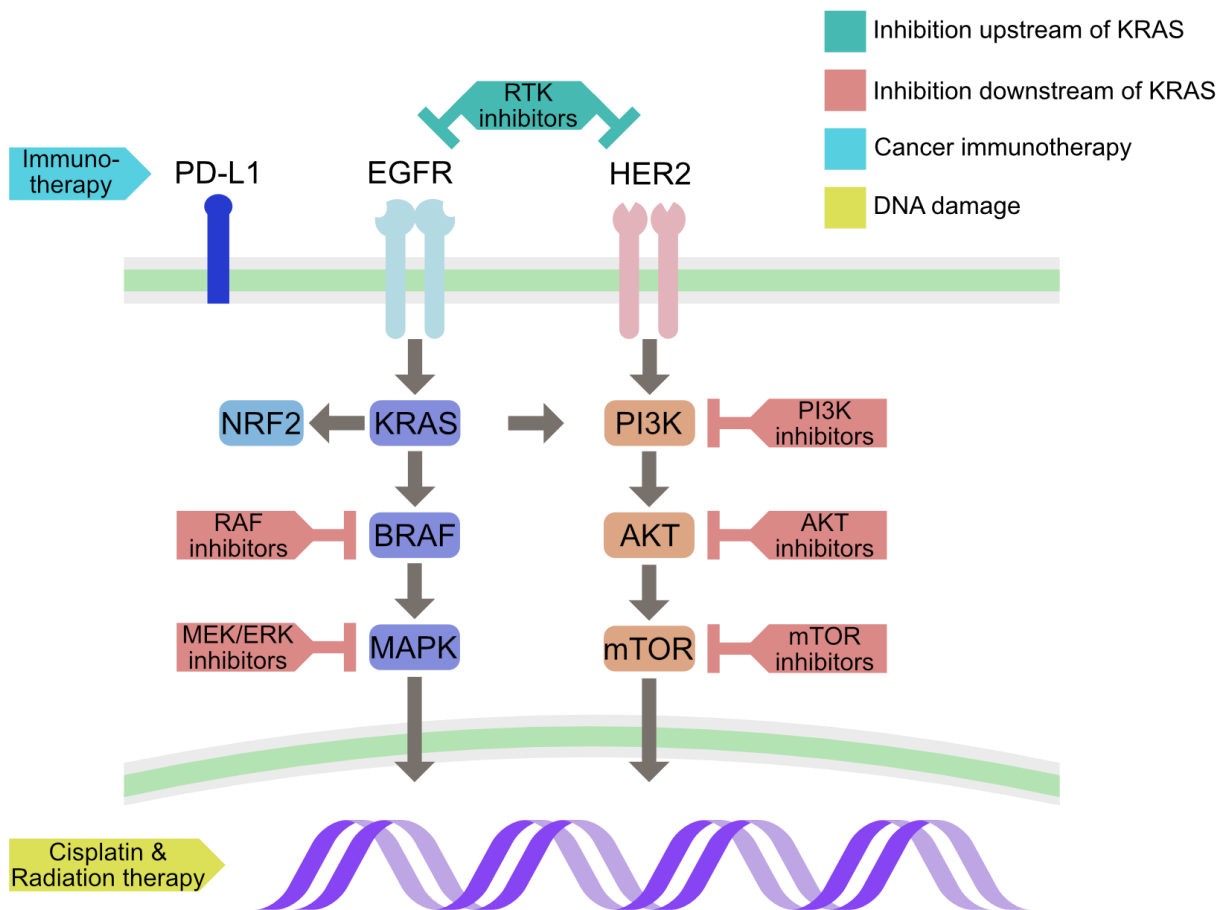


Figure 1-4: A simplified overview of current therapeutic strategies and their targeted pathways in NSCLC

Significantly altered signalling pathways in non-small cell lung cancer in a simplified overview. Arrows indicate a downstream activating effect. Turquoise box shaped connections describe inhibitors used to target the Ras pathway upstream of KRAS with receptor-tyrosine kinase (RTK) inhibitors. Red box shaped connections describe inhibitors used to target the Ras pathway downstream of KRAS, interfering with various different pathways e.g., PI3K/AKT/mTOR or RAF/MAPK. The light blue box-shaped arrow indicates Checkpoint inhibitor therapy, and the yellow arrow indicates DNA-damage therapies, such as cisplatin treatment or radiation therapy .(adopted from [Spagnuolo et al. 2022] and cbiportal.org 2023)

1.3.2. Treatment of progressed disease:

Chemotherapy is a treatment with a single component or combined drugs that can interfere with the DNA repair mechanism, induce apoptosis and DNA damage and/or interfere with the cell cycle. Commonly used to treat early and metastatic NSCLC, either as adjuvant therapy or as first-line treatment for inoperable tumours or when surgery is not possible. The final combination of chemotherapeutic agents is based on tumour stage, mutation burden and biomarker expression. However, a combination of platinum-based drugs (cisplatin or carboplatin) with cytotoxic drugs is usually given. [Zappa and Mousa 2016] Since the implementation of chemotherapy, the median survival rates of patients have only marginally improved. The first major breakthrough was the introduction of platinum-based treatment in the 1980s, which significantly

Introduction

increased OS in 1 year (5 to 15%). The next step in the treatment of advanced NSCLC was achieved with platinum doublets. This could further increase median survival significantly compared to non-platinum or single agent treatment. [Lee 2019].

The limitations of chemotherapy are the rapid development of resistant tumours and the severe side effects, which call for further improvements in this broader approach. [Heng et al. 2019].

A second mainstay treatment for inoperable NSCLC is radiotherapy, which is used for patients diagnosed with stage III NSCLC (~30%)[Ramalingam and Belani 2008]. The basis of the treatment is the local application of high energy radiation to control tumours locally through DNA damage. Despite improvements in the treatment, survival has not improved. Only side effects have been reduced. [Vinod and Hau 2020] For this reason, radiotherapy is often used in combination with other treatments such as chemotherapy. Studies have shown that this significantly increases OS by up to 4 years [Antonia et al. 2018, Rallis et al. 2021].

Improvements in diagnostic tools and the implementation of NGS have opened up a next line of treatment options for patients with advanced NSCLC. Testing for biomarkers has enabled personalised and targeted therapeutic intervention. Here, assays are utilized to identify the molecular mutations in the tumours.

The most prominent anticancer target is the member of the receptor tyrosine kinase family (RTK) the epidermal growth factor receptor (EGFR or HER1) and to date three generations of EGFR tyrosine kinase inhibitors (TKI) have been developed. Already the first two generations could improve the OS of patients with mutant EGFR [Yang et al. 2017]. However, the tumours very quickly developed resistance via subsequent mutations [Riely et al. 2006]. In particular, the T790M point mutation led to drug resistance. Third-generation TKIs were designed to circumvent this and have been able to significantly improve OS in advanced NSCLC [Cheng et al. 2021]. Besides the acquired resistance due to point mutations, another disadvantage is that only patients with sensitising EGFR mutations benefit from this treatment [Mao et al. 2010]. Mutations that occur below the EGF-receptor, e.g., in KRAS, also have a negative impact on the treatment prognosis [Reita et al. 2022].

As mentioned earlier (1.2), KRAS is one of the most altered oncogenes in lung cancer. Alterations in RAS pathways not only activate and dysregulate important cellular pathways, but also render TKI treatment inactive. To circumvent this, direct targeting

Introduction

of mutant KRAS has been the focus of recent research. To date, one inhibitor targeting KRAS G12C mutated NSCLC, has been approved and showed a beneficial effect in combination with chemotherapy [Mullard 2021].

The complexity of the KRAS pathway is shown in Figure 1 2 and Figure 1 3. Targeting downstream effectors, such as MEK or PI3K, could show that inhibitor treatment may be beneficial for patients' OS, depending on the KRAS point mutation. However, a deeper understanding at the molecular level is needed to successfully translate this into treatment strategies. [Shen et al. 2021]

Since targeting the MAPK pathway has shown promising initial results, it seems likely that targeting the Pi3K/AKT/mTOR pathway is an equally attractive target for the treatment of NSCLC. Alterations in members of this pathway have been observed for PI3K (19 %), AKT (51 %) and mTOR (90 % ADC/ 40 % SCC) and their upregulation is central for tumour development [Tan 2020]. Despite the development of first-generation inhibitors targeting either PI3K, mTOR or AKT, as well as second-generation inhibitors with a dual PI3K/mTOR targeting approach, clinical results have been disappointing. In several trials, treatment with these inhibitors had no or very weak effects on progression-free survival (PFS).

1.3.3. Beyond pathway interference: Immuno-modulatory interventions:

Immunotherapy has emerged as a promising treatment approach for non-small cell lung cancer (NSCLC) in 2015 [Rizvi et al. 2015]. In particular, immune checkpoint inhibitors, a type of immunotherapy, have shown significant efficacy in treating NSCLC [Reck et al. 2021]. By blocking checkpoint proteins such as programmed cell death protein 1 (PD-1) or its ligand (PD-L1, immune checkpoint inhibitors enhance the immune system's ability to recognise and attack cancer cells. In NSCLC, immune checkpoint inhibitors have shown significant clinical benefit, particularly in patients with advanced or metastatic disease. They have shown efficacy both as monotherapy and in combination with other treatments. Clinical trials have shown improved overall survival and long-term responses in a subset of patients treated with immune checkpoint inhibitors. [Sezer et al. 2021] PD-L1 expression on tumour cells is associated with response rates to immune checkpoint inhibitors [Brahmer et al. 2015]. Higher PD-L1 expression is often associated with higher response rates, although patients with lower PD-L1 expression may still benefit from treatment [Carbone et al. 2017]. It is important to note that although immune checkpoint inhibitors have shown

Introduction

remarkable success, not all patients with NSCLC respond to these therapies. Research efforts are focused on identifying additional biomarkers and developing combination therapies that increase response rates and overcome resistance mechanisms.

In summary, improvements in diagnostics, the implementation of NGS and biomarker determination have improved the overall understanding of lung cancer and could lead to new promising therapeutic interventions. However, the impact on the survival of lung cancer patients has increased only slightly and remains low irrespective of the type of cancer.

1.4 Animal models in NSCLC research

Non-small cell lung cancer (NSCLC) research has extensively utilized mouse models to study the disease and develop potential therapeutic strategies. Mouse models have played a crucial role in understanding the biology of NSCLC, evaluating new treatment approaches, and assessing the efficacy of various therapies before clinical trials in humans. [Day et al. 2015, Ireson et al. 2019]

Various modalities have been described previously and are still in use ranging from the subcutaneous injection of lung tumour cells to orthotopic models (into the lung) in mice. First described in 1969, the cell line xenograft model was used to study tumour growth, treatment response and potential therapeutic strategies [Rygaard and Povlsen 1969, Kelland 2004]. In order to study human lung cancer, the patient derived cells necessitated the implant in immunodeficient animals, as otherwise host-graft disease would have led to the rejection of the transplanted cells. Hence, Xenograft models using incompatible species or strains are required to be devoid of an intact immune system. As a consequence, while these transplant models aided in our strive to understand the disease and underlying mechanisms better, it limits their ability to accurately recapitulate the tumor microenvironment and immune response as seen in primary disease [Ireson et al. 2019].

With the syngeneic model not patient but mouse derived cell lines are retransplanted in isogenic recipient mice. Here, tumour cell lines established from genetically engineered mice (GEMM), chemically induced (e.g., I.p. urethane) or established from spontaneous tumours in mouse models, are retransplanted into immunocompetent animals of the same strain [Mosely et al. 2017]. This allows to study the crosstalk and

Introduction

interaction between tumor cells and the host immune system and allows for the evaluation of immunotherapeutic strategies. Both approaches are very time and cost efficient, however they fail in recapitulating tumour initiating events and other multistep processes [Ireson et al. 2019].

The most commonly used mouse model for NSCLC research is the GEMM. These mice are genetically manipulated to develop specific genetic alterations commonly observed in human NSCLC, such as genetic loss or alterations in tumor suppressor genes, such as TP53, the most commonly used and best-established tumour suppressor. By introducing these genetic changes, key aspects of human NSCLC in mice can be recapitulated and the disease progression and response to treatments can be studied. [Day et al. 2015, Janker et al. 2018]

The first generation of GEMMs was established by the ectopic and constitutive expression of transgenes under the control of lung specific promoters. Thereby, these models can mimic specific genetic events observed in human NSCLC and provide insights into the molecular mechanisms underlying tumor initiation and progression. To mimic the loss of Tp53 or Rb1 in specific lung epithelial cells, the Simian virus large T-antigen (SV40) was expressed under the control of the Club Cell Secretory Protein (CCSP/CC10) in Club cells or under the surfactant protein C (SPC) promoter in alveolar type II cells (AT2). [DeMayo et al. 1991, Wikenheiser KA 1992, Sandmüller A 1994] In the following years, the models were further extended. Variants were introduced that overexpress certain oncogenes such as Myc and JUN under the SPC or CCSP promoter [Ehrhardt et al. 2001, Geick et al. 2001].

Another approach to mimic lung malignancies has been to target frequently mutated tumour suppressors in transgenic mouse models. A dominant-negative version (dnp53) was expressed under the control of the SPC promoter and outcompeted wild-type TP53 in AT2 cells. Thus, the animals developed spontaneous lung adenocarcinomas. [Morris GF.; Hoyle GW.; Athas GB 1998]. However, recapitulation of tumour suppressor loss in conventional knockout mice is limited. Due to germline deletion, loss of many essential tumour suppressors is embryonic lethal [Jacks et al. 1992]. For less essential genes, tumour onset was sporadic and widespread, with a minor contribution to lung carcinogenesis [Meuwissen and Berns 2005].

With the advent of knock-in alleles, the second generation of NSCLC mouse models was established. Here, the expression of oncogenes under the control of the

Introduction

endogenous expression system and locus was achieved, with KRas as a prime example of the targeting strategy. In 2001, the sporadic *KRAS*^{G12D} knock-in allele (*Kras*^{LA2}) was first described as an efficient method to induce lung adenocarcinoma [Johnson et al. 2001]. Several subsequent studies have used this model to demonstrate the high overlap between KRAS-driven mice and human lung cancer [Inoue et al. 2013]. In the same year, the introduction of a conditionally activated KRAS (*lox-stop-lox-Kras*^{G12D}) via a Cre recombinase abolished the development of other cancers except lung cancer. By delivering a Cre-encoding adenovirus directly into the lungs of animals, the timing and location of tumour initiation can be controlled. [Jackson et al. 2001].

In 2005, conditional TP53 alleles were added to the LSL-KRAS model. These are mono-allelic TP53 point mutations with an LSL cassette. There is also a variant in which both TP53 alleles are flanked by loxP sites. Treatment with Cre recombinase encoding viruses leads to the expression of TP53^{mut} or to the complete loss of Tp53 in combination with KRAS^{G12D} expression. [Jackson et al. 2005]

Recently, the genetic toolbox to develop NSCLC relevant mouse models has been extended by the introduction of Clustered regularly interspaced short palindromic repeats (CRISPR) genome editing to create novel mouse models for cancer research [Mou et al. 2015]. CRISPR is a gene-editing tool that can be used to precisely modify the DNA of organisms, including mice, by introducing, altering, or deleting specific genetic sequences. It evolved as a defence system of prokaryotes against bacteriophages.. [Barrangou et al. 2007]. The CRISPR-associated protein (Cas) from *Streptococcus pyogenes* is the most commonly used Cas9 variant. Targeting of Cas9 to specific genomic sequences is achieved by the expression of a 20-base pair long RNA sequence (sgRNA), homologous to the genomic target site and a 82 base pair long trRNA, enabling Cas9 recruitment. Ultimately, Cas9 is used as an endonuclease to target specific DNA sequences that are complementary to the sgRNA. [Thomsen 2022].

In NSCLC research, CRISPR/Cas9 technology has been used to create somatic engineered mouse models (SEMMs) with precise alterations in genes relevant to the development and progression of the disease. Of particular note is the model of [Platt et al. 2014], who were able to induce the formation of *Kras*^{G12D}, *Tp53*^{mut} and *Lkb*^{mut} lung tumours by combining Cre-activated expression of Cas9 in combination with the

Introduction

viral application of sgRNAs and Cre recombinase. By supplementing a repair template, that encoded the dominant active mutation of Kras^{G12D} they were able to engineer gain-of-function mutations endogenously. [Platt et al. 2014]

In summary, CRISPR/Cas9 technology has significantly advanced NSCLC research in mouse models by enabling precise genetic modifications, replicating the complexity of human tumours, and investigating the functional consequences of specific genetic alterations.

Introduction

1.5 Aim of the thesis

Mouse models have contributed significantly to our understanding of NSCLC and have been instrumental in the development of new therapeutic strategies. They have helped to identify potential drug targets, evaluate treatment regimens, and understand the mechanisms underlying drug resistance. In addition, mouse models have helped to understand the mechanisms of tumour induction and maintenance. However, the implementation of novel genetic alterations in the conservative mouse model is time consuming, costly, and not applicable for many laboratories.

The aim of this work was to develop a versatile model that could reduce the number of animals required, reduce the need for breeding and accelerate the desired genetic changes. CRISPR was therefore used to rapidly generate clinically relevant mouse models.

The first step is to compare CRISPR/Cas9-mediated tumour formation in the $KRAS^{G12D}/TP53^{mut}$ genetic background with the classic genetically engineered mouse model $Trp53^{fl/fl} KRas^{lsI-G12D/wt}$. In order to evaluate similarities and differences, the efficacy of tumour induction, marker expression and morphological and molecular characteristics will be compared. Second, to further expanded the genetic complexity of the tumours and evaluated the applicability of targeting additional tumour suppressors shall be tested. Therefore, additional sgRNAs will be integrated and a multiplexed *in vivo* approach will be carried out. This will allow us to better reflect the complex genetic heterogeneity of NSCLC.

Finally, a dual viral approach will be used to infect animals with both target sequences and a Cas9-expressing virus, allowing independence from the genetic background of mice. Thus, implementing the 3-R rule to refine and reduce animal experiments.

Materials and Method

2 Materials and Method

2.1 Materials

2.1.1. Buffers and Solutions

Table 1: Buffer and Solutions

Buffer	Composition
β -Mercaptoethanol	1 M β -Mercaptoethanol in MilliQ
Blocking Buffer (Western Blot)	0.1% casein, 0.2x PBS, 0.1% Tween20 in MilliQ
Blocking Buffer (Western Blot, commercial)	10 % Blocker™ FL Fluorescent Blocking Buffer in MilliQ
Blocking Buffer (IF/IHC)	10 % goat serum, 1% BSA in 1x TBS
Bradford reagent	0.01% (w/v) Coomassie Brilliant Blue G250, 8.5% phosphoric acid, 4.75% ethanol
Colloidal Coomassie (Staining Solution)	60 ml MilliQ, 20 ml methanol, 20 ml 5x Roti®-Blue
Colloidal Coomassie (Destaining Solution)	25 % methanol in MilliQ
Coomassie Blue (Staining Solution)	2 g/l Coomassie Brilliant Blue R250 (2.4 mM) in Coomassie Destaining Solution
Coomassie (Destaining Solution)	40 % methanol, 10 % acetic acid, in MilliQ
DNA loading buffer (10x)	60 % Sucrose, 0.25 M EDTA, 0.001 % Bromophenol Blue
Glycerol (60 %)	6.5 M Glycerol in MilliQ
GST Elution Buffer	50 mM Tris-HCl pH 8.0, 25 mM reduced Glutathione
ECL solution	1:1 ECL Substrate A; Peroxidase solution B
HEPES Lysis Buffer	20 mM HEPES pH 7.9, 150 mM NaCl, 0.2 % NP-40, 0.5 mM EDTA pH 8.0, 10 % glycerol, 2 mM MgCl ₂
Laemmli Running Buffer (10x)	250 mM Tris, 2 M Glycine, 1 % SDS, pH 8.4
Laemmli Sample Buffer (5x)	312.5 mM Tris-HCl pH 6.8, 500 mM DTT, 0.001 % Bromophenol Blue

Materials and Method

Lysis Buffer	1 % TritonX-100 in 1x PBS, 1 µg/mL Aprotinin/Leupeptin, 1 mM Pefabloc, 1 mg/mL Lysozym, 1 mM DTT
Orange G DNA loading Buffer (6x)	0.4 g/ml Sucrose (1.17 M), 2 mg/ml Orange G (4.4 mM)
PBS	1.8 mM KH ₂ PO ₄ , 10.1 mM Na ₂ HPO ₄ , 137 mM NaCl, 2.7 mM KCl, pH 7.4
PBS-T	1.8 mM KH ₂ PO ₄ , 10.1 mM Na ₂ HPO ₄ , 137 mM NaCl, 2.7 mM KCl, pH 7.4, 1 % Triton X
RIPA Lysis Buffer	10mM TRIS HCl (pH 8.0), 1 mM EDTA, 0.5 mM EGTA, 1 % Triton X100, 0.1 % Sodium Deoxycholate, 0.1 % SDS, 140 mM NaCl
S1	50 mM Tris-HCl pH 8.0, 10 mM EDTA, 100 µg/ml RNaseA
S2	200 mM NaOH, 1 % SDS
S3	3.1 M KAc pH 5.5
Separation gel buffer	1.5 M Tris-HCl pH 8.8, 0.4 % SDS
Stacking gel buffer	0.5 M Tris-HCl pH 6.8, 0.4 % SDS, 0.001 % Bromophenol Blue
SUMO Protease Buffer	50 mM Tris-HCl pH 8.0, 150 mM NaCl, 0.2% NP-40, 1 mM DTT
1x SDS Running Buffer	25 mM Tris base, 250 mM glycine, 0.1% (v/v) SDS n MilliQ
SDS stacking gel	4% (v/v) acrylamide/bisacrylamide, 125 mM Tris HCl (pH 6.8), 0.1% (w/v) SDS, 0.1% (w/v) APS, 0.1% (v/v) TEMED
SDS separating gel.	7.5-12.5% (v/v) acrylamide/bisacrylamide, 375 mM Tris HCl, (pH 8.8), 0.1% (w/v) SDS, 0.1% (w/v) APS, 0.1% (v/v) TEMED
T25	25 mM Tris-HCl pH 7.5
50x TAE	2 M Tris-Base, 1 M acetic acid, 50 mM EDTA (pH 8.0)

Materials and Method

10x TBS (IF/IHC)	20 mM Tris-Base, 1,35 M NaCl in MilliQ
TBS (IF/IHC)	1/10 10x TBS in MilliQ
TBS-T (IF/IHC)	TBS 0.1 % Tween 20 in MilliQ
TUBE lysis buffer	20 mM Na ₂ HPO ₄ , 20 mM NaH ₂ PO ₄ , 1% (v/v) NP-40, 2 mM EDTA, 5 mM NEM, 50 µg/ml GST-TUBE added prior to use
10x Transfer buffer	250 mM Tris base 1.5 M glycine
1x Transfer buffer	1/10 Transfer buffer 10x dilution 20% (v/v) methanol in MilliQ
Primary antibody buffer (IF/IHC)	10 % goat serum, 1% BSA in 1x TBS
Secondary antibody buffer (IF)	10 % goat serum, 1% BSA in 1x TBS
Primary antibody buffer (WB)	0.1% casein, 0.2× PBS, 0.1% Tween20
Secondary antibody buffer (WB)	0.1% casein, 0.2× PBS, 0.1% Tween20, 0.01% SDS
Ubiquitin pull-down lysis buffer	6M guanidine HCl, 0.1 M Na ₂ HPO ₄ , 0.1 M NaH ₂ PO ₄ , 0.01 M Tris (pH 8.0), 10 mM β-Mercaptoethanol
Virus resuspension buffer	PBS (pH 7.4), 0.001% Pluronic F68
Warhead lysis buffer (HR lysis buffer)	50 mM TRIS HCl (pH 7.4), 5 mM MgCl ₂ , 250 mM sucrose, 0.1 % NP40, 1 mM DTT, 2 mM ATP
Wash buffer (Western Blot)	0.2xPBS, 0.1% Tween20 in MilliQ

2.1.2. Chemicals

Table 2: List of Chemicals

Chemical	Manufacturer
2-Propanol/ Isopropanol	Roth
4',6-diamidino-2-phenylindole (DAPI)	Thermo Scientific
Acrylamide	Sigma-Aldrich

Materials and Method

Agarose	Roth
Agencourt AMPure XP Beads	Beckman Coulter
Ampicillin (Amp)	Roth
Amplify	GE Healthcare
Aprotinin/Leupeptin	Sigma-Aldrich
APS (Ammoniumperoxodisulfate)	Roth
Aqua Pure (nuclease free water)	
ATP (Adenosine triphosphate)	Jena Bioscience
β -Mercaptoethanol	Merck
BCA Assay Kit	Thermo Fisher
Bovine serum albumine (BSA)	Merck Millipore
Chloroform	Roth
Coomassie Brilliant Blue R-250 Dye	Thermo Scientific
Cytoseal™ 60	Thermo Scientific
Deoxynucleotidetriphosphates (dNTPs) Mix	Promega
Differentiation Solution	Sigma
Dimethyl sulfoxide (DMSO)	Sigma-Aldrich
DNase	Applichem
DTT (Dithiothreitol)	Sigma-Aldrich
Dynabeads. Protein A/G	Life Technologies
ECL (enhanced chemiluminescence)	Perkin Elmer
EDTA (ethylenediaminetetraacetic acid)	Roth
Ethidium bromide	Sigma
Ethanol (Etoh)	Carl Roth
Eosin	Sigma
Glutathione reduced	Sigma-Aldrich
Glutathione-S-Sepharose™ 4B beads	GE Healthcare
Glycerine	Roth
Glycine	Roth
Gene Ruler 1 kb Plus DNA ladder	Thermo Scientific
Guanidine hydrochloride	Roth
Hematoxylin	Sigma

Materials and Method

Hoechst	Thermo Scientific
Hydrogen peroxide (H ₂ O ₂)	Sigma
Isopropanol (2-Propanol)	Sigma-Aldrich
Kanamycin	Roth
Magnesium chloride (MgCl ₂)	Thermo Fisher
Methanol (MeOH)	Roth
Mowiol® 40-88	Sigma-Aldrich
N, N-Dimethylformamid (DMF)	Sigma
NP-40 (IGEPAL®CA-630)	MP Biomedicals
Orange G	Roth
PageRuler Prestained Protein Ladder	Thermo Scientific
Paraformaldehyde (PFA) 37.5 %	Roth
PBS (Phosphate-buffered saline)	Gibco
Phenol:Chloroform:IAA, 25:24:1, pH 4-5	Sigma/Merck
Pierce™ Protein A/G Magnetic Beads	Thermo Scientific
Pluronic F68	Gibco
Protease Inhibitor Cocktail	Roche
RNase A	Roth
RNase-free DNase	Qiagen
Roti®-Blue	Roth
SDS (sodium dodecyl sulfate)	Roth
Sodium acetate (NaOAc)	Merck
Sodium chloride (NaCl)	Roth
Sodiumhydroxid (NaOH)	Roth
Streptavidin conjugated agarose beads (high capacity)	Pierce
TCEP (tris(2-carboxyethyl)phosphine)	Roth
TEMED (N, N, N', N'-Tetramethylethylenediamine)	Roth
Triton-X-100	Roth
Trizma®Base (Tris)	Sigma
Tris-HCl	Sigma
Triton X100	Roth
Tween-20	Roth

Materials and Method

Urea	VWR Chemical
Xylene	Sigma

2.1.3. Consumables

Table 3: List of Consumables

Consumable	Manufacturer
Chambered cell culture slides (8, 12, 24 well)	Ibidi
Cell culture plates (15 cm, 10 cm)	Sarstedt
Cell culture plates (6, 12, 24, 96 well)	Greiner
Centrifuge tubes (15 ml, 50 ml)	Greiner
Cytiva Whatman™ Soil Analysis Filter Papers	Fisher scientific
Filtropur S 0,45 µm, 0.2 µm	Sarstedt
Glass Pasteur Pipettes	Hartenstein
Glasspipetts 5ml, 10ml, 25ml	Hartenstein
Immobilon-P PVDF 0,2 µm	Merck
Microscope cover glasses (Ø 10 mm)	Roth
Microscope cover slides (50 mm, 60 mm)	
Microscope slides (Superfrost Plus)	Omnilab GMBH & Co. KG
Pipette tips	Nerbe
Semi-micro cuvette, 3 ml, (HxW): 45 x 12 mm, PS, transparent,	Sarstedt
Reaction tubes (1.5 ml, 2 ml)	Sarstedt
Whatman filter paper	A.Hartenstein

2.1.4. Bacterial culture media

Table 4: Bacterial culture media

Culture media	Composition
LB medium	LB medium 10% (w/v) Bacto tryptone (Roth) 0.5% (w/v) yeast extract (Roth) 1% (w/v) NaCl (Roth)
LB agar	LB-medium with 1.2% (w/v) agar-agar (Roth)

Materials and Method

2.1.5. Bacterial strains

Table 5: Bacterial strains

E. coli strain	Genotype
DH5 α	F- endA1 glnV44 thi-1 recA1 relA1 gyrA96 deoR nupG Φ 80dlacZ Δ M15 Δ (lacZYA-argF)U169, hsdR17(rK-mK+), λ -
BL21	-(DE3) F - ompT gal dcm lon hsdS B (r B - m B -) λ (DE3 [lacI lacUV5-T7 gene 1 ind1 sam7 nin5])
XL1 blue	recA1 endA1 gyrA96 thi- 1 hsdR17 supE44 relA1 lac [F' proAB lacIqZ Δ M15 Tn10 (Tetr)]

2.1.6. Cell culture media, supplements, and antibiotics

Table 6: Cell-culture medium and buffer

Media, supplement, antibiotic	Manufacture
Antibiotic-Antimycotic (100X)	Thermo Fisher Scientific
Cycloheximide	Sigma-Aldrich
DMEM, high glucose, pyruvate	Thermo Fisher Scientific
Doxycycline hyclate	Sigma-Aldrich
DRAQ5™ Fluorescent Probe Solution (5 mM)	Thermo Fisher Scientific
IMDM GlutaMAX Supplement, Gibco, 500 ml	Thermo Fisher Scientific
Fetal Bovine Serum Advanced	Capricorn Scientific GmbH
MEM Non-essential Amino Acid Solution (100 \times)	Merck
MG132	Millipore
Polybrene	Sigma-Aldrich
Penicillin-Streptomycin Solution stab.	Sigma
Penicillin-Streptomycin-Amphotericin B Mixture	Lonza / Biozym
Puromycin (solution)	InvivoGen
RPMI-1640 Medium, with L-Glutamin	Thermo Fisher Scientific
Sodium pyruvate solution (100x)	Merck
2,5 % Trypsin (10X)	Thermo Fisher Scientific

2.1.7. Cell lines

Table 7: Cell-lines

Cell line	Species	Origin	Identifier
HEK 293T	Human:	ATCC	ATCC® CRL-11268™

Materials and Method

HEK 293T AAV pro	Human	Takara	632273
A549	Human	ATCC	CRM-CCL-185™
BEAS-2B	Human	ATCC; gifted Calzado	Marco ATCC® CRL-9609
CALU1	Human	ATCC	ATCC® HTB-54
EKVX	Human	National Cancer Institute	CVCL-1195
H1299	Human	ATCC	ATCC® CRL-5803
H1703	Human	ATCC	CRL-5889
H23	Human	ATCC	ATCC® CRL-5800
H520	Human	ATCC	HTB-182™
H727	Human	ATCC	CRL-5815™
LUDLU-1	Human	ECACC	92012463
SK-MES1	Human	ATCC	ATCC® HTB-58
KP	Mouse primary tumor	N/A	
KPF3	Primary tumor	N/A	
KPL	Primary tumor	N/A	
KPP	Primary tumor	N/A	
KPA9	Primary tumor	N/A	

2.1.8. Antibodies

Table 8: Primary Antibodies

1 st Antibodies	Company	Identifier	RRID
Polyclonal rabbit anti-USP28	Sigma-Aldrich	HPA006778	AB_1080520
Polyclonal rabbit anti-USP28	Sigma-Aldrich	HPA006779	AB_1080517
Monoclonal mouse anti-ACTIN/	Santa Cruz	sc-47778	AB_626632

Materials and Method

Monoclonal mouse anti-VINCULIN (hVIN-1)	Sigma-Aldrich	V9131	AB_477629
Monoclonal mouse anti-TUBULIN (1E4C11)	Proteintech Europe	66031-1-Ig	AB_11042766
Monoclonal mouse anti-HA (16B12)	Abcam	ab130275	AB_11156884
Monoclonal mouse anti-FLAG (M2)	Sigma-Aldrich	F3165	AB_259529
Monoclonal rabbit anti-KRT5 recombinant mAb	Bimake	A5439	
Polyclonal rabbit anti-KRT5	Santa Cruz	sc-66856	AB_2249757
Polyclonal rabbit anti-TTF1 (H-190)	Santa Cruz	sc-13040	AB_793532
Polyclonal rabbit anti-TP63	Biolegend	619002	AB_2207170
Monoclonal rabbit anti-p63 recombinant	Bimake	A5182	
Polyclonal rabbit anti-p63	ThermoFisher	PA5-36069	AB_2553354
Monoclonal mouse anti-GFP (B-2)	Santa Cruz	sc-9996	AB_627695
Polyclonal rabbit anti-c-MYC (N-262)	Santa Cruz	sc-764	AB_631276
PCNA (PC10)	Santa Cruz	Sc-56	AB_628110
p-ERK (E-4)	Santa Cruz	sc-7383 Lot: # L1714	AB_627545
CC10/Scgba1a1	Proteintech Europe / PTGlab	10490-1-AP	AB_2183285
SFTPC	Proteintech Europe / PTGlab	10774-1-AP	AB_2185497
Sox2	Sino Biological	101284-T42	AB_2810307
anti-p63 (4A4)	Ventana	Cat# 790-4509	AB_2335989

Materials and Method

NICD1 (active Notch1)	Abcam	ab8925	AB_306863
Notch 3	Proteintech Europe / PTGlab	55114-1-AP	AB_10858393
Anti-Jun Clone 3/Jun (RUO) (8159868)	BD Biosciences	610327	AB_397717
JunD	Sigma	HPA063029	AB_2684925
JunB	Santa Cruz	sc-8051	AB_2130023
mouse anti beta-Catenin	BD Biosciences	610153	AB_397554
c-Myc (Y69)	Abcam	ab32072	AB_731658
APC	Sigma	HPA013349	AB_1844913
Keap1	Proteintech Europe / PTGlab	10503-2-AP	AB_2132625
Lkb1/Stk11	Proteintech Europe / PTGlab	10746-1-ap	AB_2271311
Pten	Proteintech Europe / PTGlab	10047-1-AP	AB_2174343
NFE2I2/Nrf2	Invitrogen	PA5-27882	AB_2545358
Cas9 (bD-20) antibody - Lot: L0314	Santa Cruz	sc-392737	
Polyclonal rabbit anti-53BP1	Santa Cruz	sc-22760	
Polyclonal rabbit anti p-ATR (ser428)	Cell signalling	2853	
Monoclonal rabbit anti-p-H2a.x (ser139)	Cell signalling	2577	
Polyclonal rabbit anti-53BP1	Santa Cruz	sc-22760	
Polyclonal rabbit anti p-ATR (ser428)	Cell signalling	2853	
Monoclonal mouse anti FANCD2	Abcam	ab108928	
Polyclonal rabbit anti P53BP1	NOVUS	NB100-904	
Polyclonal rabbit anti P-P53 (ser15)	Cell signalling	9284	

Materials and Method

Monoclonal rabbit anti p- (Ser/Thr) ATM + ATR Substrate	Thermo Scientific	MA5-14872
Monoclonal rabbit anti cleaved caspase 9	Bimake	A5074
Monoclonal rabbit anti RAD51	Abcam	ab133534
Monoclonal rabbit anti FANCI	Abcam	ab15344

Table 9: Secondary Antibodies

2nd Antibodies	Company	Identifier	RRID
SuperBoost™ Goat anti-Mouse Poly HRP	ThermoFisher	B40961	
SuperBoost™ Goat anti-Rabbit Poly HRP	ThermoFisher	B40962	
Donkey anti-Mouse IgG (H+L) Cross-Adsorbed Secondary Antibody, DyLight 680	ThermoFisher	SA5-10170	AB_2556750
Donkey anti-Goat IgG (H+L) Cross- Adsorbed Secondary Antibody, DyLight 680	ThermoFisher	SA5-10090	AB_2556670
Donkey anti-Rabbit IgG (H+L) Cross- Adsorbed Secondary Antibody, DyLight 800	ThermoFisher	SA5-10044	AB_2556624
Donkey anti-Mouse IgG (H+L) Cross-Adsorbed Secondary Antibody, DyLight 800	ThermoFisher	SA5-10172	AB_2556752
Donkey anti-Goat IgG (H+L) Cross- Adsorbed Secondary Antibody, DyLight 800	ThermoFisher	SA5-10092	AB_2556672
Donkey anti-Rabbit IgG (H+L) Highly Cross-Adsorbed Secondary Antibody, Alexa Fluor 488	ThermoFisher	A21206	AB_2535792

Materials and Method

Donkey anti-Mouse IgG (H+L) Highly Cross-Adsorbed Secondary Antibody, Alexa Fluor 488	ThermoFisher	A21202	AB_141607
Donkey anti-Mouse IgG (H+L) Highly Cross-Adsorbed Secondary Antibody, Alexa Fluor 555	ThermoFisher	A31570	AB_2536180

2.1.9. Enzymes and corresponding buffers

Table 10: Commercial enzymes and buffers

Enzyme, Buffer	Manufacture
ClonExpress MultiS One Step Cloning Kit	Absource
ClonExpress II One Step Cloning Kit	Absource
Collagenase 1	Thermo Scientific
DNase	Applichem
M-MLV reverse transcriptase	Promega
M-MLV RT 5X Buffer	Promega
Phanta Max Master Mix 2 × (± Dye Plus)	Absource
Phusion HF DNA polymerase	Thermo Scientific
Phusion High-Fidelity buffer (10x)	Thermo Scientific
Restriction endonucleases	NEB
RNase A	Roth
S7 Fusion Polymerase	Biozym
SYBR™ Green PCR Master Mix	Thermo Scientific
T4 DNA ligase	Thermo Scientific
T4 DNA ligase buffer (10x)	Thermo Scientific
Tandem ubiquitin binding entity (TUBE)	Gifted by Rune Busk Damgaard
Taq Master Mix 2x Rapid	Absource
Taq Master Mix 2x (± Dye Plus)	Absource

Materials and Method

2.1.10. Oligonucleotides

Table 11: Oligonucleotide sequences

Oligonucleotides	Sequence	Company
sgRNA murine Stk11/Lkb1 for	CACCGCGAGACCTTATGCCGCAGGG	Sigma
sgRNA murine Stk11/Lkb1 rev	AAACCCCTGCGGCATAAGGTCTCGC	Sigma
sgRNA murine APCex9 for	CACCGCCGCTAGAACTCAAACAC	Sigma
sgRNA murine APCex9 rev	AAACGTGTTTTGAGTTCTAGCGGC	Sigma
sgRNA murine KEAP1 for	CACCGCGCCCGCTGTGTAGATGAGG	Sigma
sgRNA murine KEAP1 rev	AAACCCCTCATCTACACAGCGGGCGC	Sigma
sgRNA murine Pten 1 for	CACCGTGTGCATATTTATTGCATCG	Sigma
sgRNA murine Pten 1 rev	AAACCGATGCAATAAATATGCACAC	Sigma
sgRNA murine KRas #1 for	CACCGACTGAGTATAAACTTGTGG	Sigma
sgRNA murine KRas #1 rev	AAACCCACAAGTTTATACTCAGTC	Sigma
sgRNA murine Trp53 #1 for	CACCGATGGTGGTATACTCAGAGC	Sigma
sgRNA murine Trp53 #1 rev	AAACGCTCTGAGTATAACCACATC	Sigma
KrasG12D repair template for	TTTTGTGTAAGCTTTGGTAACTCCATG TATTTTTATTAAGTGTT	Sigma
KrasG12D repair template rev	GAGCTTATCGATACCGTCGACACACC CAGTTTAAAGCCTTGGAA	Sigma

2.1.11. Plasmids

Table 12: Plasmids and Distributors

Recombinant DNA	Company/Source	Identifier
pHelper	Cell Biolabs, INC.	VPK-400-DJ
pAAV-DJ Vector	Cell Biolabs, INC.	VPK-420-DJ
AAV:ITR-U6-sgRNA(Kras)-U6-sgRNA(p53)-pEFS-2A-mCherry-shortPA-KrasG12D_HDRdonor-ITR	doi: 10.15252/emmm.201911101	N/A
AAV:ITR-U6-sgRNA(KRas)-U6-sgRNA(p53)-U6-sgRNA(Lkb1)-	doi: 10.15252/emmm.201911101	N/A

Materials and Method

pEFS-2A-mCherry-shortPA- KrasG12D_HDRdonor-ITR		
AAV:ITR-U6-sgRNA(Kras)-U6- sgRNA(p53)-U6-sgRNA(Lkb1)- U6-sgRNA(Pten)-pEFS-2A- mCherry-shortPA- KrasG12D_HDRdonor-ITR	this work	N/A
AAV:ITR-U6-sgRNA(Kras)-U6- sgRNA(p53)-U6-sgRNA(Lkb1)- U6-sgRNA(Apc-Exon9)-pEFS- 2A-mCherry-shortPA- KrasG12D_HDRdonor-ITR	this work	N/A
AAV:ITR-U6-sgRNA(Kras)-U6- sgRNA(p53)-U6-sgRNA(Lkb1)- U6-sgRNA(Keap1)-pEFS-2A- mCherry-shortPA- KrasG12D_HDRdonor-ITR	this work	N/A
AAV:ITR-U6-sgRNA(Kras)-U6- sgRNA(p53)-U6-sgRNA(Lkb1)- pEFS-Rluc-2A-Cre-shortPA- KrasG12D_HDRdonor-ITR (AAV-KPL)	AAV:ITR-U6-sgRNA(Kras)-U6- sgRNA(p53)-U6-sgRNA(Lkb1)- pEFS-Rluc-2A-Cre-shortPA- KrasG12D_HDRdonor-ITR (AAV- KPL) was a gift from Feng Zhang (Addgene plasmid # 60224 ; http://n2t.net/addgene:60224 ; RRID:Addgene_60224)	Addgene plasmid # 60224
psPAX2	psPAX2 was a gift from Didier Trono (Addgene plasmid # 12260 ; http://n2t.net/addgene:12260 ; RRID:Addgene_12260)	Addgene plasmid # 12260
pMD2G	pMD2.G was a gift from Didier Trono (Addgene plasmid # 12259 ; http://n2t.net/addgene:12259 ; RRID:Addgene_12259)	Addgene plasmid # 12259

Materials and Method

pHelper	Cell Biolabs, INC.	VPK-400-DJ
pAAV2/8	AAV2/8 was a gift from James M. Wilson (Addgene plasmid # 112864 ; http://n2t.net/addgene:112864 ; RRID:Addgene_112864)	Addgene plasmid # 112864
pLKO.DEST.EGFP	pLKO.DEST.EGFP was a gift from Ming-Sound Tsao (Addgene plasmid # 32684 ; http://n2t.net/addgene:32684 ; RRID:Addgene_32684)	Addgene plasmid # 32684
pLKO.1 puro	pLKO.1 puro was a gift from Bob Weinberg (Addgene plasmid # 8453 ; http://n2t.net/addgene:8453 ; RRID:Addgene_8453)	Addgene plasmid # 8453
pINDUCER20	pInducer20 was a gift from Stephen Elledge (Addgene plasmid # 44012 ; http://n2t.net/addgene:44012 ; RRID:Addgene_44012)	Addgene plasmid # 44012

2.1.12. Commercial kits

Table 13: Commercial Kits

Commercial kits	Company	Identifier
Blocker™ FL Fluorescent Blocking Buffer 10 x	Thermo Fisher Scientific	37565
High-Sensitivity Chemiluminescence Detection Kit (Ready-to-Use)	ECL GeneBio Systems	E412-01
VAHTS Universal Plus DNA Library Prep Kit for Illumina	Absource	ND617-01

Materials and Method

VAHTS Universal V6 RNA-seq Library Prep Kit for Illumina®	Absource	NR604-01
VAHTS mRNA Capture Beads	Absource	N401-01
VAHTS DNA Clean Beads	Absource	N411-02
TruePrep DNA Library Prep Kit V2 for Illumina® (5 ng)	Absource	TD502-01
NEBNext® Sample Purification Beads	New England Biolabs® Inc	Cat #E7767S; Lot: 10058432
ReliaPrep™ RNA Cell Miniprep System Protocol	Promega	TM370
NEBNext® Ultra™ II Directional RNA Library Prep Kit for Illumina®	New England Biolabs (NEB)	Cat #E7760L; Lot: 10065726
NEBNext® Multiplex Oligos for Illumina® (Dual Index Primers Set 1)	New England Biolabs (NEB)	NEB #E7600S
NEBNext® Poly(A) mRNA Magnetic Isolation Module	New England Biolabs (NEB)	NEB #E7490S
PureLink HiPure Plasmid Maxiprep Kit	Invitrogen	
GeneJET Gel Extraction Kit	Thermo Scientific	
MiniElute PCR Purification Kit	Qiagen	
GeneEditor™ in vitro Site-Directed Mutagenesis System	Promega	
One-Step TB Green® PrimeScript™ RT-PCR Kit	Takara	
ReliaPrep™ FFPE Total RNA Miniprep System	Promega	
SignalStainR DAB Substrate Kit	Cell Signaling	8059 S
Actin Cytoskeleton / Focal Adhesion Staining Kit	Merck	

Materials and Method

2.1.13. Software/Websites

Table 14: Software and websites

Software/Websites	Company/Source
cBioportal	https://www.cbioportal.org
GEPIA and GEPIA2	http://gepia.cancer-pku.cn
Excel	Microsoft
Image Studio	Licor
Panther Classification system	http://pantherdb.org
PRISM8	GraphPad Software, Inc.
Affinity Designer	Serif Europe
ImageJ	National Insistute of Health
Pannoramic Case Viewer	3dHistech
Uniprot	https://www.uniprot.org/
R	https://www.r-project.org
GenomicAlignments	https://bioconductor.org/packages/release/bioc/html/GenomicAlignments.html
GSEA v2.2	http://software.broadinstitute.org/gsea/downloads.jsp
SPLASHRNA	http://splashrna.mskcc.org/
Acrobat TM	Adobe Inc.
Integrated Genome Browser	Nicol et al. 2009
QuPath	https://qupath.github.io
UCSC Genome Bioinformatics	http://genome.ucsc.edu
ApE plasmid editor	By Wayne Davis
Zhang lab gRNAs design resources	https://zlab.bio/guide-design-resources
CHOPCHOP	http://chopchop.cbu.uib.no/
RNAi Consortium	www.broadinstitute.org/rnai-consortium/rnai-consortium-shrna-library
Catalogue Of Somatic Mutations in Cancer (COSMIC)	https://cancer.sanger.ac.uk/cell_lines

Materials and Method

Gene Expression and <https://www.kobic.kr/GEMICCL/>
Mutations in Cancer Cell Lines
(GEMiCCL)

2.1.14. Instruments

Table 15: Instruments

Instruments	Company
Odyssey® CLx Imaging System	Licor
iBright™ FL1000 Imaging System	Invitrogen
StepOnePlus Real-Time PCR System	Thermo Scientific
Pannoramic DESK scanner	3DHISTECH
FSX100 microscope	Olympus Life Science
Operetta High-Content Imaging System	Perkin Elmer
Fragment Analyzer	Agilent
Branson Sonifier 250	Branson
EASY-nLC™ 1200 System	Thermo Scientific
Orbitrap Fusion Lumos mass spectrometer	Thermo Scientific
1.9 µm C18 particles	ReproSil-Pur, Dr. Maisch
Hyrax M55 Rotary Microtome	Leica
Mr. Frosty freezer container	Thermo Scientific
PCR cycler: SimpliAmp thermo cycler	Life technologies
Experion™ Automated Electrophoresis System	Bio-Rad
Cell culture incubator BBD 6220	Heraeus
Casy® cell counter	Innovatis
Centrifuge Avanti J-26 XP	Backman Coulter
Centrifuge Eppendorf 5417 R	Eppendorf
Centrifuge Eppendorf 5425	Eppendorf
Centrifuge Eppendorf 5430	Eppendorf
Centrifuge Galaxy MiniStar	VWR
Centrifuge Multifuge 1S-R	Heraeus
Deep-sequencer Genome Analyzer Iix	Illumina
Dry Bath System	Starlab

Materials and Method

Thermomixer® comfort	Eppendorf
Incubator shaker Model G25	New Brunswick Scientific
Luminometer GloMax	Promega
Microscopes Axiovert 40CFL	Zeiss
PCR thermal cycler Mastercycler pro S	Eppendorf
Spectrofluorometer NanoDrop 1000	Thermo Scientific
Ultrospec™ 3100 pro UV/Visible	Amersham Biosciences
SDS page system Minigel	Bio-Rad
SDS page system Tetra Cell	Bio-Rad
Maxi UV fluorescent table	Peqlab
Mixer Vortex-Genie 2	Scientific Industries
Julabo ED-5M water bath	Julabo
Memmert waterbath	Memmert
Immunoblot transfer system: Perfect Blue Tank Electro Blotter Web S	Peqlab
Power supply: Power Pac	Bio-Rad
Chemiluminescence imaging LAS-4000 mini Fujifim	Fujifim
Illumina GAIx sequencer	Illumina
Sterile bench HeraSafe	Heraeus
Siemens linear accelerator for X-ray irradiation	Siemens
Dionex Ultimate 3000 analytical HPLC	Thermo Scientific
NextSeq 500 sequencer	Illumina
Leica VT 1200S	Leica
Microscope TCS SP5	Leica
BD FACS Aria III	BD Biosciences
Pipetboy acu 2	Integra
Consort EV243 electrophoresis power supply	Sigma
Ventana DP 200 slide scanner	Roche

Materials and Method

2.2 Methods

2.2.1. Molecular biology methods

2.2.1.1 Restriction Digest

The respective restriction enzymes were obtained from New England Biolabs. The enzymes were incubated with the DNA supplemented with recommended buffer in a total volume of 30 μ l for 1 h at 37 °C.

2.2.1.2 Polymerase Chain Reaction

In order to amplify DNA for cloning or to generate expression constructs a polymerase chain reaction was carried out with the S7 Fusion High-Fidelity DNA polymerase (Biozym). Following buffer compositions ([Table 6](#)) and PCR settings were used ([Table 7](#)).

Table 16: PCR buffer compositions

	20 μ l	50 μ l
Water	Add to 20 μ l	Add to 20 μ l
5x HF or GC Buffer	4 μ l	10 μ l
dNTPs (10 mM)	0.4 μ l	1 μ l
Forward primer	0.5 μ M f.c.	0.5 μ M f.c.
Reverse primer	0.5 μ M f.c.	0.5 μ M f.c.
Template	100 – 500 ng	100 – 500 ng
S7 Fusion	0.2 μ l	0.5 μ l

Table 17: 3 step PCR settings

Cycles	Step	Temperature	Time
1	Initial denaturation	98 °C	30 s
	denaturation	98 °C	10 s
20-40	Annealing	X °C	30 s
	Extension	72 °C	15 s/kb
1	Final extension	72 °C	10 min
1	cooling	4 °C	hold

Materials and Method

The annealing temperature for the primers were calculated with the basic melting temperature formula $Tm = (wA + xT) * 2 + (yG + zC)$, where w,x,y,z are the number of bases in the primer, respectively.

2.2.1.3 T4 Ligation

To ligate DNA, achieved via restriction digest ([2.2.1.1](#)) or oligo cloning ([2.2.1.4](#)), into a linearized vector, the T4 DNA ligase (Thermo Fisher) was used according to manufacturer's instructions. A 1:2 molar ratio of vector to insert was chosen if not stated otherwise.

2.2.1.4 Oligo cloning

In order to insert Crispr/Cas gRNAs into the target vectors, oligonucleotides were annealed first. Therefore, 10 µM sense and anti-sense oligonucleotides were mixed with 1 µl of 10x T4 ligase buffer and 0.5 µl PNK in a total volume of 10 µl. After 30 min at 37 °C followed by 5 min incubation at 95 °C, the mix was cooled down slowly to 25 °C and diluted 1:200.

The vector was linearized with BsmB1 at 55 °C for 1 h and purified as described in [2.2.17](#).

Vector and insert were mixed in a 1:2 ratio and the ligation was carried out as described in [2.2.1.3](#). Eventually, 8 µl product was transformed into E. coli DH5α.

2.2.1.5 Agarose gel electrophoresis

For the separation, the DNA was mixed with 6x DNA loading buffer. According to the size, samples were loaded onto 1 - 2 % (w/v) agarose gel, containing 0.001 % ethidium bromide and separated with 2.5 V/cm in 1x TAE. The samples were visualised with UV-light at 254 nm and the Gene Ruler 1 kb Plus DNA ladder was used, to determine the size of the DNA fragments. Colony PCR samples were loaded directly.

2.2.1.6 Heat Shock Transformation

Ligation products or purified DNA plasmids were added to 100 µl chemical competent E. coli DH5α. After 30 min incubation on ice, a heat shock at 42 °C for 90 s was performed. The mix was cooled on ice for 2 min and 500 µl of LB-medium was added. The bacteria were incubated at 37 °C at 700 rpm for 60 min and plated onto LB agar plates supplemented with the corresponding antibiotic and incubated over night at 37 °C. For DNA isolation ([2.2.1.8](#)) the bacteria were added to 50 ml of LB medium with the corresponding antibiotic.

Materials and Method

2.2.1.7 DNA Purification

DNA was purified with the FastPure Gel DNA Extraction Mini Kit (Absource) according to manufacturer's instructions.

DNA achieved by restriction digest was separated by gel electrophoresis (2.2.1.5). PCR products were loaded onto the column directly.

2.2.1.8 DNA Isolation (MidiPrep)

Plasmid DNA was purified with the alkaline lysis method [Stephen 1990]. 50 ml of an overnight bacteria culture was centrifuged for 30 min at 4000 rcf, 4 °C and resuspended in 5 ml S1. Then, 5 ml S2 Buffer was added for lysis. After 5 min incubation at 25 °C, 5 ml Buffer S3 was added and incubated for 10 min on ice. Samples were centrifuged for 30 min at 4000 rcf and the supernatant was filtered into a new tube. Afterwards, 10 ml isopropanol was added and centrifuged for 20 min at 8000 rcf. The DNA pellet was resuspended with 400 µl aqua pure, mixed with phenol/chloroform/isoamyl (25:24:1) in a new reaction tube and centrifuged at 12000 rcf for 20 min at 25 °C. The upper phase was transferred, and 1 ml of 100 % ethanol was added. The DNA was pelleted at 12000 rcf for 15 min at 4 °C and washed twice with 70 % ethanol. Lastly, the DNA was solved in aqua pure.

2.2.1.9 DNA Quantification

The DNA concentration was determined by measuring absorbance at a wavelength of $\lambda = 260$ nm using a Spectrofluorometer NanoDrop 1000 (Thermo Fisher).

2.2.1.10 DNA Sequencing

DNA was sequenced by Macrogen Europe (Amsterdam, Netherlands). For sequencing, 250 ng of DNA was mixed with the corresponding primer (10 nM) in a total volume of 50 µl.

2.2.1.11 RNA Isolation

RNA from cell pellets was isolated using the ReliaPrep™ RNA Cell Miniprep System Protocol (Promega) according to manufacturer's instructions. Isolated RNA was stored at – 80 °C.

2.2.1.12 cDNA synthesis

RNA was isolated from cells as described in 2.2.1.11 and the concentration was measured with a Spectrofluorometer NanoDrop 1000 (Thermo Fisher) at 260 nm. In order to determine the quality and purity of the RNA the A_{260}/A_{280} and A_{260}/A_{230} ratios

Materials and Method

have been measured. In order to synthesize cDNA, 2 µg of RNA was mixed with 1 µl of random primer mix in a total volume of 14 µl aqua pure. After 5 min incubation at 65 °C, 4 µl First-Strand RT Buffer (5X, Promega), 1 µl dNTPs (10 mM) and 1 µl Reverse Transcriptase (M-MLV, 200 U/µl, Invitrogen) were added. The First-Strand synthesis was carried out with the following settings:

Table 18: First-Strand Synthesis

Time	Temperature
10 min	22 °C
50 min	37 °C
15 min	70 °C
hold	8 °C

Eventually, the cDNA was diluted 1:200 with nuclease free water and stored at – 20 °C or used for qPCR.

2.2.1.13 Quantitative real-time PCR (qPCR)

In order to quantify mRNA abundance and thereby measure gene expression, quantitative real-time PCR (qPCR) was performed. Therefore, 2 µl of diluted cDNA (2.2.1.12) was mixed with 2 x SYBRGreen Mix (Thermo Scientific) and 1 µl qPCR primer mix (forward/reverse 10 µM stock) in a total volume of 20 µl. The qPCR (Table 9) was carried out in a StepOne® plus (Applied Biosystem) real-time PCR machine and the DNA amplification was measured via the fluorescent signal of the intercalating dye present in the SYBRGreen master mix.

Table 19: qPCR settings with melting curve

Cycles	Step	Temperature	Time
1	Initial denaturation	95 °C	15 min
	Denaturation	95 °C	30 s
38	Annealing	60 °C	20 s
	Extension	72 °C	15 s
1	Melting curve	95 °C	60 s
		60 °C	30 s
		95 °C	30 s

Materials and Method

2.2.1.14 AAV titration

Viruses were quantified using the AAV Titration by qPCR protocol from Addgene.

2.2.1.15 RNA sequencing

In order to analyse global changes in a transcriptome RNA-sequencing was carried out. Isolated RNA (2.2.1.11) was measured with a Spectrofluorometer NanoDrop 1000 (Thermo Fisher). The quality of the RNA was determined with a Fragment analyser (Advanced Analytical) according to manufacturer 's instruction. Only RNA with an RNA integrity number (RIN) > 9.0 was used for the library preparation. Therefore, 500 ng of RNA input was purified using the NEBNext Poly(A) mRNA Magnetic Isolation Module (#E7490L) according to manufacturer 's instruction. Next, the library was prepared using the NEBNext® Ultra™II Directional RNA Library Prep Kit for Illumina® (#E7760L) according to manufacturer 's instruction. The cDNA was purified with the Agencourt XP Beads and the library was amplified with 10 PCR cycles. After a final quality control with the Fragment analyser (Advanced Analytical), 50 fmol per sample war sequenced with the Illumina NextSeq 500.

The resulting sequencing data were mapped on the mouse genome build 39 (GRCm39; 2020). For the alignment Bowtie2 [Langmead et al, 2009] was used, with 1 mismatch allowed. The index for Bowtie and the pre-built chromosome sizes were obtained from NCBI. The Refseq coordinates for rRNA cluster, exons, introns, and genes were obtained from the University of California (UCSC, Santa Cruz). The gene set enrichment analysis (GSEA) was done with the M2 and M5 mouse hallmark database from Molecular Signature (Broad Institute).

Fragment Analyser, Flow cell loading, and Illumina NextSeq 500 was operated by group members of the department or Prof. Dr Eilers.

Bioinformatics was carried out by Michaela Reißland.

2.2.2. Biochemical methods

2.2.2.1 Protein Isolation

To isolate proteins from cells or tissue to carry out an immunoblotting analysis, the samples were lysed in RIPA buffer, supplemented with protease- and phosphatase inhibitor (1:1000).

For harvesting cells, the medium was removed, and the dish was washed with sterile PBS. Afterwards, PBS was added, and the cells were scraped, transferred into a reaction tube, and centrifuged for 5 min at 800 x g at 4 °C. The cell pellet was

Materials and Method

resuspended in RIPA and in addition mechanically lysed with a three times freeze-thaw cycle. To remove cell debris, the sample was centrifuged at 12.000 x g for 30 min at 4 °C. Subsequently, the protein amount was determined with a Bradford assay. 1 µl of Protein lysate was added to 1 ml of Bradford solution and mixed well. The absorption was measured at 595 nm with an Ultrospec™ 3100 pro and the concentration was calculated using a standard curve of BSA solutions with known concentrations.

To achieve a sufficient lysis of tissue samples, an additional mechanical maceration was done. Therefore, 500 mg of tissue in RIPA were dissociated using an Ultra Turrax® (IKA) at 14.000 rpm on ice.

2.2.2.2 SDS-PAGE

Proteins obtained by cell lysis (2.2.2.1) were separated by sodium dodecyl sulfate polyacrylamide gel electrophoresis (SDS-PAGE) [Laemmli 1970] according to their molecular weight. Depending on the protein size a final concentration of polyacrylamide from 7.5 % up to 15 % was chosen for the separation gel. Per sample 25 µg of protein was diluted in 25 µl total volume and heated in 1x Laemmli buffer at 95 °C for 5 min. Electrophoresis was carried out at 40 mA per gel. As size reference the PageRuler Prestained Protein Ladder (Thermo Fisher) was used.

2.2.2.3 Immunoblot

Proteins separated by SDS-PAGE have been visualised by Western blot. Prior to the transfer, the PVDF membrane (Thermo Fisher) was activated for 10 min in 100 % methanol and the SDS-gel, as well as the Whatman paper (Hartenstein), have been equilibrated with Transfer buffer. For a 'wet transfer' a sandwich of soaked Whatman paper, SDS-gel and PVDF membrane have been assembled, that the negative charged proteins will be transferred in the electric field (30 V, overnight, 4 °C) towards the positive charged membrane. Afterwards, the membrane has been washed with deionized water and blocked for 1 h at room temperature with 1 x Blocker™ FL Fluorescent Blocking Buffer. Next, the membrane has been washed with Wash Buffer and incubated with the respective primary antibody overnight rolling at 4 °C. The Western blot was washed thrice and incubated with the respective secondary antibody for 1h at room temperature. Prior to detection the membrane was washed three times. To detect fluorescent signals, the iBright™ FL1000 Imaging System was used. HRP coupled secondary antibodies were treated

Materials and Method

with fresh prepared ECL solutions and imaged on the iBright™ FL1000 Imaging System.

2.2.2.4 Immunoprecipitation

In order to study protein interaction Co-immunoprecipitation (Co-IP) assays were done. Cells were harvested and lysed as described in 2.2.2.1 with HEPES lysis buffer. Additionally, DTT (Sigma) was added fresh prior to usage. This prevents false positive interaction via disulfide bonds. For the Co-IP 500 mg of proteins were incubated with the respective antibody targeting the protein of choice overnight at 4 °C rotating together with Agencourt AMPure XP Beads (50 % slurry). As a negative control the same amount of protein was incubated with IgG. Furthermore, 1-10 % of the lysate were separated as input control, heated to 95 °C for 5 min in 1x Laemmli and stored at -20 °C.

Next, the beads were washed three times with HEPES lysis buffer, resuspended in 25 µl 1x Laemmli-HEPES lysis buffer and heated for 10 min at 95 °C. Eventually, the samples were separated via SDS-PAGE and western blot.

2.2.2.5 Tandem Ubiquitin Binding Entities (TUBE)

The Tandem Ubiquitin Binding Entities (TUBE) were obtained from the laboratory of David Komander and expressed in *E. coli* [Damgaard *et. al.* 2019].

Cells were harvested as described in 2.2.2.1 and lysed in TUBE lysis buffer (~150 µl/1.5*10⁶ cells). Add GST-TUBE (100 µg/ml) prior to lysis. Lysates were cleared at 12000 x g at 4 °C for 15 min and transferred to a new reaction tube. For the pull-down 50 % slurry of Glutathione-Sepharose 4B (GE Healthcare) was added and incubated overnight rotating at 4 °C. As input, 10 % of the cleared lysate was stored at -20 °C after 5 min incubation at 95 °C in 1 x Laemmli-TUBE buffer.

Next, the beads were washed 3 times with cold PBS-T, resuspended in 1 x Laemmli-TUBE buffer and heated at 95 °C for 15 min. Eventually, the samples were separated via SDS-PAGE and western blot.

2.2.2.6 Warhead assay

Warhead-ubiquitin suicide probes were obtained from UbiQ and used according to the manufactures instructions. The cells were lysed in HR-lysis buffer and 25 µg protein were supplemented with 20 µM warhead-probe. Next, the samples were incubated for 60 min at 37 °C and subjected to a western blot.

Materials and Method

2.2.3. Cell biology methods

2.2.3.1 Cultivation of cells

Human cell lines were obtained from American Type Culture Collection (ATCC) and the European Collection of Authenticated Cell Cultures (ECACC). Primary mouse tumour cell lines were produced during this work. All cell lines were cultivated in an incubator at 37 °C, 5 % CO₂ and at 95 % relative humidity.

All human lung cancer cell lines were maintained in RPMI 1640 medium, supplemented with 10 % FCS, 1 % Penicillin/Streptomycin, 1 % GlutaMAX, 1 % NEAA and 1 % Na-Pyruvate. Beas-2B, HEKT-293 and all primary mouse tumour cell lines were maintained in DMEM medium, supplemented with 10 % FCS and 1 % Penicillin/Streptomycin.

For passaging and seeding, cells were detached with Trypsin/EDTA. At first, the medium was removed, and the cells were washed with sterile PBS. Depending on the cell line, the incubation was carried out for 5 to 10 min at 37 °C and stopped by adding the corresponding medium.

For passaging, the cells were split onto new cultivation plates in an appropriate ratio. For seeding, the cells were counted with the Countess (Thermo Fisher).

2.2.3.2 Establishment of primary tumour cell lines

In order to establish primary lung tumour cell lines tumour bearing animals (2.2.4.3) were sacrificed (2.2.4.5). Next, the lungs were dissected and washed in sterile ice-cold PBS. Afterwards, the lungs were transferred into a fresh plate with sterile PBS and visible tumour nodules were excised under the binocular microscope. The nodules were placed in reaction tubes and PBS Mg²⁺/Ca²⁺ was added. In order to individualize the cells, the tumours were broken up mechanically and Collagenase 1 (100 U/ml) was added. After 1 h at 37 °C the mixture was centrifuged at 800 x g, 4 °C for 10 min and washed 3 times with DMEM 10 % FCS, 1 % Pen/Strep. The pellet was resuspended in DMEM 10 % FCS, 1 % Pen/Strep and poured onto a 70 µm cell strainer. Eventually, the cells were seeded in DMEM 10 % FCS, 1 % Pen/Strep, 1 % AntiAnti™ (Gibco) into 6 well plates and cultivated at 37 °C, 5 % CO₂ and 95 % relative humidity.

Individual growing colonies were expanded, and cancer cells were selected by harsh trypsinization.

Materials and Method

2.2.3.3 Transfection of cells

For the transient transfection of plasmid DNA or for the production of virus, the cells were seeded and cultivated until a confluence of ~70 %. As a transfection reagent polyethylenimine (PEI 1 µg/µl) was used. The necessary amount of DNA was mixed with PEI in a 1:3 ratio in DMEM without supplements and incubated for 15 min at room temperature. Afterwards, the transfection mix was added to the cells.

2.2.3.4 Lentivirus production

HEKT293T AAVpro cells were seeded the day prior the transfection on 15 cm cell culture dish. On the next day, the cells were supplemented with fresh DMEM 10 % FCS, 1 % Pen/Strep. For the transfection, the plasmid of interest, the viral packaging plasmid pPAX2 and the viral envelop plasmid pMD2 were mixed in a 4:2:1 molar ratio in DMEM. Then, PEI (1 µg/µl) was added in a 3:1 ratio and the transfection mix was mixed immediately. After 15 min incubation at room temperature, the mix was added dropwise onto the cells.

Three days post transfection the virus containing supernatant was filtered through a 0.45 µm filter with a syringe. For immediate infection, seeded cells were treated with the virus directly. For longer term storage of the virus, the medium was mixed with autoclaved PEG8000 to a final concentration of 10 %. After an overnight incubation at 4 °C the precipitated virus was centrifuged at 2000 x g, 4 °C for 20 min and resuspended in PBS and stored at -80 °C.

2.2.3.5 Adeno-associated virus production

To produce AAVs 5×10^6 Hekt293T-cells were seeded in 15 cm cell culture dishes and cultivated for 24 h or until a confluence of ~60-70 % was achieved. Cells were transfected with the pRepCap (pRC), the cis-plasmid (pAAV) and the pAdDeltaF6 (Table 1) in a 1:1:2 molar ratio. Therefore, the DNA was mixed in 2 ml DMEM (w/o FCS) and PEI (1 µg/µl) (DNA:PEI ratio of 1:2) was added. The mixture was incubated 15 min at room temperature and added dropwise to the plates.

To harvest the AAV, cells and supernatant were collected after 96 hours and transferred into a 50 ml conical tube. At first, NaCl was added (f.c. 0.5 M) and slowly mixed for 1h at 4 °C. Next, Chloroform was added (f.c. 10 %) and slowly mixed for 30 min at 4 °C. Eventually, the suspension was centrifuged at 2000 x g for 30 min at 4 °C. The water phase was transferred into a new conical tube and PEG8000 was added (f.c. 10 %) and mixed well. The AAV was precipitated overnight at 4 °C.

Materials and Method

After the centrifugation at 2000 x g for 20 min at 4°C the pellet was resuspended in AAV resuspension buffer (PBS + 0.001% pluronic F68 + 200mM NaCl) (~100 µl/15 cm dish used) and protease inhibitor and DNase/RNase were added (f.c. 1x). Incubate for 2 h at 37 °C, add Chloroform (1:1 ratio) and centrifuge at 12000 x g for 5 min at 4 °C. Repeat the chloroform step and collect the water phase. Proceed with the titration or store at -80 °C.

2.2.3.6 Infection of cells

In order to infect cells with the prior produced viruses, cells were seeded in 6 well plates. For the Lentivirus infection, the cells were treated with Polybrene (1 µg/µl) and 20 to 50 µl of virus were added. 24 h post infection, the medium was changed, and the positive infection was checked either by fluorescence or the cells were selected with the corresponding selection marker.

For the AAV infection, the titrated virus was added to the cells with a MOI of 10.000. Similarly, the Lentivirus infection, the cells were selected by the respective marker.

2.2.3.7 Immunofluorescence

To conduct an immunofluorescence staining, cells were seeded in Ibidi™ slides. 24 h post seeding the cells were treated for the respective amount of time. Afterwards, the cells were washed with PBS and fixed for 30 min with 10 % NBF. Next, the cells were washed with PBS, permeabilized with 0.1 % Tween20 in PBS for 5 min and blocked with 3 % BSA in PBS for 1 h at room temperature. The primary antibodies were diluted in 1 % BSA in PBS to achieve the working solution and the cells were incubated with the respective antibodies overnight at 4 °C. The slides were washed 3 times with PBS and incubated with the diluted secondary antibodies for 1 h at room temperature. Eventually, the slides were washed 3 times with PBS for 10 min. In the first washing step, the DNA intercalating dye Hoechst 33342 was added 1:1000 to stain the nuclei. The slides were analysed at the Olympus FSX100 microscope.

2.2.4. Animal models

2.2.4.1 Licences

All *in vivo* experiments were approved by the Regierung Unterfranken and the ethics committee under the license numbers 2532-2-362, 2532-2-367, 2532-2-374 and 2532-2-1003. The mouse strains used for this publication are listed.

Materials and Method

2.2.4.2 Animal welfare

All animals are supervised daily, and animal health is monitored with a sentinel mouse. Furthermore, a disease screening was conducted every three months. Animals are housed in standard cages in pathogen-free facilities on a 12-h light/dark cycle with *ad libitum* access to food and water. FELASA2014 guidelines were followed for animal maintenance.

2.2.4.3 AAV induced lung tumours

Adult mice were anesthetized with Isoflurane in a chamber with a constant flow of 3 % Isoflurane and intratracheally intubated with 60 µl AAV virus (1×10^{11} PFU/ml). For endotracheal instillation, a gauge 24 catheter was used and the AAVs were pipetted to the top of the catheter. During normal animal breathing, the virus was distally expanded and delivered into the lungs. Viruses were quantified using the AAV Titration by qPCR protocol from Addgene. As a control, some animals were intratracheally intubated with 60 µl AAV-resuspension buffer without AAVs. Animals were sacrificed after 12 weeks by cervical dislocation and lungs were fixed using 5% NBF. IF animals showed severe symptoms or lost more than 10 % of their weight, they were taken out at that point.

2.2.4.4 Orthotropic transplantation of lung tumour cell lines

Established primary lung tumour cell lines (2.2.3.2) were cultivated in DMEM 10 % FCS and 5 % Pen/Strep until confluence. In order to achieve a single-cell suspension, the cell lines were trypsinized with TripLE™ (Sigma) for 15 min at room temperature. Next, the cells were washed and resuspended in PBS. After counting the cells with the Countess (Thermo Fisher), 200.000 per 60 µl were orthotropic re-transplanted as described in 2.2.4.3.

6 weeks post transplantation, the mice were sacrificed, and the lungs were fixed using 10 % NBF.

2.2.4.5 Mice euthanasia

The mice were euthanized by cervical dislocation. Therefore, pressure was applied to the neck and the spinal column was dislocated from the brain. Death must be verified by loss of consciousness, loss of reflex, loss of muscle response and loss of response to noxious stimuli or comparable stimuli.

Materials and Method

2.2.5. Immunohistochemistry

2.2.5.1 Formalin-fixated and paraffin embedded tissue

Tumour bearing lungs were dissected and fixated in 10 % NBF for 24 h. The lung lobes were separated and put into an embedding cask, together with the heart, the oesophagus, and the upper airway. Afterwards, the tissue was processed in the tissue processor [FIRMA] overnight with the following steps: 2 x 70 % EtOH, 2 x 90 % EtOH, 2 x 95 % EtOH, 2 x 100 % EtOH, 3 x Xylol and pre-heated paraffin.

2.2.5.2 Immunohistochemistry (IHC)

Human samples were obtained from the Institute of Pathology, University Würzburg after informed consent was given. Paraffin-embedded sections of human and murine samples were cut into 2 - 4 µm sections with a microtome (Leica). Before staining, slides were de-paraffinized and rehydrated using the following protocol: 3 × 5 min in xylene, 2 × 3 min in EtOH (100%), 2 × 3 min in EtOH (95%), 2 × 3 min in EtOH (70%), 2 min in EtOH (50%) and 3 min in H₂O. After de-paraffinization and rehydration, antigen retrieval was performed with 10 mM sodium citrate buffer (pH 6.0) in a microwave oven at 800 W, 650 W and 360 W for 5 min, respectively. The samples were permeabilized with TBS 0.1 % Tween20 for 10 min and washed with TBS and blocked for 1 h at room temperature with 10 % goat-serum, 1.5 % BSA in TBS. The respective primary antibodies were diluted in blocking solution and incubated overnight at 4 °C. Next, the endogenous Peroxidase was blocked with TBS containing 3 % H₂O₂ for 10 min. Slides were developed with the SuperBoost™ HRP coupled secondary antibodies and with SignalStain® DAB Substrate Kit and counterstained with Hematoxylin (Sigma H3136). Slides were scanned in 40x resolution using a Panoramic SLIDE II slide scanner and analysed using QuPath (version 0.3.0).

Results

3 Results

3.1 CRISPR/Cas9 mediated genome editing to generate murine *KRas*^{G12D}/*Trp53*^{mut} driven lung cancer

In the year 2022, Non-small-cell lung cancer (NSCLC) will account for the largest number of estimated cancer cases and cancer-related deaths, with the exception of breast and prostate cancer [Siegel et al. 2022]. In past years, genetic profiling and novel therapeutic interventions have improved the overall treatment success [Cancer Genome Atlas Research 2012, Research 2012, Cancer Genome Atlas Research 2014]. However, the overall 5-year survival rate of NSCLC patients remains below 6 % [Ruiz et al. 2019, Pottier et al. 2020]. This observation signifies the importance of the availability of better suited experimental and pre-clinical models for recapitulating, identifying, and testing novel vulnerabilities in NSCLC.

Over the past decade the main *in vivo* model to study NSCLC was the mouse model *Trp53*^{fl/fl} *KRas*^{Isl-G12D/wt} developed by Tuveson, Jacks and Berns [Jackson et al. 2005, Talmadge et al. 2007, DuPage et al. 2009]. Although it recapitulates a large proportion of ADC and SCC patients, this conditional model is limited in representing the genetic complexity of NSCLC. With the advent of CRISPR/Cas9, reflecting this complexity in the genetic landscape of NSCLC has been simplified. [Sanchez-Rivera et al. 2014, Wang et al. 2014]

In this work, we use the versatility of CRISPR/Cas9 to recapitulate the conditional NSCLC mouse model and compare both models in terms of morphology, marker expression and transcriptional profiles.

3.1.1. TP53 and KRAS are frequently altered in ADC and SCC NSCLC subtypes

The predominant murine model to study NSCLC is represented by the use of conditional alleles targeting the tumour suppressor *Trp53* and a Lox-Stop-Lox cassette controlling the expression of a mutant allele of the proto-oncogene *KRas*, *KRas*^{G12D} (*Trp53*^{fl/fl} *KRas*^{Isl-G12D/wt} genotype). Upon infection with a Cre-recombinase encoding virus, the loss of the Stop cassette will allow for the expression of the mutant variant from the endogenous locus of *KRas*, *Kras*^{G12D}, and the Cre recombinase will further delete both alleles of *Trp53*, resulting in tumour formation.

Results

In order to recapitulate the patient relevant mutational burden by using CRISPR/Cas9 *in vivo*, we first analysed the occurrence of driving mutations in TP53 and KRAS with publicly available datasets of human non-small-cell lung cancer patients (Figure 3-1A).

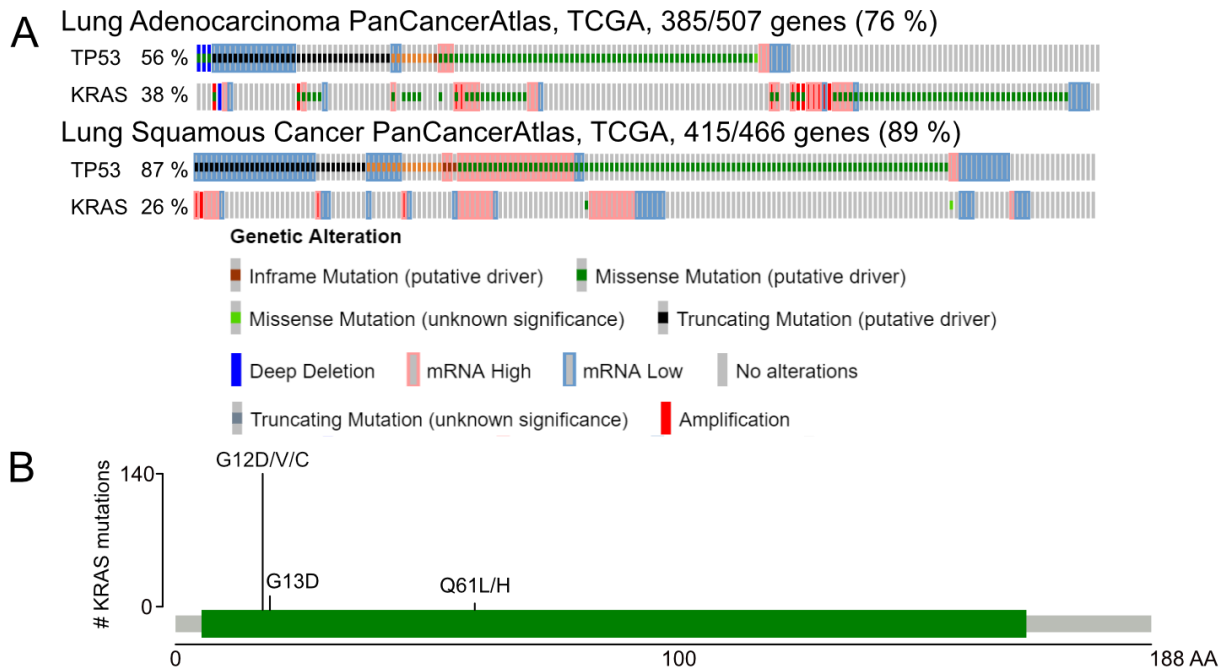


Figure 3-1: TP53 and KRAS are frequently altered in NSCLC subtypes

A Diagram of occurring alterations in TP53 and KRAS in lung Adenocarcinoma (n= 507) and lung Squamous-cell carcinoma (n= 466). Analysed was the PanCancerAtlas (TCGA) with the mRNA expression z-scores relative to all samples (log RNA Seq V2 RSEM $z \pm 1.5$). The legend of the depiction of alterations is below. (cBioportal.com)

B Point mutations in KRAS analysed in publicly available human patient adenocarcinoma cases (n= 503 PanCancerAtlas, TCGA). In 140 out of 157 cases with point mutations, KRAS was mutated at position G12. (modified from cBioportal)

In both tumour entities alterations in TP53 were observed. For Adenocarcinoma (Figure 3-1, upper panel) the overall rate of change in TP53 is 56 % and lower than compared to Squamous-cell carcinoma (87 % Figure 3-1A lower panel). However, in both cases, nearly 95 % of all alterations observed in *Trp53* were either point- and/or truncation mutations rather than complete loss of *Trp53*, thereby presenting an intriguing possibility to use CRISPR genome editing rather than classic genetic targeting by loxP sites.

In addition, alterations of KRAS in association with TP53 alterations can be observed in both subtypes. However, while the alteration of KRAS is comparable at 38 % in ADC and 26 % in SCC, the nature of the alteration is different. Over 80 % of all ADC cases with alterations in KRAS have a point mutation, predominantly at codon 12 (Figure

Results

3-1B). On the other hand, the majority of SCC cases shows an amplification or an upregulation in mRNA level (Figure 3-1).

In addition to alterations in KRAS, ADC and SCC have a combination of activating mutations within the members of the MAPK-pathway (Figure 3-2).

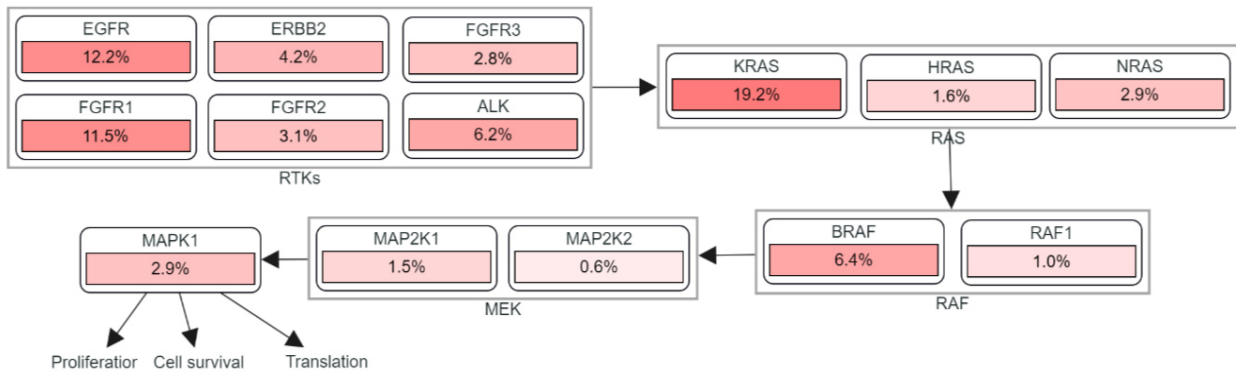


Figure 3-2: Deregulated oncogenic driver in ADC and SCC

Schematic overview of commonly deregulated oncogenic driver pathways in NSCLC, ADC and SCC (PanCancerAtlas, TCGA). Frequency of alteration is shown in percentage. (modified from www.cbioportal.org)

Taking these results together, targeting *Trp53* and *KRas* in mice with CRISPR/Cas9 may lead to a suitable model for NSCLC reconstruction. Especially considering that the majority of TP53 alterations found in patients are point or truncation mutations rather than complete loss.

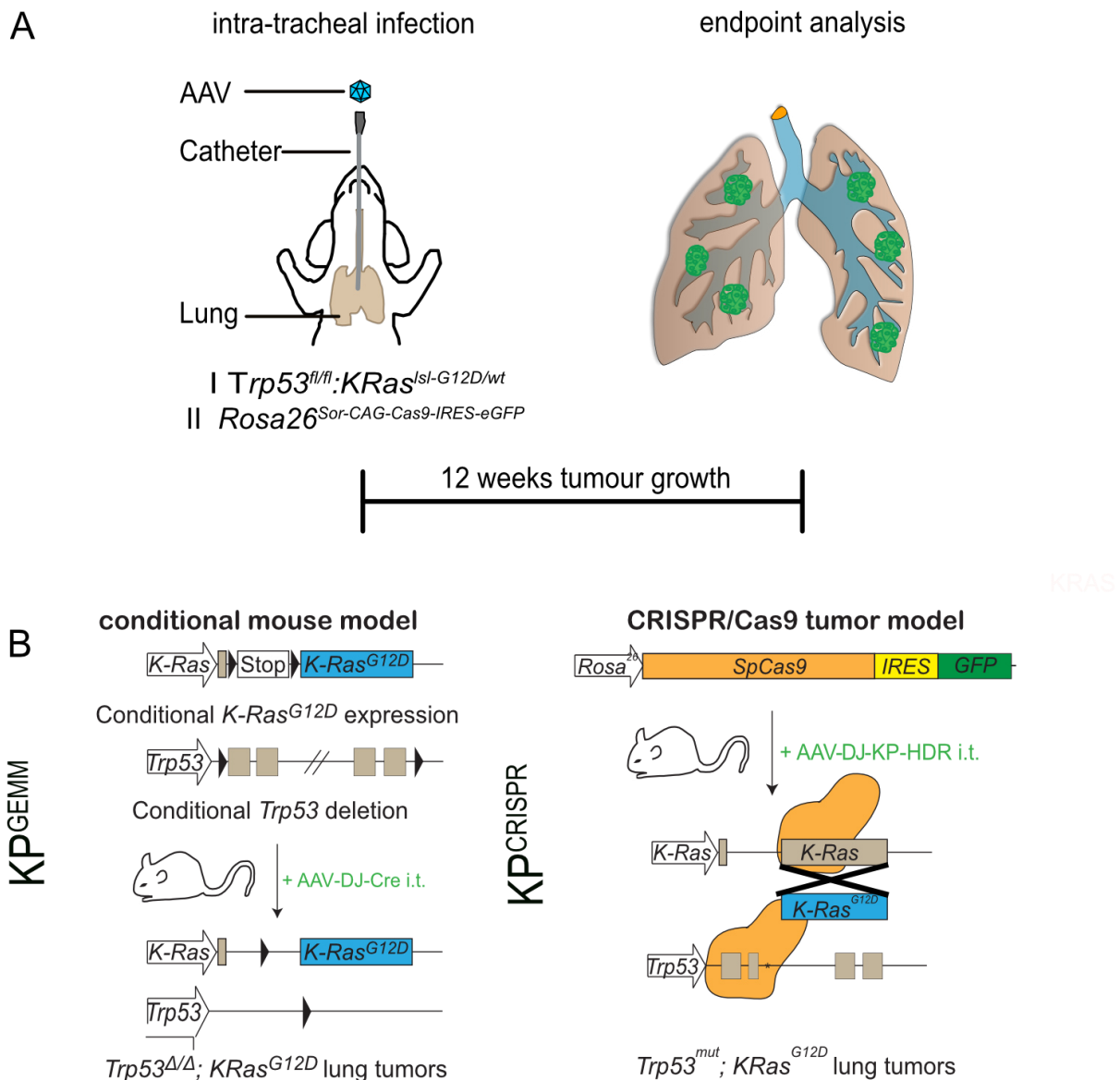
3.1.2. Intratracheal installation of AAV-DJ in KP^{GEMM} shows the highest efficacy

In order to assess if CRISPR/Cas9-mediated gene editing can be utilized for *in vivo* recapitulation of NSCLC, we compared the conditional Cre-recombinase model (KP^{GEMM}) with the CRISPR/Cas9 model (KP^{CRISPR}). As an experimental setup, we chose to infect mice intra-tracheally with an adeno-associated virus (AAV) and performed an endpoint analysis 12 weeks post-infection (Figure 3-3A). To induce lung tumor formation in the conditional mouse model, *Trp53^{fl/fl}:KRas^{Isl-G12D/wt}* mice (C57BL6/J background) were infected with an AAV coding for a Cre-recombinase under the control of an ubiquitous promoter (CMV) (Figure 3-3 B left panel). In infected lung cells, the Cre-mediated recombination of the lox-stop-lox cassette (Isl) induces the heterozygous expression of constitutive active *KRas^{G12D}*. Furthermore, the homozygous loxP targeted *Trp53^{fl/fl}* alleles, encoding wild-type Trp53 containing loxP sites flanking exon 2 and 10, were removed [Jackson et al. 2005], resulting in *Trp53^{Δ/Δ}*. To recapitulate the *KRas^{G12D}* as well as the *Trp53* mutation with CRISPR/Cas9, mice were intra-tracheally infected with an AAV (Figure 3-3B right). The sgRNA targeting

Results

Trp53, *KRas* as well as the homologous repair donor for *KRas*^{G12D} (HDR) have been adopted from [Platt et al. 2014].

The subsequent induced DNA double-strand breaks mediated by CRISPR/Cas9 and the corresponding sgRNA, can be repaired either non-homologous end joining (NHEJ), leading to indels, or homology-directed repair (HDR) [M. Bibikova et al. 2002, M. Bibikova et al. 2003, Kim and Kim 2011]. Thus, deletions or insertions integrated into the gene by the error-prone repair mechanism of NHEJ can subsequently lead to loss-of-function mutations or even complete loss of the target protein. On the other hand, HDR can be used to endogenously mutate a gene of interest by adding an extrachromosomal repair template (blue; Figure 3-3B right panel). Here, the HDR donor encodes the G12D mutational homolog for the first exon of *KRas* as well as silent single nucleotide changes to prevent further CRISPR/Cas9 activity after HDR.



Results

Figure 3-3: Schematic of the intratracheal tumor induction

A Schematic diagram of the intra-tracheal tumor induction in $Trp53^{fl/fl};KRas^{Isl-G12D/wt}$ (KPG^{GEMM}) and CRISPR/Cas9 mediated tumor modelling and targeting of $Trp53\Delta$; $KRas^{G12D}$ in $Rosa26^{Sor-CAGG-Cas9-IRES-GFP}$ mice (KPC^{CRISPR}) via AAV infection.

B The promoters of the respective genes are shown as arrows. **Left Panel** To induce lung tumour formation in the classic conditional mouse model (KPG^{GEMM}), the $Trp53^{fl/fl};KRas^{Isl-G12D/wt}$ mice were i.t. infected with an adeno-associated virus (AAV-DJ-Cre). Upon successful infection, the Cre-recombinase will recognize the loxP sites (black triangle) in the lox-stop-lox-cassette (Isl) in the intron 0 of the $KRas^{IslG12D}$ allele (blue). Thus, the dominant active $KRas^{G12D}$ will be expressed. In addition, the $Trp53^{fl/fl}$ allele encodes the wild type p53 protein and contains LoxP sites flanking exons 2 and 10 (brown). The Cre-mediated recombination will lead to a complete loss of p53 expression.

Right Panel To induce lung tumour formation in the CRISPR/Cas9 (KPC^{CRISPR}), the $Rosa26^{Sor-CAGG-Cas9-IRES-GFP}$ mice were i.t. infected with an adeno-associated virus (AAV-DJ-KP-HDR). Upon successful infection, the Cas9 (orange) together with the corresponding sgRNAs targeting either KRas or Trp53 (brown squares) will induce double-strand breaks. In order to achieve a $KRas^{G12D}$ mutation, the AAV is supplemented with a homologous repair donor (blue) encoding for the G12D mutation.

In order to compare KPG^{GEMM} and KPC^{CRISPR}, we wanted to ensure the optimal virus delivery and infection rate. The intratracheal application (i.t.) of the virus has previously described as optimal delivery path [Platt et al. 2014].

To ensure sufficient infection, several AAV pseudo-serotypes, i.e., incorporation of the genome of one serotype (here: AAV2) into the capsid of another serotype (Table 20). [Burger et al. 2004], were tested, as capsids allow for target cell specificity.

Table 20: AAV serotypes and preferred cell type for infection (adopted from Addgene)

Serotype pRC	Tissue	Comment
AAV2-2	Muscle, Liver, Retina	
AAV2-5	Lung	
AAV2-6	Lung, Muscle	
AAV2-6-2	Lung, Muscle	Variant of AAV2-6
AAV2-7	Muscle, Retina, Neurons	
AAV2-8	Liver	
AAV2-9	Heart, Liver, Lung, Brain	
AAV-DJ	Various	Combination of 8 serotypes; broad spectrum of infection

$Trp53^{fl/fl};KRas^{Isl-G12D/wt}$ mice (C57BL6/J background) were intratracheally infected with $1 * 10^{11}$ PFU (plaque forming unit) of the different AAV-serotypes coding for a Cre-recombinase and analysed 6 weeks post infection. For this purpose, the lungs were

Results

dissected, formalin fixated, paraffin embedded and cut into 4 μm slices. Afterwards, a haematoxylin and eosin (H&E) staining was conducted, and the tumour burden determined (Figure 3-4).

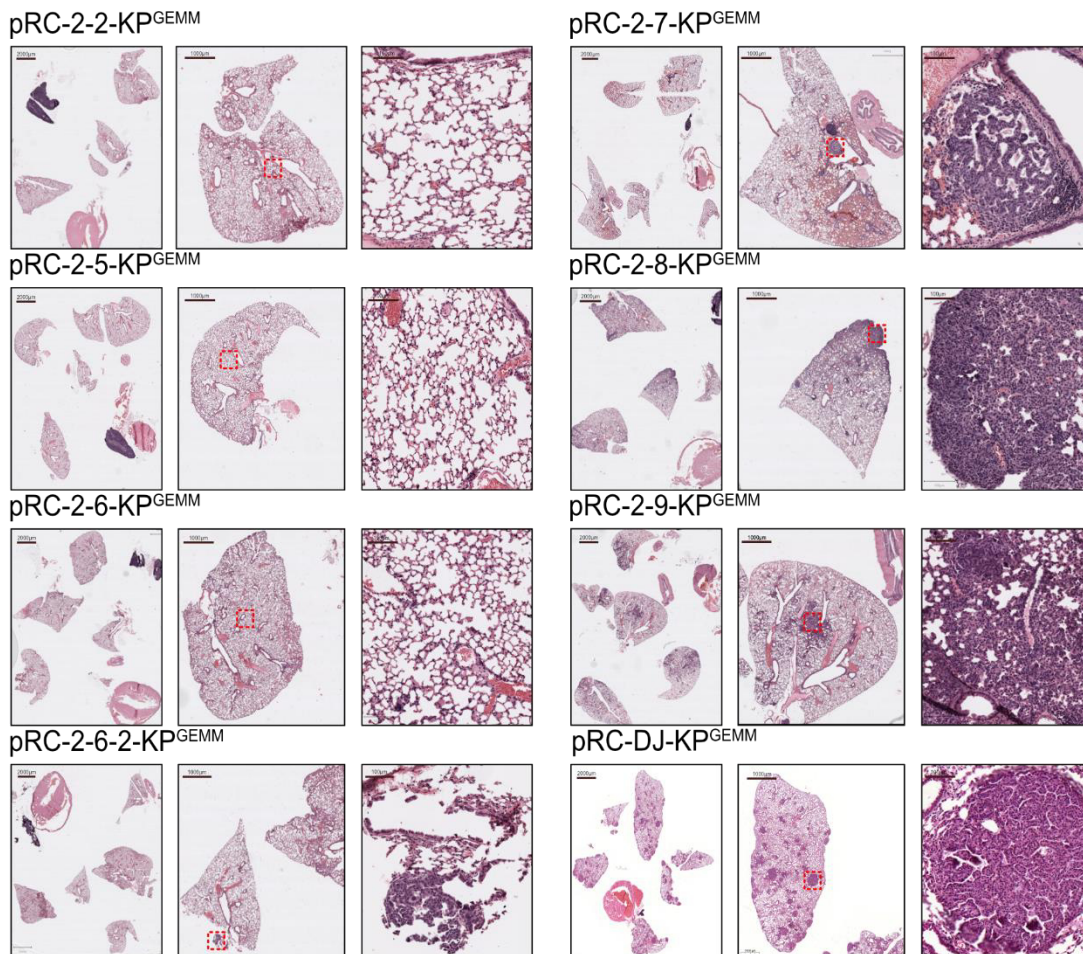


Figure 3-4: Intratracheal administration of AAV-DJ yields the highest efficacy

Representative Haematoxylin and eosin staining of *Trp53^{fl/fl};KRas^{ls1-G12D/wt}* (KPGE)MM). Animals were intratracheally infected with $1 * 10^{11}$ PFU of different Cre-recombinase encoding AAV, packaged with the indicated pseudo-serotype and capsid compositions to test target organ tropism *in vivo*. Animals were sacrificed 6 weeks post intratracheal instillation. Highlighted areas are marked with red dashed squares. (scale bar 2000 μm , 1000 μm and 100 μm)

The combination of the serotypes pRC2-2,2-5 and 2-6 did not result in any tumour formation in animals within 6 weeks. AAV encapsulated with AAV-2-6-2, 2-7, and 2-8 showed low frequency of tumor formation with only a single-digit number of lesions. In contrast, pRC2-9, and the shuffle capsid AAV-DJ, generated by combining amino acid sequences from all major AAV capsids, did show robust tumour formation as early as 6 weeks, with AAV-DJ exhibiting the highest infection efficiency, with more than 40 lesions. Based on these results, all further *in vivo* experiments were conducted with i.t. application of AAV packed with pRC-DJ.

Results

3.1.3. Crispr/Cas9 mediated editing of *Trp53* and *KRas*^{G12D} induces formation of NSCLC morphological indistinguishable from the classical model

Next, we directly benchmarked KP^{GEMM} versus KP^{CRISPR} using the experimental setup as outlined above. Animals were i.t. infected with $1 * 10^{11}$ PFU of either AAV-DJ-Cre (KP^{GEMM}; n=4) or AAV-DJ-KP-HDR (KP^{CRISPR}; n=8) and analysed 12 weeks post infection. The formalin-fixed paraffin-embedded (FFPE) tissue was histological processed, and H&E stained (Figure 3-5).

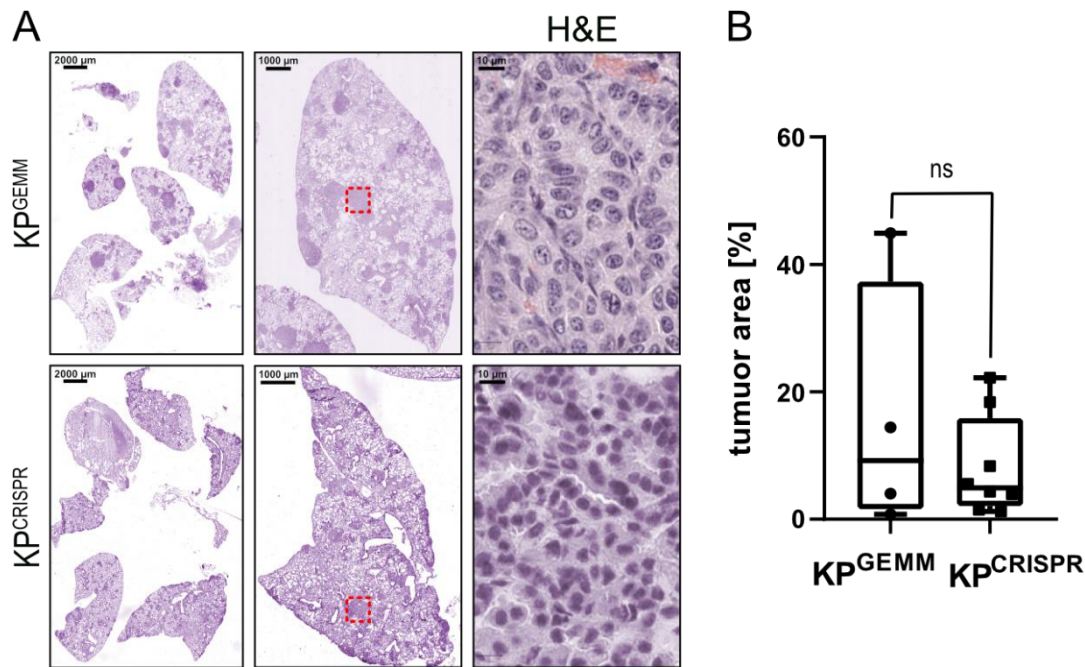


Figure 3-5: Type of tumour induction in *KRas*/*Trp53*-driven NSCLC shows no significant difference in tumour burden

A Representative H&E images of tumour bearing animals 12 weeks post intratracheal infection. *Trp53*^{fl/fl}:*KRas*^{sl-G12D/wt} (KP^{GEMM}; n=4) and *Rosa26*^{Sor-CAGG-Cas9-IRES-GFP} mice (KP^{CRISPR}; n=8) were infected i.t. with $1 * 10^{11}$ PFU. Highlighted tumour areas are marked with red dashed squares. (scale bar 2000 μ m, 1000 μ m and 10 μ m).

B Quantification of the tumour area in % normalized to total lung area in KP^{GEMM} (n=4) and KP^{CRISPR} (n=8). Data are shown as boxplot, with each box representing the group's median, upper, and lower quantiles, and min/max confidence interval. Individual data points are shown. (p=0.3423 unpaired two-tailed t-test)

The expression of the constant active *KRas*^{G12D} mutant as well as the loss of *Trp53* in the classical KP^{GEMM} after the Cre-mediated recombination, led to the formation of lung tumours (Figure 3-5A top). In a comparable manner, a similar tumour formation was observed in the CRISPR/Cas9-mediated targeting of *KRas* and *Trp53* (KP^{CRISPR}, Figure 3-5A bottom). Tumour morphology (Figure 3-5A high magnification) and individual tumour size were also comparable. Thus, the occurrence of lesions indicated

Results

a successful CRISPR-mediated mutation of KRas to KRas^{G12D}, as along with a loss-of-function mutation in Trp53.

Quantification of tumour area in % normalized to total lung area showed no significant difference in tumour burden of KP^{CRISPR} compared to KP^{GEMM} (Figure 3-5B). However, at least one animal has a higher tumour burden, compared to all other KP^{CRISPR} experimental animals. To investigate, if the complete loss of Trp53 in KP^{GEMM} has an impact on the overall proliferation and tumour growth we carried out an immunohistochemistry (IHC) staining for the proliferation marker Proliferating cell nuclear antigen (PCNA) (Figure 3-6).

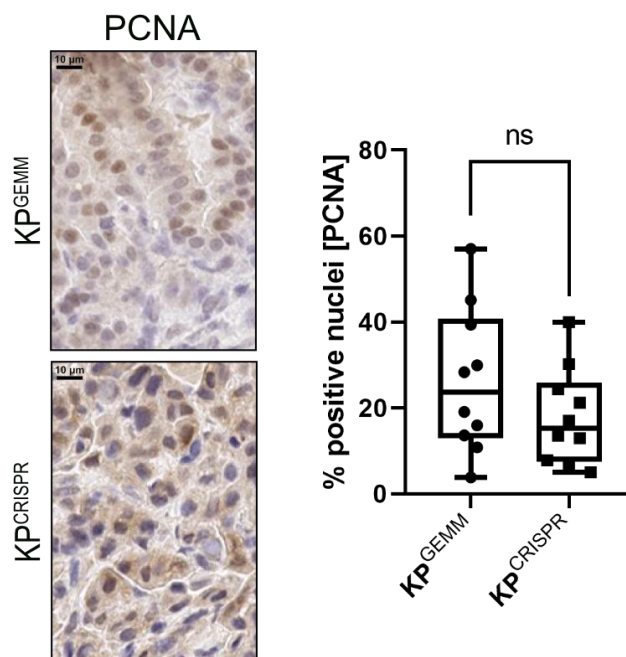


Figure 3-6: Quantification of PCNA indicates no significant difference in proliferation

Representative IHC analysis of PCNA from tumor bearing animals 12 weeks post intratracheal infection. (KP^{GEMM}; n=4). (KP^{CRISPR}; n=8) Quantification of % PCNA positive nuclei in 10 tumours in KP^{GEMM} and KP^{CRISPR}. Data are shown as boxplot, with each box representing the group's median, upper, and lower quantiles, and min/max confidence interval. Individual data points are shown. (p=0.3051 Mann-Whitney-Test)

Quantification of 10 individual tumours with a combined minimum of n=20,000 cells revealed no significant difference in the frequency of PCNA-positive nuclei. This suggests a comparable proliferative state in KP^{GEMM} and KP^{CRISPR} lung tumours.

Since there was no significant difference in tumour burden or proliferation between KP^{GEMM} and KP^{CRISPR}, we wondered if the tumour grades differ. To address this question, we have adopted the staging system established by the American Cancer Society for evaluating the grade of solid tumours [AmericanCancerSociety 2019]. Depending on the size and abnormal shape and structure of the nuclei, individual

Results

tumours were blindly graded from 1 (atypical alveolar hyperplasia) to 4 (large tumours; high amount of abnormal nuclei), with 1 being the lowest grade and 4 being the highest (Figure 3-7A). Comparing both tumour induction methods, KP^{GEMM} and KP^{CRISPR} , no significant difference could be observed in the abundance and distribution of the stages (Figure 3-7B).

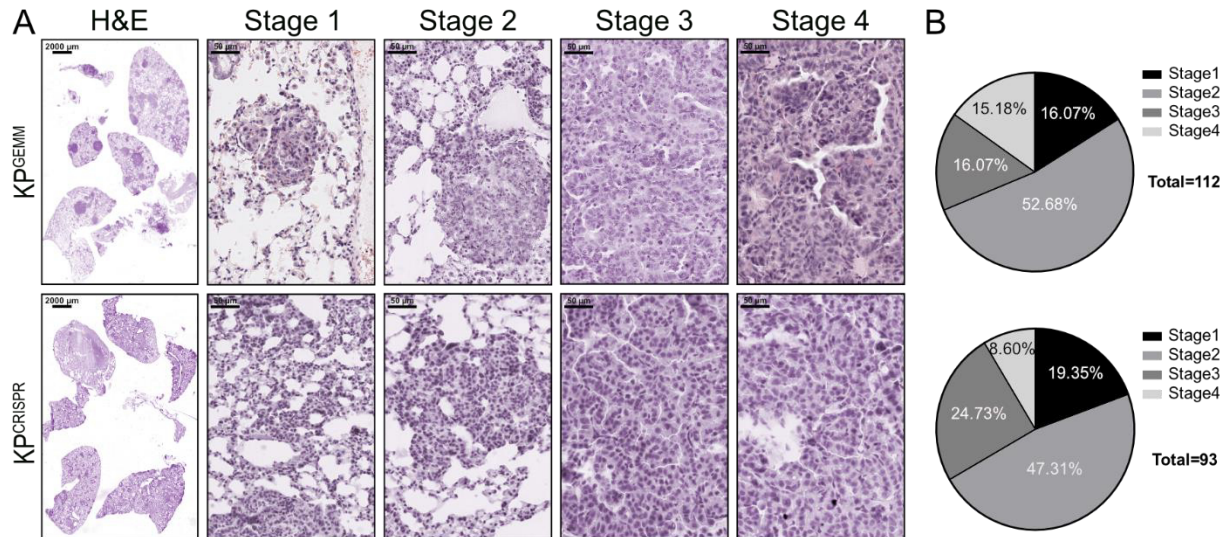


Figure 3-7: KP^{GEMM} and KP^{CRISPR} presented comparable distributions of all stages

A Representative H&E images of tumor stages in KP^{GEMM} and KP^{CRISPR} according to the adopted American Cancer Society guidelines. Stages ranging from atypical alveolar hyperplasia (AAH, stage I) to stage IV Cancer. (scale bar 2000 μm and 50 μm) **B** Quantification of the tumour stages blindly determined in KP^{GEMM} (n=112) and KP^{CRISPR} (n=93) (p Value=0.1589 one-way Anova)

In both cases, close to 20% of all tumours presented stage 1 (atypical alveolar hyperplasia (AAH)). This could indicate insufficient recombination in KP^{GEMM} or CRISPR/Cas9-mediated DSB and HDR were not efficient in KP^{CRISPR} . Since the AAV genome persists as an exosome and hence non-integrative in infected cells, tumour induction could occur at a later time point than immediately after i.t. infection.

Half of all tumours in both KP^{GEMM} and KP^{CRISPR} were in stage 2, whereas the remaining 30 % of tumours presented features representative of stage 3 and 4. It was observed that twice as many late-stage tumours progressed to stage 4 in KP^{GEMM} than in KP^{CRISPR} . This is in line with previous publishes studies, which could be inked to a faster progression due to complete loss of Trp53 [Zheng et al. 2007].

Next, we wanted to confirm the successful CRISPR/Cas9-mediated targeting of Trp53 and KRas. For this purpose, genomic DNA was isolated, and Sanger sequencing was performed. Since the genomic events of a CRISPR/Cas9 approach can vary in length, the PCR primers were designed to bind 500 base pairs (bp) upstream and 500 bp

Results

downstream of the respective sgRNA: The result is a PCR product of 1000 bp covering the target site (Figure 3-8A). The PCR for the isolated wildtype DNA revealed a product length of 1000 bp for both: Trp53 and KRas, confirming the success of the PCR strategy.

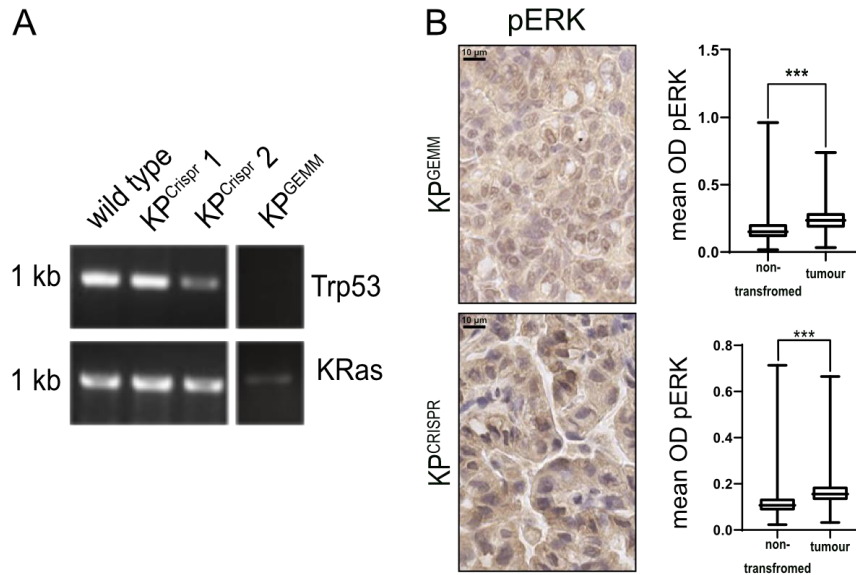


Figure 3-8: Analysing genomic DNA and the MAPK-pathway confirms successful targeting of Trp53 and KRas in KPCRISPR

A Exemplary DNA gel electrophoresis image of representative tumor explants 12 weeks post i.t. of AAV containing sgRNA to delete Trp53, and sgRNA and HDR encoded for CRISPR mediated genome editing to KRas^{G12D}(KPCRISPR). Sequencing primers used bind 500bp proximal and distal to sgRNA sequences. DNA of Trp53 and KRas locus of two KPCRISPR, compared to KPGEEMM DNA after recombination.

B Representative IHC analysis of p-ERK from tumor bearing animals 12 weeks post intratracheal infection. (KPGEEMM; n=4). (KPCRISPR; n=8) Quantification of the mean optical density of positive cells (n ≥ 15000 cells) in non-transformed and tumour tissue in KPGEEMM and KPCRISPR. Data are shown as boxplot, with each box representing the group's median, upper, and lower quantiles, and min/max confidence interval. (KPGEEMM <0.0001/ KPCRISPR<0.0001 Mann-Whitney-Test, scale bar 10 μm)

The Cre-recombination should remove both Trp53 alleles in KPGEEMM. This could be confirmed by the missing PCR product for the Trp53 locus. In addition, a band at 1000 bp can be observed for KRas, however with a lower band intensity compared to wild type. This could indicate a successful recombination with subsequent loss of heterozygosity (LOH), which has been described for KRas^{G12D/wt} before [Ma et al. 2022].

In both KPCRISPR tumours, a band at 1000 bp was observed for Trp53, whereas KPCRISPR2 had a lower band intensity. This again could indicate a heterozygous event. In addition, a PCR product comparable in intensity to the wildtype sample was detected in both KPCRISPR clones isolated and analysed. The bands could indicate either

Results

successful recombination to KRas^{G12D}, homologous repair to wild-type KRas, or no CRISPR/Cas9 event at all. However, because the PCR did not reliably indicate a genetic alteration of Trp53 or KRas mediated by CRISPR/Cas9, the purified PCR products were subjected to Sanger sequencing. Here we could confirm the mutation of KRas to the active G12D variant, as well as depletions in Trp53 in various length (Figure 6-1).

Furthermore, we confirmed the activation of the MAPK-pathway due to the mutation of KRas^{G12D} by an IHC staining of the phosphorylated MAPK1/3 (p-ERK) (Figure 3-8B). Comparison of p-ERK abundance by optical density in non-transformed and tumour tissues in KP^{GEMM} and KP^{CRISPR} revealed a significant increase in p-ERK in tumours. Taken together, the sequencing results and IHC staining confirmed a successful activating mutation of KRas and a loss-of-function mutation in Trp53 in KP^{GEMM} and KP^{CRISPR}.

To finalize the comparison at the morphological level, we analysed the KP^{GEMM} and KP^{CRISPR} tumour bearing lungs regarding their marker expression, for the respective NSCLC subtypes: Adenocarcinoma (ADC) and Squamous-cell carcinoma (SCC).

For this purpose, a set of clinically relevant markers for both subtypes were selected: Surfactant protein C (Sftpc), specific for alveolar type II cells, and thyroid transcription factor-1 (Nkx2-1/TTF1), expressed in lung epithelial cells, were used to classify NSCLC-ADC, while Cytokeratin 5 (Krt5) and Sox2 were used to identify NSCLC-SCC [Gurda et al. 2015, Ferone et al. 2016]. In addition, the tracheal club cell marker Scgb1a1 (CC10), exclusively expressed in wild type tracheal cells, was used as a control (Figure 3-9).

The IHC staining for Scgb1a1 was negative for both, KP^{GEMM} and KP^{CRISPR}, consistent with the literature.[Kurotani et al. 2011]. A positive staining could be observed in the non-transformed tracheas in both models.

Analysis of the expression of ADC specific markers demonstrated positive staining of Sftpc and Nkx2-1 in both tumor models. However, expression of the basal stem and

Results

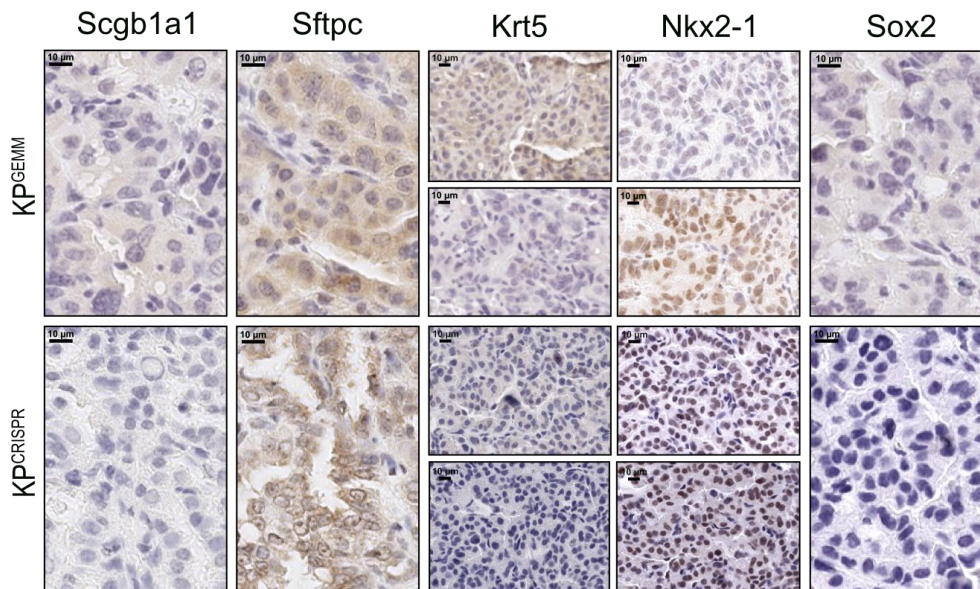


Figure 3-9: Marker expression in KP^{GEMM} and KP^{CRISPR} indicates an adeno-squamous phenotype

Representative IHC staining for Scgb1a1/CC10 and the ADC (Sftpc and Nkx2-1/TTF-1) and SCC (Krt5 and Sox2) marker expression in tumor bearing animals 12 weeks post intratracheal infection. (KP^{GEMM}; n=4). (KP^{CRISPR}; n=8) (scale bar 10 μm)

squamous cell carcinoma marker Krt5 was detectable in a subset of primary tumours only in KP^{GEMM} but was absent in KP^{CRISPR}, respectively. In order to confirm a possible squamous subtype in KP^{GEMM}, Sox2, an additional marker and driver of SCC, was stained. No staining was detected in the tumours of both models, whereas the basal cells of the trachea showed positive staining. This could be indicative of a co-abundance of Krt5 and Nkx2-1, than a real squamous phenotype in KP^{GEMM}.

These data demonstrate that CRISPR/Cas9 mediated genome editing of Trp53 and KRas results in tumours which are comparable on morphological level to the classic GEMM model Trp53^{fl/fl}:KRas^{Isl-G12D/wt}.

3.1.4. KP^{GEMM} and KP^{CRISPR} demonstrate a similar upregulation of NSCLC oncogenic transcription factors

A hallmark of cancer is the deregulation of pathways involved in cell cycle progression, apoptosis, and proliferation. Previous studies have shown the dependency of lung tumours on oncogenic transcription factors, such as members of the AP-1 family or cMYC [Hartl 2016, Sanchez-Vega et al. 2018]. Additional important transcription factors for lung cancer progression include the WNT signalling pathway and members of the NOTCH family [Nakayama et al. 2014, Xu et al. 2014]. In unperturbed lung epithelial cells, WNT is involved in alveolar stem cell maintenance, but its effector β-catenin does promote oncogenesis and is associated with poor survival of KRas-mutated NSCLC [Pacheco-Pinedo and Morrissey 2011]. The expression of Notch1 and

Results

Notch3 are crucial for the progression of *KRas* driven lung cancer and are as well associated with poorer survival [Licciulli et al. 2013].

Analysis of publicly available datasets from patients with NSCLC highlighted a frequent upregulation or amplification of oncogenic transcription (co)-factors (Figure 3-10).

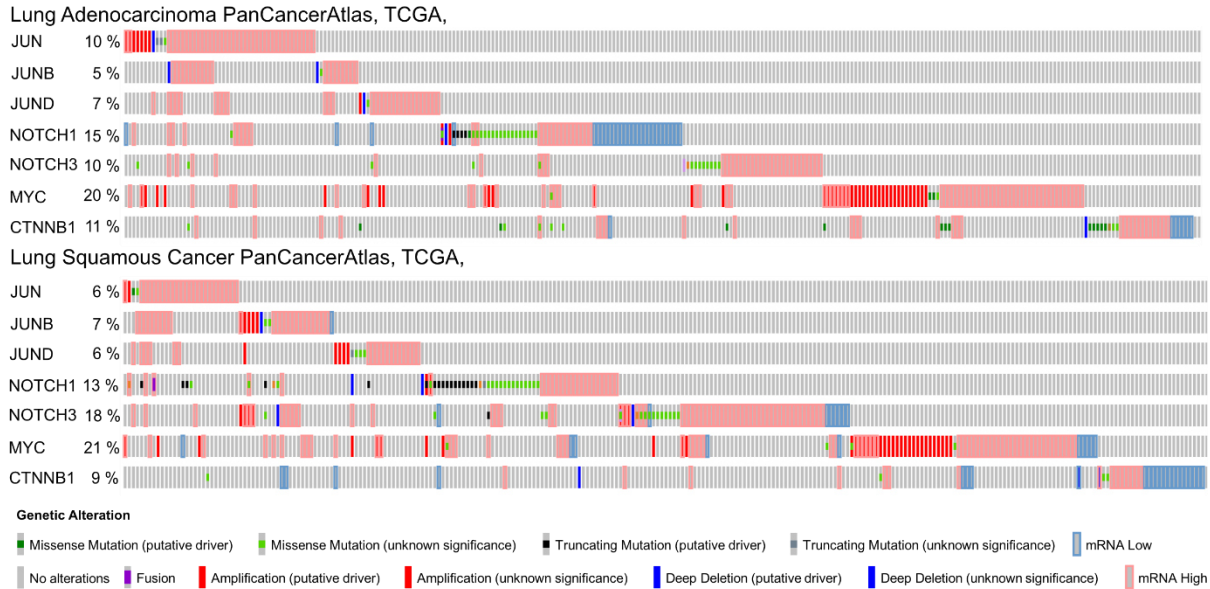


Figure 3-10: Oncogenic transcription factors a commonly upregulated in NSCLC

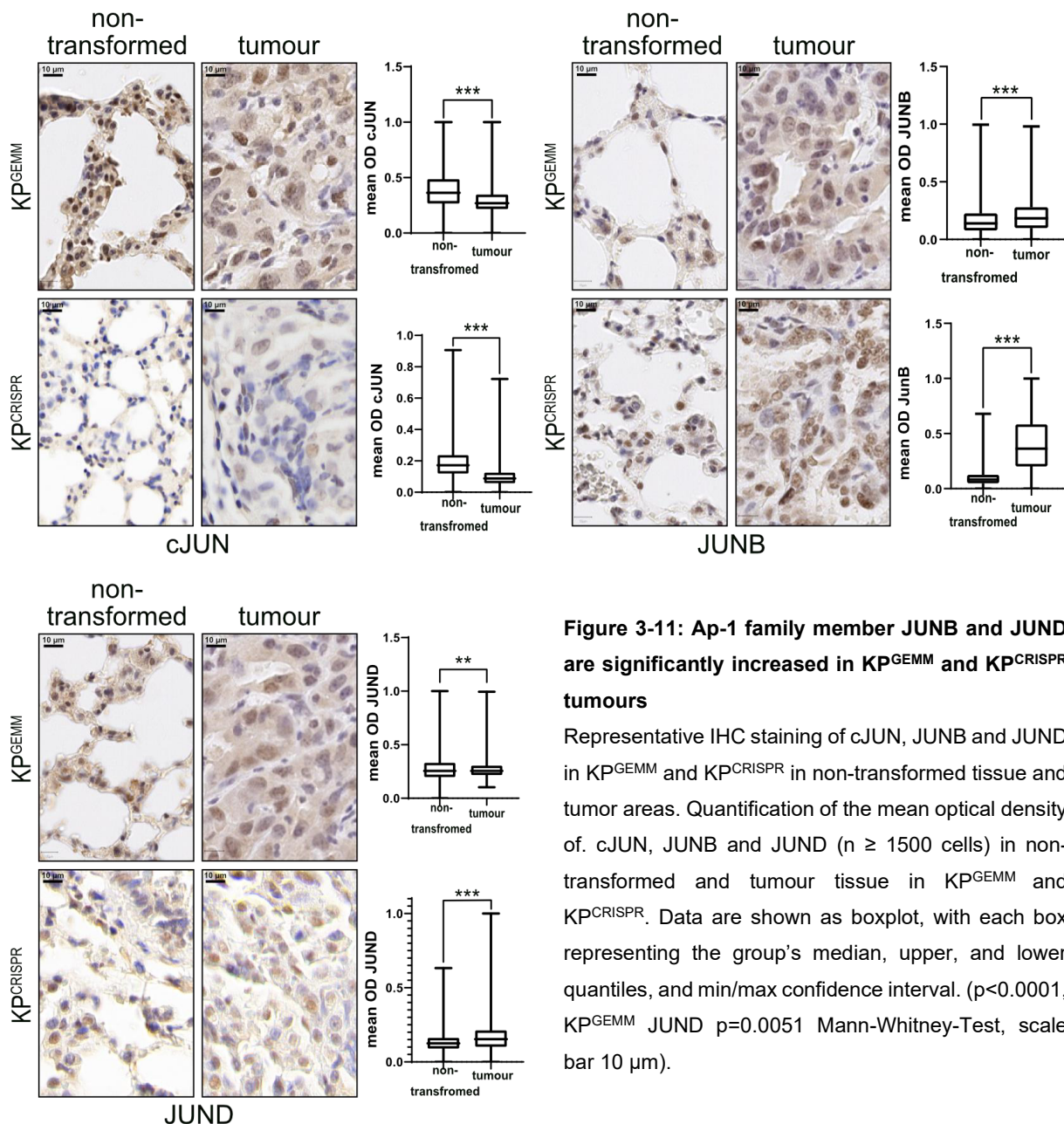
Diagram of occurring alterations in JUN, JUNB, JUND, NOTCH1, NOTCH3, MYC and CTNNB1 in lung Adenocarcinoma (n= 507) and lung Squamous-cell carcinoma (n= 466). Analysed was the PanCancerAtlas (TCGA) with the mRNA expression z-scores relative to all samples (log RNA Seq V2 RSEM $z \pm 1.5$). The legend of the depiction of alterations is below. (adopted from cbioportal.com)

In both NSCLC entities, ADC and SCC, upregulation of the factors can be observed in around 5% of cases for e.g., the AP1 family members JUNB and JUND, while 20% of patients demonstrated a deregulation of the transcription factor cMYC in these samples. It is noteworthy that the majority of patient samples demonstrated a discreet upregulation of one of the analysed oncogenes, while co-upregulations or amplifications only appear to occur irregularly.

We wondered, if a similar dysregulation of these oncogenic factors can be observed in both NSCLC tumour mouse models. Therefore, FFPE slides of tumour bearing animals were stained immunohistochemically for the mentioned factors.

At first, a IHC staining for the AP-1 family members cJUN, JUNB and JUND was carried out (Figure 3-11).

Results



Comparing protein abundance based on the mean optical staining density (OD) of non-transformed tissues and tumours (n = 10 tumours/ n ≥ 1500 cells) in KP^{GEMM} and KP^{CRISPR}, a significant increase in JUNB and JUND can be observed in both cases. Contrary to expectations (Figure 3-10), the amount of cJUN in both KP^{GEMM} and KP^{CRISPR} was significantly reduced to the same extent in tumours compared to the nearby non-transformed tissue. In wild-type lung tissue, cJUN, JUNB, and JUND can be detected exclusively in type 2 alveolar stem cells (AT2) (Figure 3-11 non-transformed tissue), whereas in tumours, the majority of cancer cells stained positive for the respective factor (Figure 3-11 tumour).

Results

As mentioned above, NOTCH family transcription factors play an important role in the progression and differentiation of NSCLC. A large proportion of NSCLC patients exhibit dysregulation in 2 of the 4 members of the NOTCH family: Notch1 and Notch3 [Zou et al. 2018]. Hence, we analysed the total protein abundance of the cleaved and transcriptionally active variant of NOTCH1, the intracellular domain of Notch-1 protein (NICD), and total and cleaved NOTCH3 (Figure 3-12).

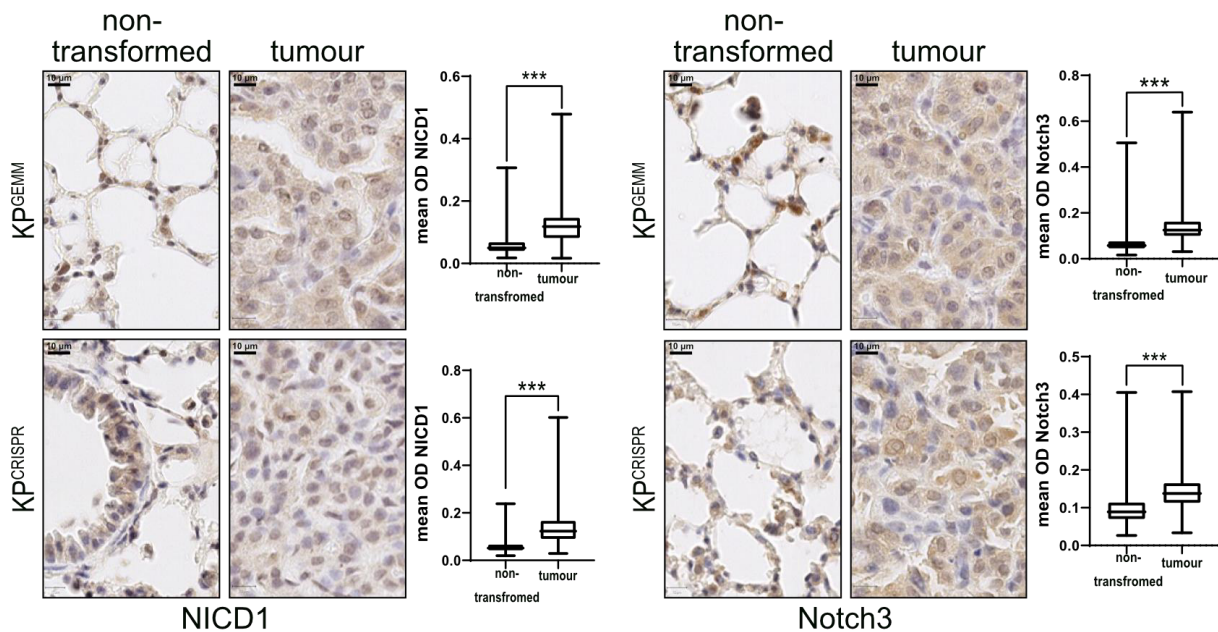


Figure 3-12: NICD and NOTCH3 are significantly more abundant in KP^{GEMM} and KP^{CRISPR} compared to non-transformed tissue

Representative IHC staining of the intracellular domain of Notch-1 protein (NICD) and total and cleaved NOTCH3 in KP^{GEMM} and KP^{CRISPR} in non-transformed tissue and tumour areas. Quantification of the mean optical density of NICD and NOTCH3 ($n \geq 1500$ cells) in non-transformed and tumour tissue in KP^{GEMM} and KP^{CRISPR}. Data are shown as boxplot, with each box representing the group's median, upper, and lower quantiles, and min/max confidence interval. ($p < 0.0001$, Mann-Whitney-Test, scale bar 10 μm).

Similar to AP-1 transcription factors, the increased optical density for NICD1 and NOTCH3 also indicates increased protein abundance in the tumours. Significantly and uniformly elevated levels can be detected for KP^{GEMM} and KP^{CRISPR} for both transcription factors.

The non-transformed and wild type tissues showed rather low levels of NICD and NOTCH3 (Figure 3-12 Quantifications). However, the importance of NOTCH signalling for lung tissue development is evident from the positive NICD and NOTCH3 staining in the AT2 cells as well as in the trachea (Figure 3-12 KP^{CRISPR} NICD).

Results

To finalize the evaluation of dysregulated (co)transcription factors in the KP^{GEMM} and KP^{CRISPR} a staining for the WNT effector β -Catenin (CTNNB1) and the oncoprotein cMYC was carried out (Figure 3-13)

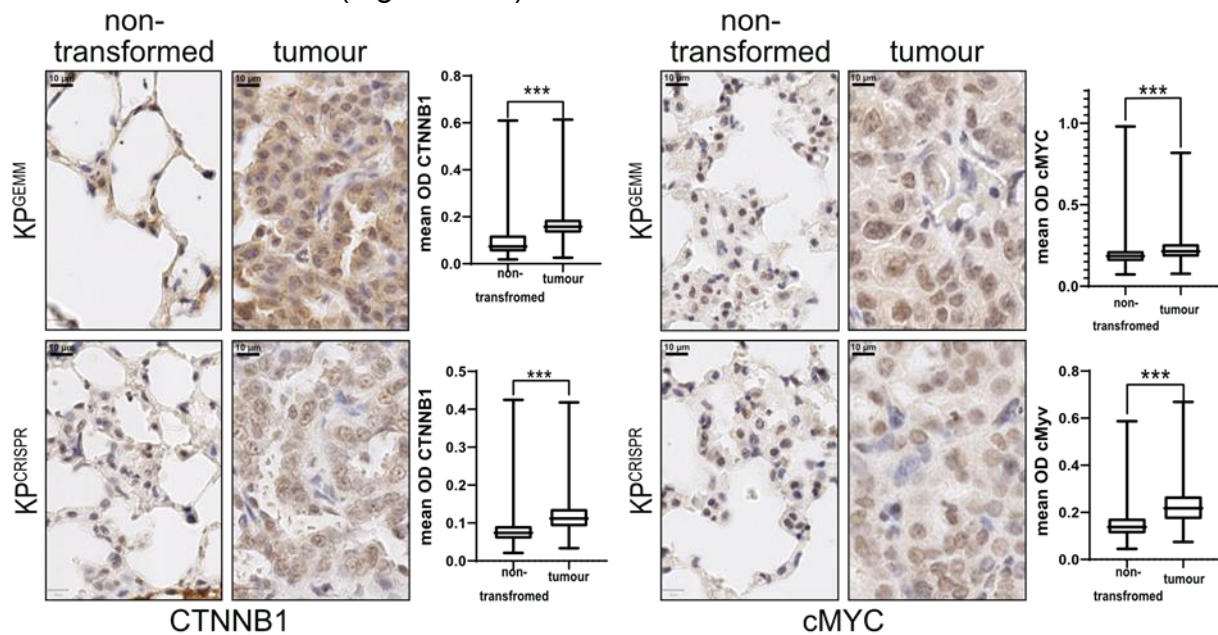


Figure 3-13: CTNNB1 and cMYC are significantly upregulated in KP^{GEMM} and KP^{CRISPR} tumours

Representative IHC staining CTNNB1 (β -Catenin) and cMYC in KP^{GEMM} and KP^{CRISPR} in non-transformed tissue and tumor areas. Quantification of the mean optical density of CTNNB1 (β -Catenin) and cMYC ($n \geq 1500$ cells) in non-transformed and tumour tissue in KP^{GEMM} and KP^{CRISPR}. Data are shown as boxplot, with each box representing the group's median, upper, and lower quantiles, and min/max confidence interval. ($p < 0.0001$, Mann-Whitney-Test, scale bar 10 μ m).

In non-transformed tissue CTNNB1 was located prevalently in the cytosol in lung epithelial cells. An exception was the stem cells AT2 of the alveolar compartment, where it has a nuclear localization. This could also be observed predominantly in the tumours. Here, β -Catenin/CTNNB1 showed a significant upregulation in both model systems.

Finally, we examined the total protein abundance of the proto-oncogene cMYC. This transcription factor coordinates a variety of biological processes and its upregulation is considered a "hallmark of cancer" [Gabay et al. 2014]. Furthermore, the expression of cMYC is directly and indirectly driven by the previous mentioned factors. Again, only a small proportion of the wildtype tissue demonstrated a positive staining for cMYC. The tumours, on the other hand, showed significant and comparable upregulation of MYC in KP^{GEMM} and KP^{CRISPR}.

Results

The general upregulation of the oncogenic (co-)transcription factors indicates the activation of signalling pathways for cancer proliferation, transformation, and cell survival.

Taken together, both model systems upregulate the clinically relevant signalling pathways of cMYC, CTNNB1, NOTCH and AP-1 and recapitulate the situation in NSCLC patients. Moreover, CRISPR/Cas9-mediated genome editing does this to the same extent as KP^{GEMM}.

3.1.5. CRISPR/Cas9-mediated NSCLC formation has similar transcriptional profile adaptations to the classical model

The aforementioned experiments demonstrated that CRISPR/Cas9-mediated induction of non-small cell lung cancer leads to tumour formation that is morphologically very similar to the classical model. Furthermore, both murine models activated pathways required for tumour progression and maintenance to comparable levels when compared to non-transformed tissue samples. To investigate whether the deregulation of oncogenes associated with the KRas^{G12D} and Trp53^{Δ/Δ} mutation have comparable effects on global transcriptional programs in KP^{GEMM} and KP^{CRISPR}, an RNA-Sequencing (RNA-Seq) of corresponding tumour samples was performed. Therefore, animals were i.t. infected with $1 * 10^{11}$ PFU of either AAV-DJ-Cre (KP^{GEMM}) or AAV-DJ-KP-HDR (KP^{CRISPR}) and sacrificed 12 weeks post intratracheal installation. The lungs of tumour-bearing animals were removed, and the visible lesions were dissected. After a collagenase digestion and mechanical separation, the cell suspensions were cultivated in DMEM supplemented with 10 % FCS and 1 % f.c. anti mycotic and anti-bacterial agents. Clonally growing cell populations were mechanically isolated and passaged as individual clones. These isogenic cell lines established via this method were subjected to RNA-Seq. A total of two single cell clones of KP^{GEMM} and KP^{CRISPR} were analysed in triplicate technical design, with wild-type lung tissue serving as control.

Results

In order to evaluate the similarities and differences in the whole transcriptome of KP^{GEMM} and KP^{CRISPR}, we compared the log₂FC of gene expression in the clone A of KP^{GEMM} and clone B in KP^{CRISPR} relative to wild type (Figure 3-14A).

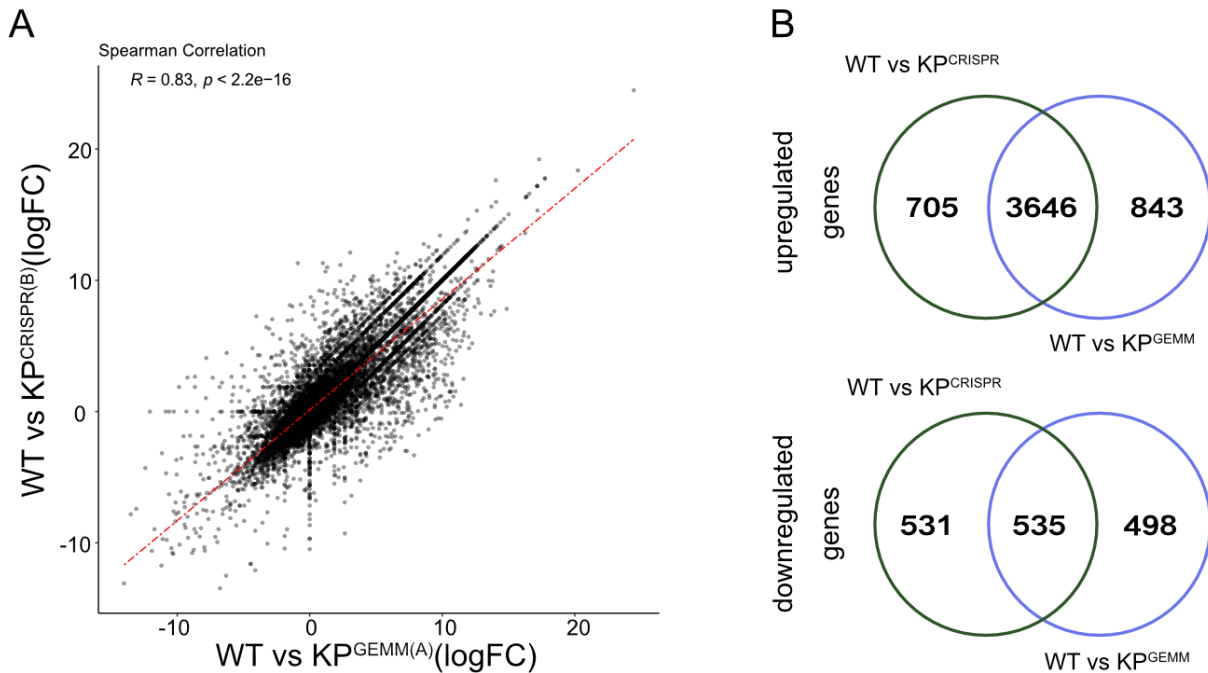


Figure 3-14: KP^{GEMM} and KP^{CRISPR} show highly similar transcriptomic profiles

A Correlation blot of gene expression in KP^{GEMM(A)} and KP^{CRISPR(A)} relative to wild type tissue with linear regression (red line). Spearman correlation of $R=0.85$, $p \leq 2.2 \times 10^{-16}$. $n=3$ each.

B Venn diagram of individually and commonly up- and downregulated genes between Wt vs. KP^{GEMM} and Wt vs. KP^{CRISPR}. ($\log_2FC > 1.5$ and $q\text{-value} < 0.05$) Average of $n=3$ each.

The significant Spearman Correlation ($R = 0.83$) confirmed a high similarity between the classical and the CRISPR/Cas9 approach. A comparable correlation can also be found in the comparison of the other two individual clones ($R = 0.77$; $R = 0.73$; $p \leq 2.2 \times 10^{-16}$). Despite the difference in both methods to achieve the tumour forming mutations, the observed global transcriptomic changes indicate that rather than the method used, the transformation inducing mutations affect changes to the global transcriptional profile. Genetic recombination or homologous repair induced oncogenesis, leading to *KRas*^{G12D} and *Trp53*^{Δ/Δ} mutations in vivo, share common adaptations. If we now compare the up-regulated and down-regulated genes ($\log_2FC > 1.5$ and $q\text{-value} < 0.05$) of KP^{GEMM} and KP^{CRISPR} versus non-transformed tissue samples, a common up-regulation of 3646 genes and down-regulation of 535 genes was detected (Figure 3-14B). CRISPR/Cas9-mediated tumour induction resulted in individual upregulation of 705 genes and downregulation of 531 genes, while the Cre recombinase approach resulted in 843 individually upregulated genes

Results

and 498 downregulated genes. To gain a deeper insight into the common dysregulated genes in both model systems, a volcano plot showing log₂FC in expression of WT vs KP^{GEMM} and WT vs KP^{CRISPR} against the -log₁₀ p-value of the expression, was generated (Figure 3-15).

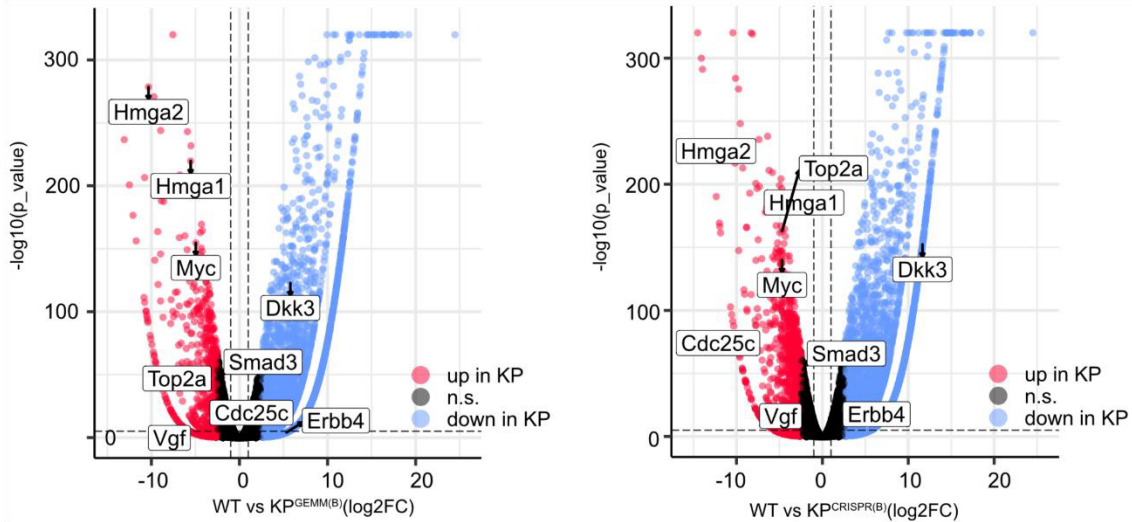


Figure 3-15: KP^{GEMM} and KP^{CRISPR} demonstrate a similar up- and down-regulation of cancer related genes

Volcano blot of genes up- and down-regulated ($n = 17243$ genes) in KP^{GEMM(B)} and KP^{CRISPR(B)}, relative to wild type tissue. Genes up-regulated in KRas^{G12D}/Trp53^{mut} (KP) are shown in red, down-regulated genes in blue, non-significant (n.s.) in black. Genes of interest are labelled. $n=3$ each

Comparing the up- and down-regulated genes for KP^{GEMM} and KP^{CRISPR} relative to the wild type, it is striking that genes associated with cancer progression behave very similarly in both cases. Among the upregulated genes are two members of the High Mobility Group (HMG) protein family Hmga2 and Hmga1. Both are commonly upregulated in several cancers and a high abundance is associated with increased proliferation and inhibition of apoptosis [Belton et al. 2012, Shah et al. 2013, Mansoori et al. 2021]. A significant upregulation in MYC protein abundance was observed in both model systems by IHC methods (Figure 3-13), and the analysis of transcriptomic datasets confirmed this result by identifying significantly upregulated MYC-driven gene signatures. Furthermore, Topoisomerase IIa (Top2a) and cell division cycle-25C (Cdc25c) are up-regulated in KP^{GEMM} and KP^{CRISPR}. Both have been linked to increased metastasis and proliferation on NSCLC [Kou et al. 2020, Liu et al. 2020].

On the other hand, among the commonly down-regulated genes is Dickkopf 3 (Dkk3), a Wnt-pathway inhibitor. Down-regulation or loss of Dkk3 is associated with increased β -Catenin signalling in lung cancer and this finding is in line with the increased protein abundance in both tumour entities (Figure 3-13).

Results

Apart from several factors deregulated upon oncogenic transformation, the fourth member of the Tyrosine kinase receptors of the ERBB family *ErbB4* is mildly downregulated in KP^{GEMM} and KP^{CRISPR} . Although the ERBB family is normally associated with tumour growth and cell proliferation, exceptionally *ErbB4* has inhibitory properties. Alterations in *ErbB4* or its down-regulation can be found in poor differentiated or aggressive tumours [Hu et al. 2021].

Despite the strong similarities in both tumour models, it is noteworthy that distinct differences in the regulation of several genes was observed in the transcriptomes of KP^{GEMM} and KP^{CRISPR} (Figure 3-16).

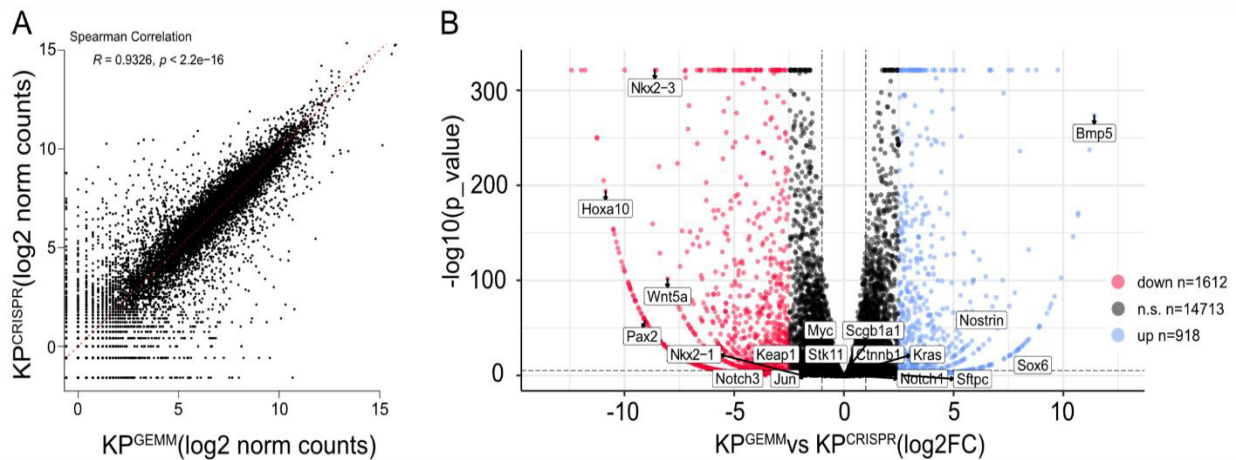


Figure 3-16: Direct comparison of KP^{GEMM} and KP^{CRISPR} highlights difference in oncogenic pathways

A Correlation plot of gene expression in KP^{GEMM} and KP^{CRISPR} relative to each other with linear regression (red line).

Spearman correlation of $R = 0.9326$, $p \leq 2.2 * 10^{-16}$. $n=3$ each

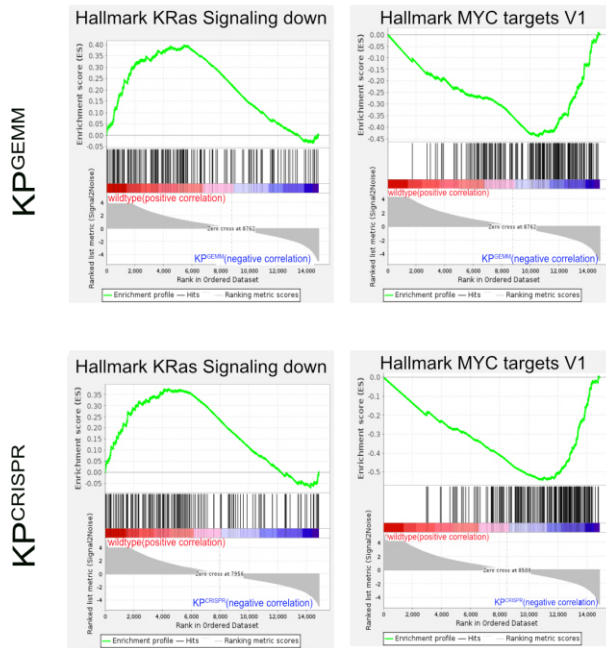
B Volcano blot of genes up- and downregulated ($n = 17243$ genes) in $KP^{GEMM(B)}$ and $KP^{CRISPR(B)}$, relative to relative to each other. Genes up-regulated in KP^{GEMM} are shown in blue, up-regulated in KP^{CRISPR} are shown in red, non-significant (n.s.) in black. Genes of interest are labelled. $n=3$ each

At first, the Spearman correlation ($R = 0.9326$; $p \leq 2.2 * 10^{-16}$) confirms the previous results of a high similarity of KP^{GEMM} and KP^{CRISPR} (Figure 3-16A). In addition, common key players in the development and progression of NSCLC, such as *Scgb1a1/CC10*, *Stk11/Lkb1*, *Keap1*, *cJun*, *cMyc*, *Notch1*, *Notch3* or *Nkx2-1* show no differences when comparing KP^{GEMM} and KP^{CRISPR} directly. However, in KP^{CRISPR} a stronger upregulation of genes involved in the Wnt pathway could be observed, whereas in KP^{GEMM} genes of the TGF-beta pathway as well as genes involved in inflammatory response were up-regulated (Figure 3-16B).

Previous studies demonstrated that a *KRAS* mutant allele-specific imbalance (MASI) significantly correlates with a worse prognosis in patients [Chiose et al. 2011]. Our analysis could show that in KP^{CRISPR} *KRAS* is predominantly homozygous mutated

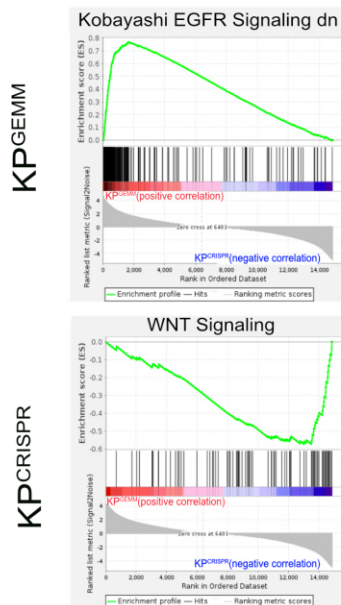
Results

A



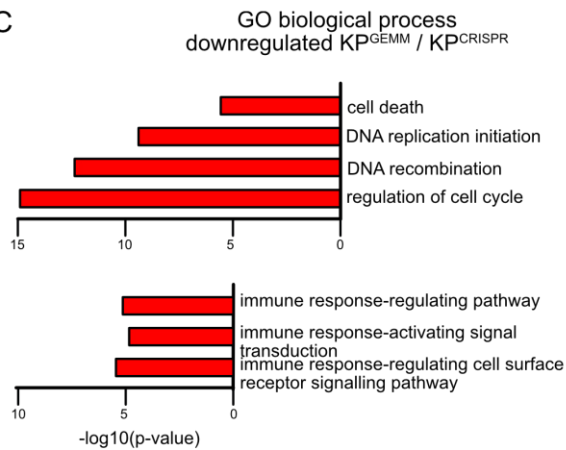
Geneset	(N)ES	pValue
KP^{GEMM}		
KRAS down	1.45	0.006
INFL.RESP.	1.74	<0.0005
MYC target V1	-2.45	<0.0005
MYC target V2	-2.33	<0.0005
DNA_REP.	-2.13	<0.0005
KP^{CRISPR}		
KRAS down	1.43	0.008
INFL.RESP.	1.99	<0.0005
MYC target V1	-3.06	<0.0005
MYC target V2	-2.88	<0.0005
DNA_REP.	-1.74	<0.0005

B

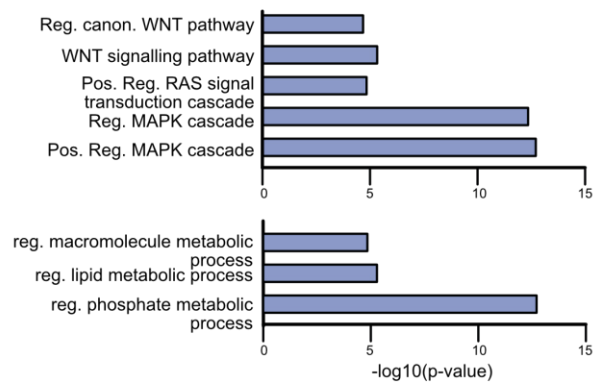


Geneset	(N)ES	pValue
KP^{GEMM}		
EGFR_Signaling	3.45	<0.0005
KP^{CRISPR}		
WNT_Signaling	-2.06	<0.0005

C



GO biological process upregulated KP^{GEMM} / KP^{CRISPR}



Results

Figure 3-17: Gene set enrichment and GO term analysis show the same comparatively deregulated tumour pathways in KP^{GEMM} and KP^{CRISPR}

A Gene set enrichment analyses of significant up and down regulated pathways in KP^{GEMM} and KP^{CRISPR} compared to wild type: negative regulation upon oncogenic KRAS signalling (KRas Signaling down), Myc targets V1 and V2, Inflammatory response (INFL RESP.) and DNA Repair. (N)ES, normalized enrichment score and p Values are depicted in the table. n=3 each.

B Gene set enrichment analyses of EGFR Signaling (up in KP^{GEMM}) and WNT Signaling gene expression (up in KP^{CRISPR}) in KP^{GEMM} and KP^{CRISPR}. (N)ES, normalized enrichment score and p Values are depicted in the table. n=3 each.

C GO biological processes analysis of commonly down (left) and upregulated (right) genes in KP^{GEMM} and KP^{CRISPR} relative to wild type tissue. n=3 each, ranking according to $-\log_{10}(p\text{-value})$

(Figure 3-5 and Sanger Sequencing Figure 6-1), which could be indicative for the up regulation of oncogenic pathways in KP^{CRISPR} compared to the exclusive heterozygous mutational status of KRas^{G12D} in KP^{GEMM}.

In order to gain deeper insights into the distinctly regulated pathways, Gene Set Enrichment Analysis (GSEA) as well as gene ontology biological process (GO-term) analysis were performed (Figure 3-17).

Analysing the commonly up and downregulated gene sets upon oncogenic transformation via KRas^{G12D} and Tp53^{mut} confirmed a high similarity between KP^{GEMM} and KP^{CRISPR}. We found a downregulation of gene set involved in the negative response to the oncogenic KRAS signalling in a comparable manner in both. This further confirms the successful targeting of KRas and the subsequent homologous repair in the KP^{CRISPR} model.

In previous studies, mutations in KRas have been associated with pro-inflammatory as well as anti-inflammatory effects in the tumour microenvironment (TME) and consequent effects on tumour immune responses [Caetano et al. 2016, Cullis et al. 2018]. Here, a downregulation of the gene set for inflammatory response could be observed relative to wild type for both model systems. However, genes that showed a higher expression in this KRas mutant lung cancer would result in a reduced T-cell activation and recognition as well as an inhibition of apoptotic CD3⁺ T-cells (data not shown), which is in line with an immune evasive phenotype of KRas mutant lung cancer [van Maldegem and Downward 2020].

As aforementioned, differences between KP^{GEMM} and KP^{CRISPR} could be observed in the regulation of several genes (Figure 3-16). This observation could be further confirmed with the GSEA of both KP models. The direct comparison of KP^{GEMM} and

Results

KP^{CRISPR} demonstrated an upregulated expression of EGFR signalling in KP^{GEMM} (Figure 3-17B upper panel). On the other hand, the GSEA could confirm the aberrant signalling of the WNT pathway in KP^{CRISPR} compared to KP^{GEMM} (Figure 3-16; Figure 3-17B lower panel).

Lastly, gene ontology (GO) analysis of the most up and down regulated pathways in KP^{GEMM} and KP^{CRISPR} were carried out (Figure 3-17C).

Noteworthy, in both tumour models the most downregulated pathways according to the GO analysis were associated with cell cycle regulation as well as cell death. In line with previous results, we could also observe a strong downregulation in pathways involved in immune response.

Among the significant upregulated pathways, the most enriched processes were regulatory pathways of the MAPK cascade. This further confirms the mutant status of KRas in both tumor models. Additionally, the aberrant WNT signalling we already observed histopathological (Figure 3-13), was present in the GO-term. Finally, to cope with the increased proliferation of both tumour models, metabolic pathways such as lipid, phosphate metabolism processes and macromolecule synthesis are upregulated.

Conclusively, the conducted experiments highlighted, that the classic model and the CRISPR/Cas9 mediated tumour induction led to similar tumour formation at molecular level. Most of the dysregulated signalling pathways analysed here for tumour proliferation, maintenance, immune evasion, and metabolism are similarly altered. Only the restriction of the exclusive heterozygous mutation of KRas in the classical model led to minor differences in the expression of certain oncogenic signalling pathways. Overall, our data suggest that CRISPR/Cas9-mediated tumour induction is suitable substitute for the classical model to target *Trp53* and *KRas*.

3.2 CRISPR/Cas9 mediated genome editing to generate murine NSCLC models reflecting patient relevant *loss-of-function* mutations.

Lung cancer is not only the most common cause for cancer related death [Siegel et al. 2022], the subtype NSCLC is one of the solid tumours with the most somatic mutations [Cancer Genome Atlas Research 2012, Cancer Genome Atlas Research 2014]. This mutational burden and the heterogeneity of tumours have a negative impact on the

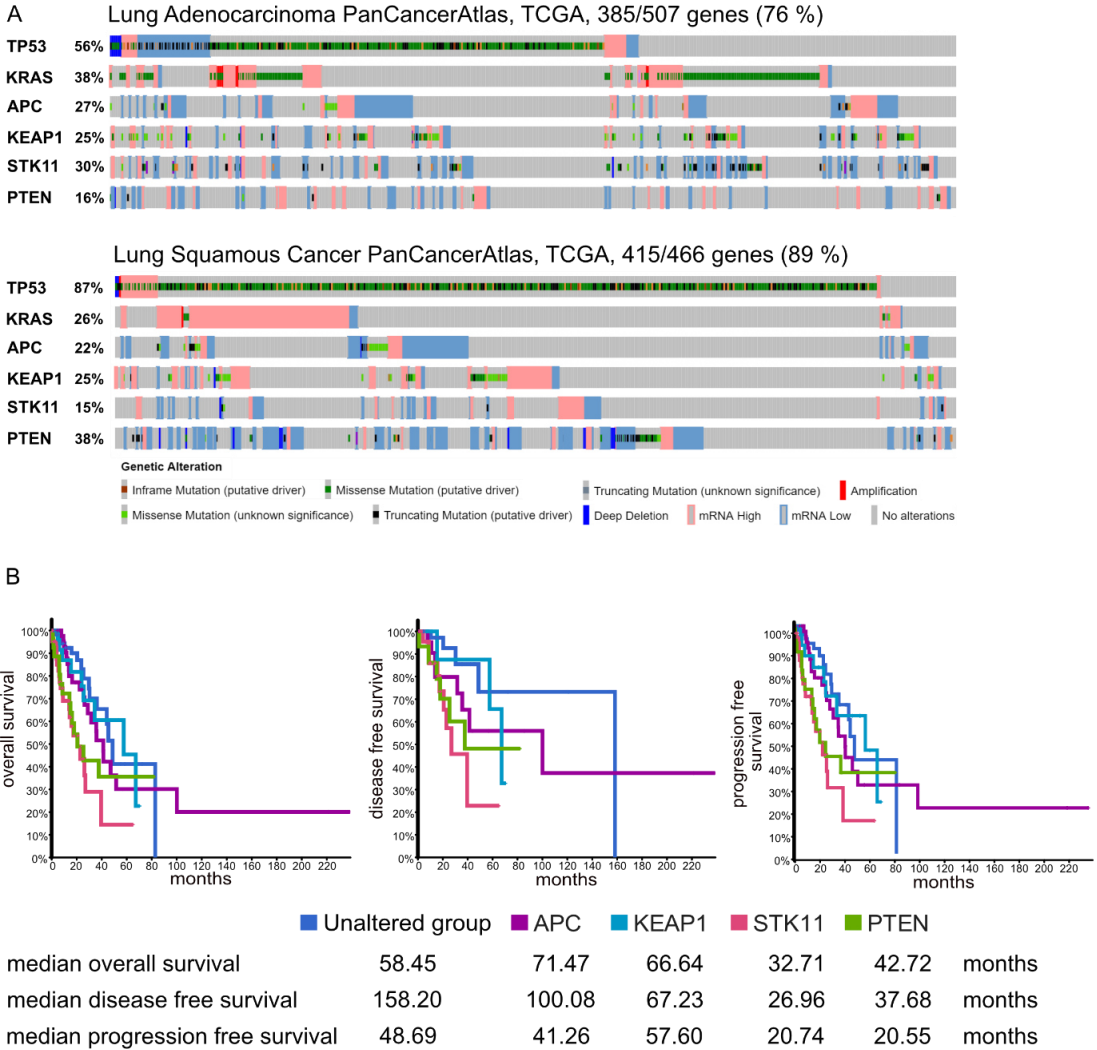
Results

therapy of patients, especially when diagnosed with late stage disease [Rodak et al. 2021]. With the advent of next-generation sequencing, the individual mutations of patients can be determined, allowing for targeted therapy. In order to further refine therapeutic strategies as well as address novel driving mutations or to target therapy resistance mechanisms, we wanted to interrogate if CRISPR/Cas9-mediated somatic mutations for tumour induction can be utilized to swiftly model commonly occurring patient survival relevant mutations *in vivo*.

3.2.1. APC, KEAP1, STK11/LKB1 and PTEN are frequently altered and thus negatively impact patient survival

To recapitulate the mutational burden found in patients with CRISPR/Cas9, we first analysed the occurrence of mutations in tumour suppressors in ADC and SCC with publicly available datasets of patients with NSCLC (Figure 3-18A).

Here we could identify that the members of the ubiquitin proteasome pathway APC and KEAP1, as well as regulator of cell growth and proliferation STK11 and LKB1 and



Results

Figure 3-18: APC, KEAP1, STK11/LKB1 and PTEN are frequently altered and thus negatively impact patient survival

A Diagram of occurring alterations in TP53, KRAS, APC, KEAP1, STK11/LKB1 and PTEN in lung Adenocarcinoma (n= 507) and lung Squamous-cell carcinoma (n= 466). Analysed was the PanCancerAtlas (TCGA) with the mRNA expression z-scores relative to all samples (log RNA Seq V2 RSEM $z \pm 1.5$). The legend of the depiction of alterations is below. (adopted from cbiportal.com)

B Median overall, disease free and progression free survival of patients plotted as KM-Plot with the indicated alterations, relative to patients with no mutations (blue) in APC (purple), KEAP1 (turquoise), STK11 (red) or PTEN (green). The median values in months are shown below the plots. . $p < 0.005$

PTEN are frequently altered in ADC and SCC. Furthermore, alterations in any of the aforementioned tumour suppressors co-occurs with loss of function mutations within the tumour suppressor Trp53 and aberrant MAPK signalling.

The tumour suppressor adenomatous polyposis coli (APC) is a crucial member of the destruction complex for β -Catenin and the governing regulator for the WNT signalling pathway. Infamous are loss-of-function mutations of APC in colorectal cancer, in which more than 80% of all patients lose APC wild type activity [Kwong and Dove 2009]. In addition to colon cancer, studies could link aberrant WNT signalling to poor prognosis as well as a dedifferentiation state of early and late stage non-small-cell lung cancer [Shapiro et al. 2013]. The analysis of public available patient cohorts showed a comparable rate of change of 27% for ADC and 22% for SCC in APC. Furthermore, alterations in APC decreased the disease-free survival relative to the unaltered group by ~37 % and the progression free survival by ~ 15 % (Figure 3-18B), whereas no immediate effect could be observed on the overall survival.

Apart from KRAS and TP53, Kelch-like ECH-associated protein 1 (KEAP1) is commonly mutated in NSCLC [Cancer Genome Atlas Research 2014]. This E3 ligase regulates the protein stability and abundance of NRF2 (nuclear factor erythroid 2-related factor 2) and is thus a crucial factor in the regulation of the antioxidant transcription factor. Furthermore, KEAP1 acts as a tumour suppressor and its loss is associated with resistance to checkpoint inhibition, immune cold tumours, and tumour progression [Romero et al. 2017, Lignitto et al. 2019].

Overall, we could identify alterations in 25 % of ADC as well as SCC patients in the PanCancerAtlas cohort for KEAP1. Comparable to APC, changes on KEAP1 negatively impact the disease-free survival (~ 60%) but showed no significant effect on disease free and progression free survival (Figure 3-18A/B).

Results

Another known tumour suppressor, frequently mutated in KRas/Tp53 driven NSCLC, is the liver kinase B1 (LKB1), encoded by the serine/threonine kinase 11 (STK11) gene [Ding et al. 2008]. Genomic alterations in STK11/LKB1 with co-occurring KRas mutations lead to immunosuppressed, and hence immune-evasive tumours. Given its contribution to the control of the AKT-mTOR pathway, by negatively regulating AMPK, *LKB1*-mutant tumours demonstrate a dysregulated energy metabolism and a decreased survivability [Galan-Cobo et al. 2019]. With regard to patient significance for this particular mutation, 30 % of all ADC patients had an alteration in STK11/Lkb1, whereas only 15 % of all SCC patients in this cohort showed an alteration/mutation in STK11 (Figure 3-18A). Consistent with the literature, 70 out of 149 cases showed co-occurrence of KEAP1 and STK11 alterations in adenocarcinoma and 22 out of 69 cases in SCC [Sitthideatphaiboon et al. 2021]. Loss of regulatory function of STK11/Lkb1 had a significant impact in each survival cohort, with a reduction in overall survival and progression-free survival of about 50% and disease-free survival of about 83% (Figure 3-18B).

Lastly, we were interested in the tumour suppressor PTEN (Phosphatase and tensin homolog) in both cohorts. Phosphatase and tensin homolog deleted on chromosome 10 (PTEN) was described as tumour suppressor and is the main negative regulator of the PI3K signalling pathway. Hence, it plays a vital role in cell growth, survival and metabolism [Stiles 2009]. Alterations in PTEN are associated with a poor prognosis, resistance to radio and chemotherapy as well as targeted therapies and increased metastasize [Gkountakos et al. 2019, Fischer et al. 2022].

Here, the burden of alterations is the reverse of the situation with STK11/Lkb1. Thus, patients diagnosed with SCC had an alteration of PTEN in 38 % of all cases, which manifested itself mainly in reduced expression. On the other hand, 16 % of all ADC cases demonstrated a PTEN alteration (Figure 3-18A). Similar to STK11/Lkb1, those changes in PTEN had severe impacts on the disease (~ 76 %) and progression free survival (~58 %).

Analysis of this publicly available data showed that a rapid and flexible recapitulation of the mutational burden of patient-relevant alterations might be a useful and necessary tool for exploring new treatment strategies, as commonly used murine

Results

models of NSCLC fall short to readily incorporate these additional mutations, which have a significant impact on therapy performance and patient survival.

3.2.2. Modular AAV-vector enables successful targeting of commonly mutated tumour suppressor in mice

In order to recapitulate patient-relevant mutations in a timely and efficient manner, we generated a modular vector system containing all components required for CRISPR/Cas9 mediated genome editing. Therefore, the AAV backbone was extended to harbour additional sgRNA cassettes allowing for the additional targeting of one of the tumour suppressors discussed above (Figure 3-19).

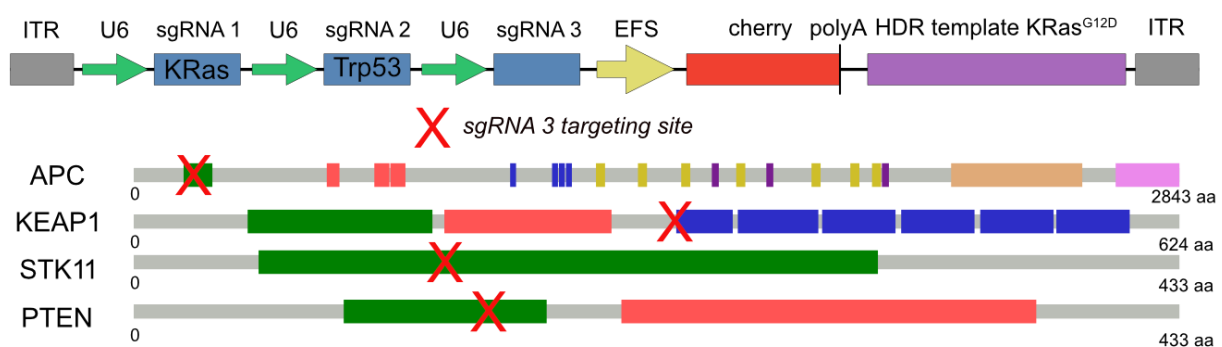


Figure 3-19: Schematic for the AAV approach to rapidly model common loss of function mutations

Schematic representation of the AAV CRISPR cassette. green arrow= murine U6 promoter, blue boxes are sgRNA-*tr*crRNA hybrid structures; yellow arrow= minimal EFS promoter; red = mCherry; purple = KRas HDR^{G12D} with 800 base pairs of murine KRAS genomic sequence encoding the G to D trans-version. sgRNA3 encodes an sgRNA for either *Apc*, *Keap1*, *Lkb1* or *Pten*. sgRNA targeting sequences are shown. Lower schematics show protein structures of APC, KEAP1, LKB1 and PTEN. Marked with a red X are the sgRNA3 recognition sites relative to protein. Schematics were adopted from cBioportal.org.

The AAV backbone first used to generate the KP^{CRISPR} mouse model (Figure 3-3) was used and an additional sgRNA cassette with U6 promoter (green arrow) and the corresponding sgRNA (sgRNA 3 blue) were added.

The sgRNAs were designed to induce CRISPR/Cas9-mediated double-strand breaks in the vicinity of frequently mutated sites of the respective tumour suppressor (red cross) and simultaneously show high efficacy according to the algorithms of Doensch and Marenco-Mateos [Moreno-Mateos et al. 2015, Doench et al. 2016].

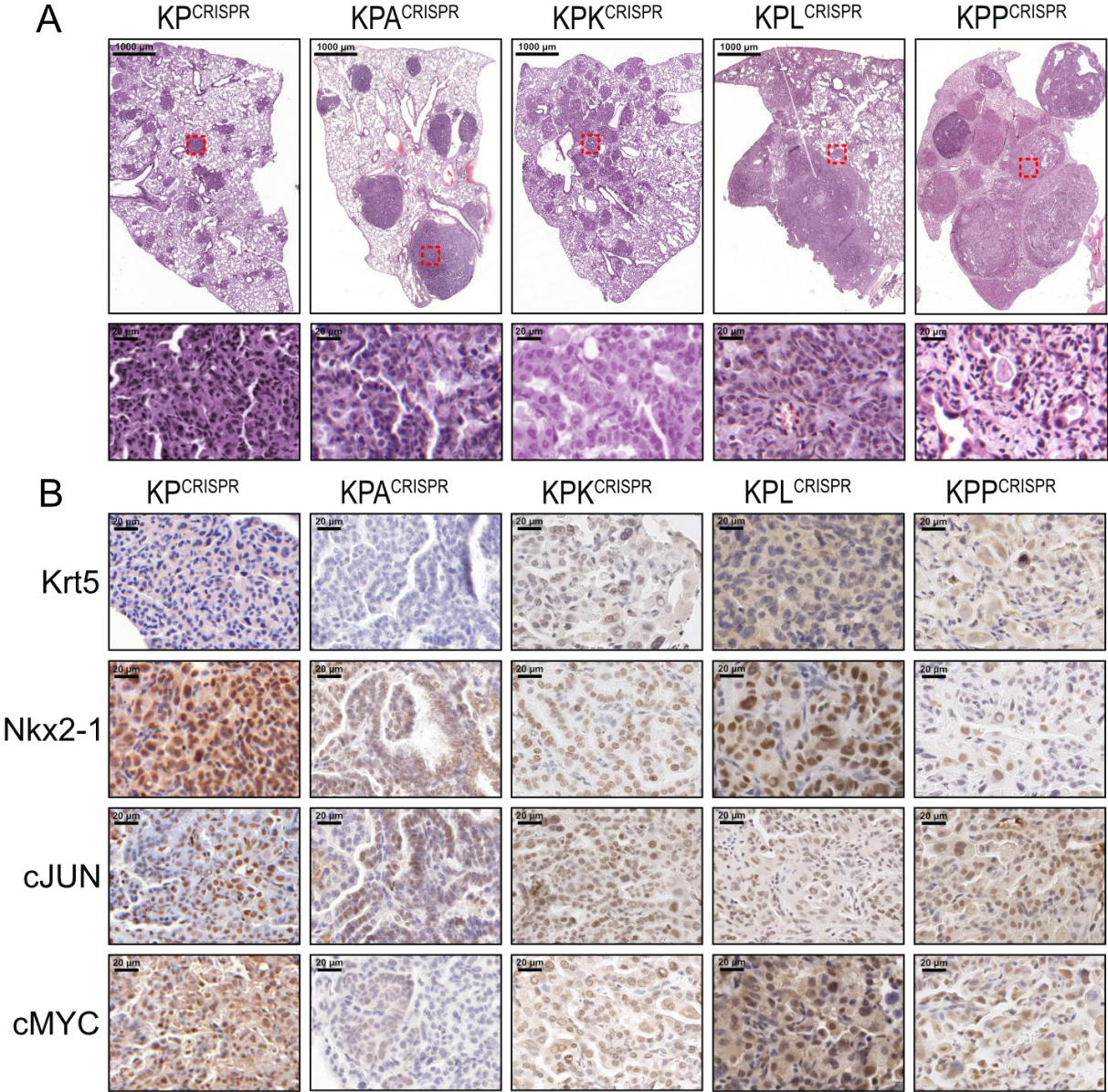
Hence, we targeted *APC* at exon 9, which is a common mutation sites for *APC* in WNT-driven cancer. We aim to achieve a truncation mutation mediated by the CRISPR/Cas9 double-strand break, thus losing the majority of APC. Additionally, APC mutant cells tend to lose the second allele of *APC* via loss of heterozygosity, which would increase

Results

the targeting efficacy of the CRISPR/Cas9-mediated mutation at endpoint [Aitchison et al. 2020].

To recapitulate inactivation or loss of function mutations in *Keap1*, the sgRNA is targeting the 5' site of the seven Kelch domains. As a result, a mutation impairs the binding of the substrate Nrf2 and thus enables translocation of Nrf2 into the cell nucleus [Tian et al. 2020]. To introduce loss of function mutations for both, STK11 and PTEN we target the kinase or phosphatase site, respectively.

In order now to induce tumour formation, animals were i.t. infected with 1×10^{11} PFU of either AAV-DJ-KRas-Trp53 (KP^{CRISPR}) as a control or with an AAV-DJ-KP- with the additional sgRNA cassette targeting APC, KEAP1, STK11/LKB1 and PTEN (KPA^{CRISPR} ; KPK^{CRISPR} ; KPL^{CRISPR} and KPP^{CRISPR} ; $n \geq 3$ each) and analysed 12 weeks post infection (Figure 3-20).



Results

Figure 3-20: Modular AAV-vector enables successful targeting of commonly mutated tumour suppressor in mice and induces lung cancer formation

Animals were infected i.t. with $1 * 10^{11}$ PFU AAV encoding sgRNA targeting KP, KP-APC (KPA^{CRISPR}), KP-KEAP1 (KPK^{CRISPR}), KP-Lkb1 (KPL^{CRISPR}) or KP-PTEN (KPP^{CRISPR}) $n \geq$ each 3.

A Representative H&E images of tumour bearing animals 12 weeks post intratracheal infection of Rosa26^{Sor-CAGG-Cas9-IRES-GFP} mice ($n \geq$ 3 each) Highlighted tumour areas are marked with red dashed squares. (scale bar 1000 μ m and 20 μ m)

B Representative IHC staining for Nkx2-1/TTF-1 and SCC Krt5 marker expression, and the oncogenes cJUN and cMYC in tumour bearing animals 12 weeks post intratracheal infection. (20 μ m)

The formalin-fixed paraffin-embedded (FFPE) tissue was histological processed, and H&E stained (Figure 3-20A).

As in previous experiments, mutation of *Trp53* and activation of *Kras*^{G12D} led to the formation of tumours in infected animals. The morphology of the tumours in KP^{CRISPR} was also identical to previous animal experiments discussed in this thesis. The additional and simultaneous targeting of *KRas* and *Trp53* with sgRNAs against the previously mentioned tumour suppressors led to the development of NSCLC in all 4 cases. It is worth noting that for KPA^{CRISPR}, KPL^{CRISPR} and KPP^{CRISPR} in particular, the additional loss of the tumour suppressor has a significant impact on tumour number, growth, and tumour burden. (Figure 3-20A). In contrast, and controversial to public data, when we compared the loss of KEAP1 to KP^{CRISPR}, the additional loss of the tumour suppressor only affected the number of tumours, but not their size.

Next, we analysed the KP^{CRISPR}; KPA^{CRISPR}; KPK^{CRISPR}; KPL^{CRISPR} and KPP^{CRISPR} tumour bearing lungs regarding their marker expression, for the respective NSCLC subtypes: Adenocarcinoma (ADC) and Squamous-cell carcinoma (SCC) (Figure 3-20B Krt5 and NKX2-1).

Here, as in the previous *Kras*^{G12D}, *Trp53*^{mut} driven lung tumours, we could only detect tumours that were positive for NKX2-1 expression. This strongly suggests an adenocarcinoma subtype, which is confirmed by the absence of Krt5 expression. This observation can also be made in the KPA^{CRISPR} cohort. Immunohistochemical analysis showed only NKX2-1-positive and Krt5-negative tumours in all animals. This is in line with studies analysing APC, were mutations and/or APC gene silencing found predominantly, but not exclusively, in patients with lung adenocarcinoma.[Guo et al. 2014]. Targeting of KEAP, STK11/LKB1 and PTEN resulted in the formation of adenocarcinomas and squamous cell carcinomas, as confirmed by positive staining for NKX2-1 (ADC marker) or Krt5 (SCC marker), respectively (Figure 3-20B).

Results

As already described in Figure 3-10, NSCLC is characterised by the upregulation of additional oncogenes, e.g., cJUN and cMYC, which influence tumour growth and survival. To assess whether additional targeting of the above tumour suppressors affected the expression of common oncogenes, immunohistochemical staining for cJUN and cMYC was performed (Figure 3-20B). Confirming previous results, strong expression of cJUN and cMYC was detected in KP^{CRISPR} . A comparable expression pattern was observed with KPA^{CRISPR} for cJUN, but the overall abundance of cMYC appears to be lower compared to KP^{CRISPR} . In contrast, the three remaining genotypes, KPK^{CRISPR} , KPL^{CRISPR} and KPP^{CRISPR} demonstrated a high abundance of both oncogenic transcription factors.

Noteworthy, KPL^{CRISPR} and KPP^{CRISPR} developed considerable large and interconnected tumour areas (Figure 3-20A).

This increase in tumour burden had a significant impact on animal survival (Figure 3-21).

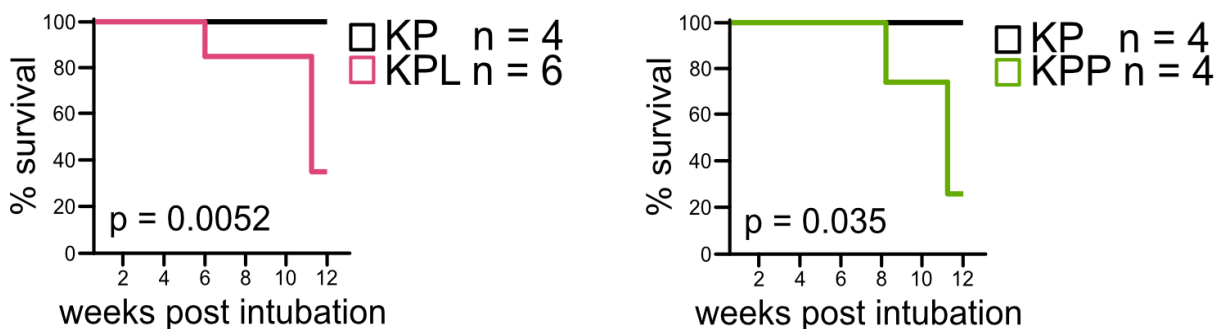


Figure 3-21: Additional loss of STK11/Lkb1 and PTEN decreases animal survival

Kaplan Meier plot of % survival of animals infected with AAV-DJ-KP (black), KPL (red) and KPP (green) in 12 weeks post intubation. (Chi-quadrat test, $p \leq 0.05$)

For KPL^{CRISPR} , the first animal succumbed within 6 weeks due respiratory distress, and in week 8 for KPP^{CRISPR} . In both cohorts, several animals necessitated termination around week 11 due to cachexia and short breath. This observation is consistent with the impact on overall survival of patients diagnosed with lung cancer associated with changes in STK11/LKB1 and PTEN (Figure 3-18).

Next, we wanted to investigate the efficacy of CRISPR-mediated genome editing of the additional targeted tumour suppressors APC, KEAP1, STK11/LKB1 and PTEN, allowing us thereby to attribute the observed phenotype to genetic ablation of desired tumour suppressors.

To this end, we immunohistochemically stained FFPE tissue samples of tumour-bearing animals for the target proteins of interest and compared the total number of

Results

tumours that showed positive staining for the PIO with the negative tumours (Figure 3-22).

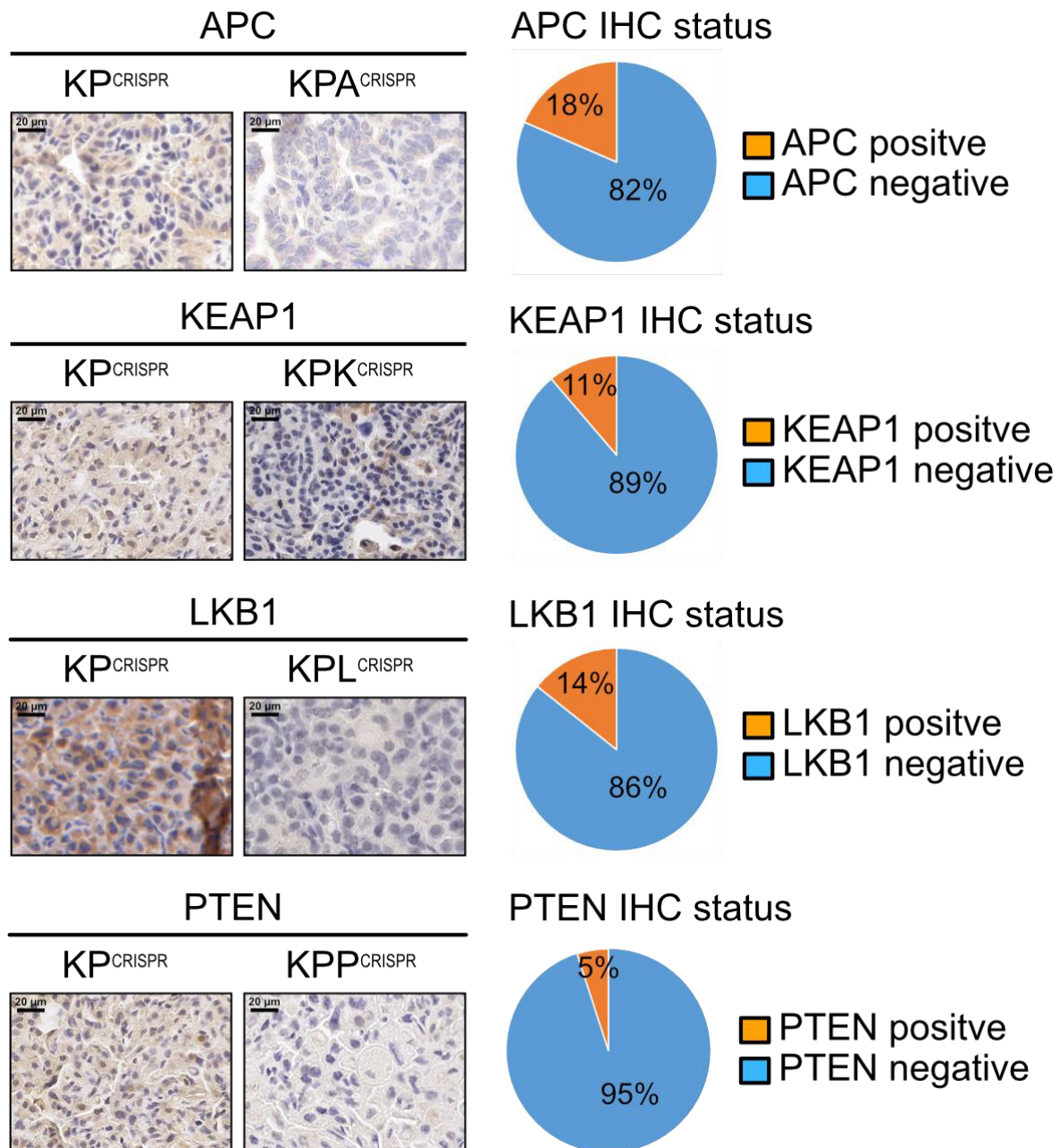


Figure 3-22: CRISPR/Cas9 mediated genome editing as a high targeting efficacy in mice on those tumour suppressors

Representative IHC stainings in KP^{CRISPR}, KPA^{CRISPR}, KPK^{CRISPR}, KPL^{CRISPR} and KPP^{CRISPR} in tumour areas against the sgRNA targets APC, KEAP1, LKB1 and PTEN. Quantification of APC, KEAP1, LKB1 and PTEN positive to negative tumours in the CRISPR/Cas9 mice infected with the respective AAV-DJ. (Scale bar 20µm)

Overall, an efficacy of over 80 % was achieved with all sgRNAs used. While APC, KEAP1 and LKB1 had a null situation in about 85 % of all tumours, only 5 % of the total tumour burden in KPP^{CRISPR} had residual expression of PTEN. The remaining amount of expressed tumour suppressors in this endpoint analysis could indicate an

Results

incomplete CRISPR/Cas9 event, a fully repaired double-strand break or small-in-frame mutations that do not affect expression but may affect protein function.

To further confirm a successful targeting of the aforementioned tumour suppressors, we immunohistochemically stained the lung tumours for known downstream pathway members or targets of the POI and compared the abundance to KP^{CRISPR}, the standard genotype of NSCLC models (Figure 3-23)

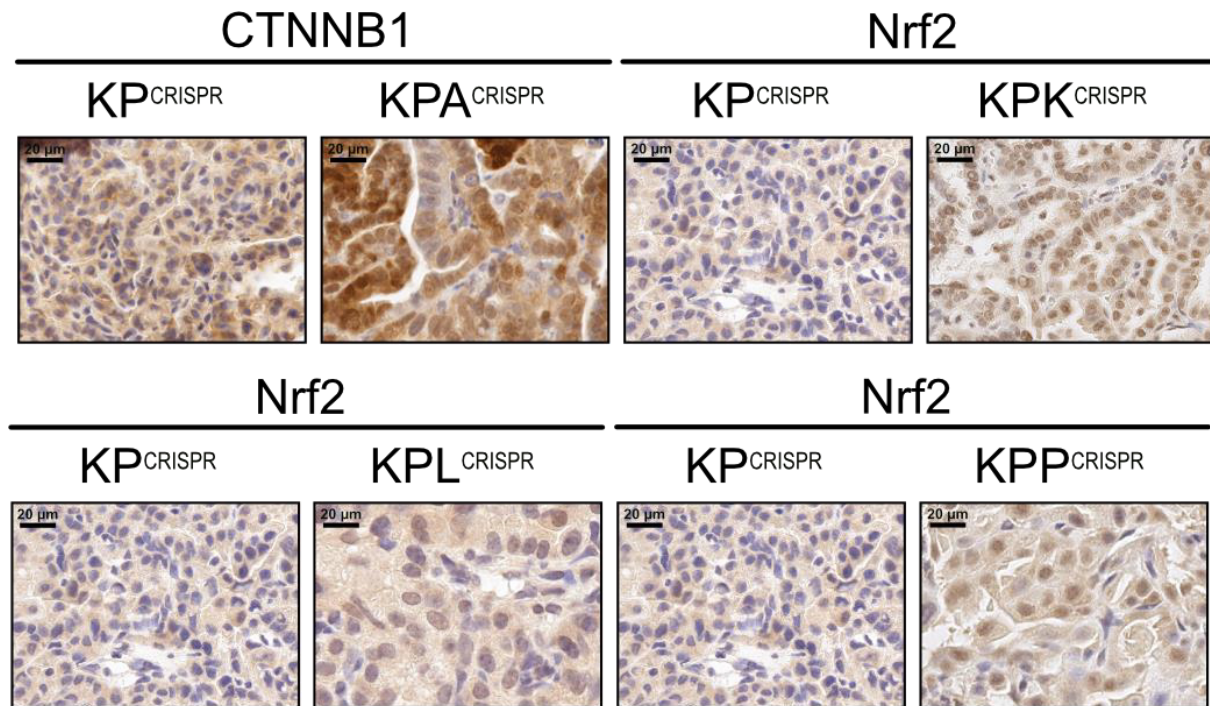


Figure 3-23: Successful targeting of APC, KEAP1, LKB1 and PTEN lead to an increased abundance of downstream pathway member

Representative immunohistochemical staining against CTNNB11 in KP^{CRISPR} and KPA^{CRISPR} and Nrf2 in KP^{CRISPR}, KPK^{CRISPR}, KPL^{CRISPR} and KPP^{CRISPR}. (Scale bar 20μm)

After the loss of APC, an increase in CTNNB1 and an accumulation of β -Catenin in the nucleus were observed.

Loss of KEAP1 increased the abundance of its bona fide target Nrf2, which is in line with recent literature[Tian et al. 2020].Furthermore, an increased amount of Nrf2 was observed in the nucleus after loss of KEAP1. In addition, Nrf2 has been linked to enable cells, especially tumour cells, to cope with oxidative stress, ROS homeostasis and a higher abundance provides tumorigenic advantages. This was not only observed in KEAP1-deficient NSCLC. Abnormal Nrf2 levels have also been observed in association with changes in LKB1 and PTEN [Ma 2013, Rojo et al. 2014, Galan-Cobo et al. 2019]. These reports could be recapitulated in the murine models established in this thesis. In detail, we could detect increased Nrf2 levels for KPL^{CRISPR} and KPP^{CRISPR}

Results

compared to KP^{CRISPR} , which is in line with published data [Kaufman et al. 2014, Rojo et al. 2014, Best et al. 2018].

Lastly, it was investigated how the loss of a tumour suppressor affected the general proliferation state. For this purpose, the FFPE tissue were stained for PCNA, and the abundance of this proliferation marker compared to adjacent wildtype tissue and KP^{CRISPR} (Figure 3-24).

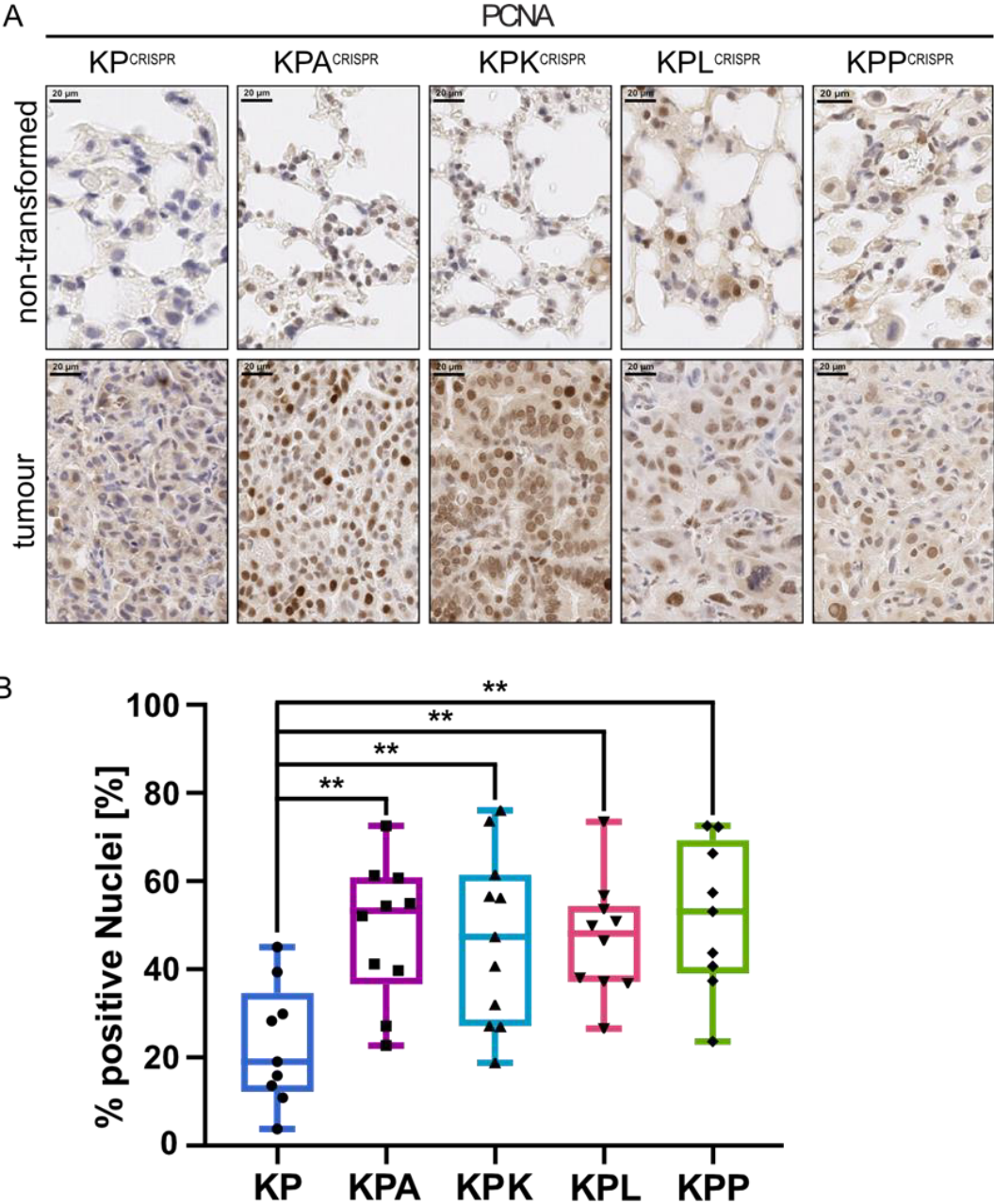


Figure 3-24: Loss of tumour suppressor increased proliferation of tumours compared to KP^{CRISPR}

A Representative immunohistochemical staining against PCNA in KP^{CRISPR} , KPA^{CRISPR} , KPK^{CRISPR} , KPL^{CRISPR} and KPP^{CRISPR} wild type tissue and tumours. (Scale bar 20µm)

B Quantification of % PCNA positive nuclei in at last 10 tumours in KP^{CRISPR} , KPA^{CRISPR} , KPK^{CRISPR} , KPL^{CRISPR} and KPP^{CRISPR} . Data are shown as boxplot, with each box representing the group's median, upper, and lower quantiles, and min/max confidence interval. Individual data points are shown. ($p < 0.05$ Mann-Whitney-Test)

Results

We observed that PCNA in tumour tissue showed strong upregulation at the protein level compared to WT tissue in all mice cohorts (Figure 3-24A). Comparable to previous results, an average of 20% of tumour cells were positive for PCNA expression in KP^{CRISPR} (Figure 3-6, Figure 3-24). It is noteworthy that proliferation is significantly increased when one of the tumour suppressors is lost. On average the amount of PCNA positive cells (~ 50 %) is doubled in KPA^{CRISPR} , KPK^{CRISPR} , KPL^{CRISPR} and KPP^{CRISPR} compared to KP^{CRISPR} (Figure 3-24B).

Taken together, the modular system of the AAV in combination with CRISPR/Cas9-mediated genome editing allows us to create a rapid *in vivo* system for recapitulation of patient-relevant NSCLC-driving mutations. Therefore, it can serve as a reliable and relevant surrogate model to investigate further treatment options and refine targeted (personalised) therapy strategies.

Results

3.2.3. Dual viral approaches enhance applicability of CRISPR for translational research, irrespective of the mouse strain

With the previous experiments, we could demonstrate that CRISPR/Cas9 is reliably suitable for inducing the formation of lung tumours in Cas9-expressing mice. Furthermore, using a modular system, different patient-relevant mutations in tumour suppressors were recapitulated. However, due to the necessity of a spCas9, the system was limited to the Rosa26^{Sor-CAGG-Cas9-IRES-GFP} mice. To test if the CRISPR/Cas9 mediated genome editing can be utilized *in vivo* irrespective of a constitutive expressed SpCas9, we intended to establish a dual AAV virus infection protocol allowing us to use any mouse strain readily available (Figure 3-25).

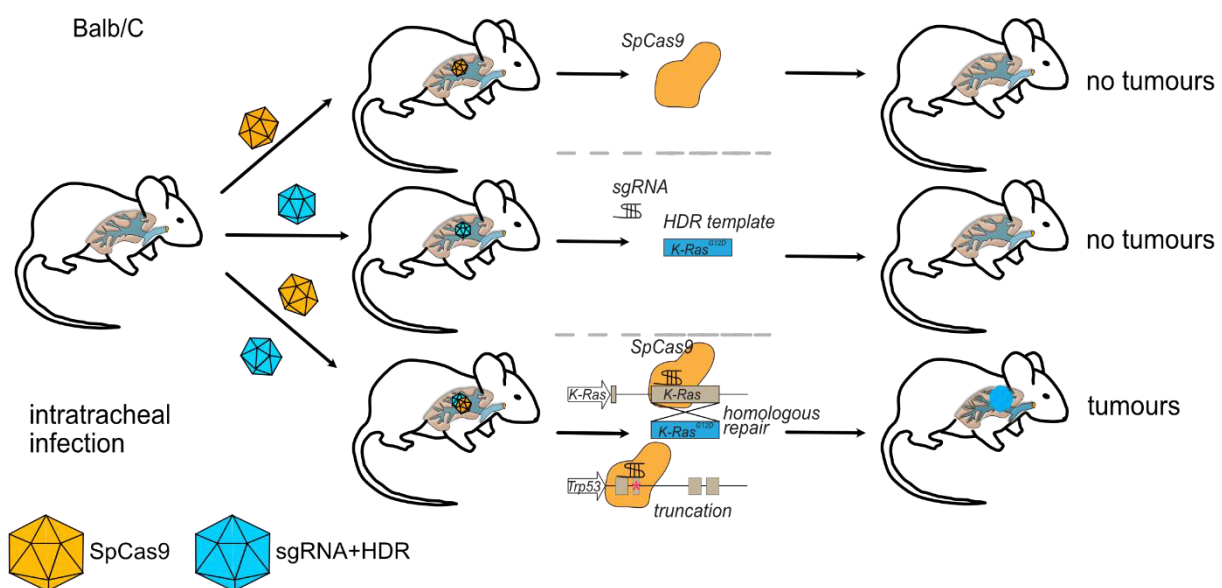


Figure 3-25: Dual viral approach to induce lung tumour formation irrespective of the mouse strain

Schematic diagram of the dual AAV approach of intratracheal infection. To induce lung tumour formation mediated by CRISPR/Cas9 genome editing the mice were i.t. infected with 2 adeno-associated viruses. One AAV encodes for the spCas9 (orange), whereas the second AAV (blue) encodes for the sgRNAs. Upon successful infection, the Cas9 (orange) together with the corresponding sgRNAs targeting either KRas or Trp53 (brown squares) will induce double-strand breaks. In order to achieve a KRas^{G12D} mutation, the AAV is supplemented with a homologous repair donor (blue) encoding for the G12D mutation.

As an experimental setup, we chose to infect mice intra-tracheally with two adeno-associated virus (AAV) and perform an endpoint analysis 12 weeks post-infection. The first AAV encodes for the SpCas9 and the second for the sgRNAs to target Trp53 and KRas including the HDR-template to induce the endogenous mutation KRas^{G12D}. Balb/C mice were infected with the single AAVs and a mix of 1×10^{11} PFU of each virus in a total volume of 60µl and analysed 12 weeks post infection.

Results

The lungs of the tumour-bearing animals were fixed in formalin and embedded in paraffin. After histo-pathological processing, the lung tumours were compared with KP^{CRISPR} . Therefore, we used the adapted staging system of the American Cancer Society, evaluate the grade of the tumours as carried out in Figure 3-7 [AmericanCancerSociety 2019]. Tumours were blindly graded, depending on the size and abnormality of the nuclei, from 1 (atypical alveolar hyperplasia) to 4 (large tumours; high amount of abnormal nuclei), with 1 being the lowest grade and 4 being the highest. Comparing both tumour induction methods, KP^{AAV} -SpCas9^{AAV} and KP^{CRISPR} , no significant difference could be observed in the abundance and distribution of the stages (Figure 3-26).

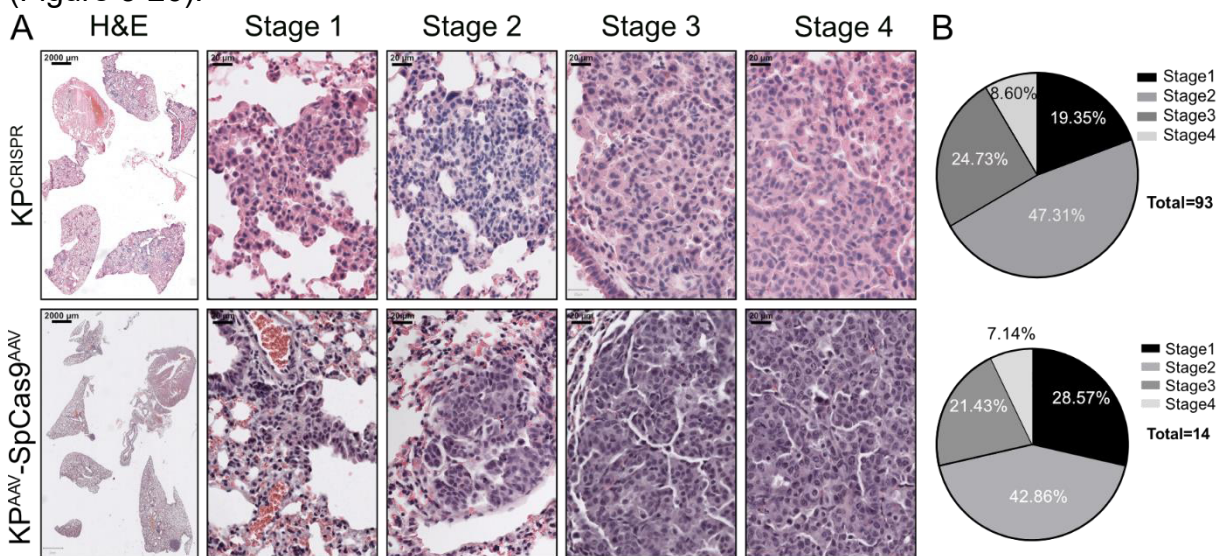


Figure 3-26: KP^{CRISPR} and KP^{AAV} -spCas9^{AAV} presented comparable distributions of all stages

A Representative H&E images of tumour stages KP^{CRISPR} and KP^{AAV} -spCas9^{AAV} according to the adopted American Cancer Society guidelines. Stages ranging from atypical alveolar hyperplasia (AAH, stage I) to stage IV Cancer. (scale bar 2000 μ m and 20 μ m)

B Quantification of the tumour stages blindly determined in KP^{CRISPR} (n=93) and KP^{AAV} -spCas9^{AAV} (n=14) (pValue=0.3433 two-way Anova)

Roughly a quarter of all tumours in KP^{AAV} -SpCas9^{AAV} were graded into stage 1, whereas close to a fifth of all tumours was in stage 1 atypical alveolar hyperplasia (AAH) in KP^{CRISPR} . As already mentioned, the AAV genome is retained as an extrachromosomal episome in infected cells. Furthermore, a double infection of the same cell is a prerequisite to induce tumour formation. It is possible that this does not occur at a high probability rate, and thereby reduces tumour onset in the double viral approach.

Results

In both KP^{CRISPR} and $KP^{AAV}\text{-SpCas9}^{AAV}$, around 47 % and 42 % of tumours were in stage 2, whereas the remaining 30 % of tumours are distributed in stage 3 and 4. In summary, the dual viral approach shows a very comparable distribution of tumour stages, without significant differences compared to KP^{GEMM} and KP^{CRISPR} .

However, we observed a significantly reduced number of tumours in $KP^{AAV}\text{-SpCas9}^{AAV}$ with just 14 tumours in 5 animals compared to 93 tumours in 8 KP^{CRISPR} animals. As the putative tumour inducing cell must be infected with both viruses in a timely manner for successful oncogenic mutation, this is the most probable cause for the low number of tumours.

Next, we wanted to compare the morphological features of occurring tumours. To this end, the marker expression of tumour bearing lungs regarding the respective NSCLC subtypes for ADC and SCC were analysed. The alveolar type II and thyroid transcription factor-1 (Nkx2-1/TTF1) was stained to classify adenocarcinoma, Keratin 5 (Krt5) to classify Squamous-cell carcinoma (Figure 3-27).

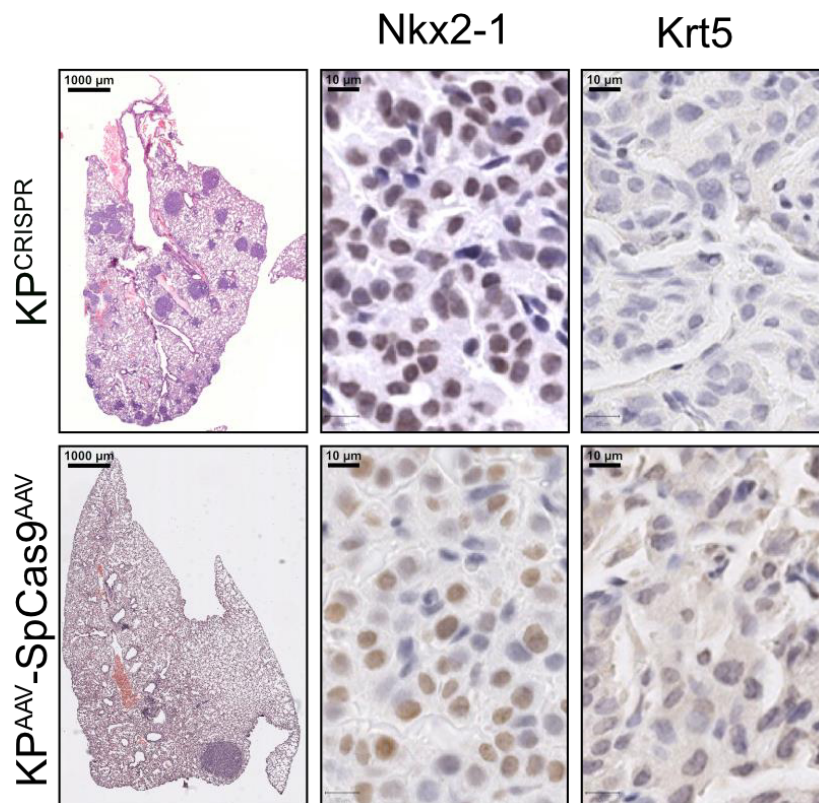


Figure 3-27: Double viral approach led to formation of adenocarcinomas comparable to KP^{CRISPR}

Representative H&E images of tumour bearing animals 12 weeks post intratracheal infection (scale bar 1000 μm and 10 μm) and representative IHC analysis of Nkx2-1 and Krt5. ($KP^{AAV}\text{SpCas9}^{AAV}$; n = 5); (KP^{CRISPR} ; n = 8)

As in the previous comparison of the classical model with CRISPR-mediated tumour induction (Figure 3-9), the dual viral approach with CRIPSR/Cas9 also resulted in the

Results

exclusive formation of ADCs. The adenocarcinoma subtype is confirmed not only by morphology but also by the expression of the typical marker Nkx2-1. Furthermore, the absence of Krt5 was observed as well.

Since we observed the strong decrease in overall tumour number in KP^{AAV}SpCas9^{AAV}, we wondered if differences in the proliferation can be observed and/or if the mutational efficacy is reduced in the dual viral approach.

To test the first hypothesis, we stained the tumour bearing lungs for the proliferation marker Proliferating cell nuclear antigen (PCNA) (Figure 3-28). The quantification of 10 individual tumours revealed no significant difference of PCNA-positive nuclei. Although there were no differences in the amount of PCNA expressing cells, higher protein abundance, indicated by staining intensity, was observed in KP^{AAV}-SpCas9^{AAV}. In order address the efficacy of the endogenous mutation of KRas by the CIRSPR/Cas9 mediated double-strand break and the supplemented repair donor, we stained the lung tumours for phosphorylated MAPK1/3 (pERK) (Figure 3-28).

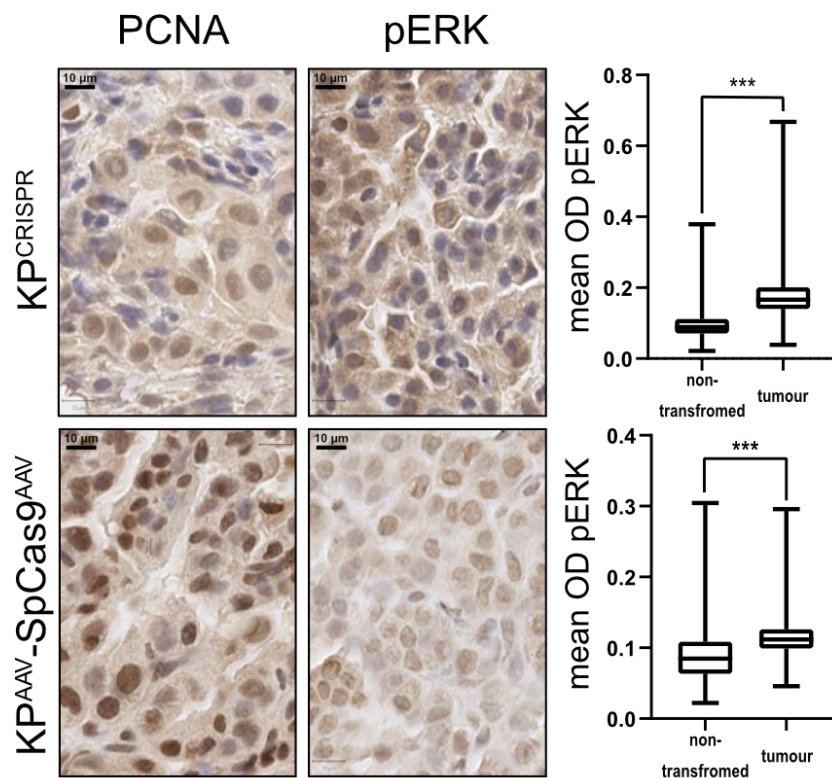


Figure 3-28: Activation of the MAPK-pathway in KP^{AAV}SpCas9^{AAV} to the same extent as in KP^{CRISPR}

Representative IHC analysis of PCNA and pERK from tumour bearing animals 12 weeks post intratracheal infection. (KP^{AAV}SpCas9^{AAV}; n = 4). (KP^{CRISPR}; n = 8) Quantification of the mean optical density (OD) of pERK in adjacent non-transformed tissue and tumours. Data are shown as boxplot, with each box representing the group's median, upper, and lower quantiles, and min/max confidence interval. (n ≥ 5000 cells p < 0.05 Mann-Whitney-Test).

Results

The significantly increased pERK abundance in tumour tissues compared to non-transformed tissue in KP^{CRISPR} and $KP^{AAV}SpCas9^{AAV}$ confirmed a successful targeting of KRas. However, a comparison of the optical density of pERK revealed a higher protein abundance of phosphorylated Erk12 in KP^{CRISPR} compared to $KP^{AAV}SpCas9^{AAV}$. This could indicate a lower efficiency in homologous repair, resulting for example in a heterodimeric mutation of KRas. One possible reason for this could be the overall abundance of the repair donor in the cells at the time when the CRISPR/Cas9 event takes place.

Taken together, the results and IHC staining confirmed successful tumour induction in wild-type Balb/c mice with the dual viral approach. Even though the efficacy is lower, the resulting tumours have a comparable proliferation and show the desired KRas^{G12D} mutation.

To further emphasise the versatility and modularity of our NSCLC mouse model, we intended to target an tumour suppressor as part of the dual viral approach. Therefore, we utilized the sgRNA to target STK11/LKB1 (Figure 3-19) together with Trp53 and KRas and infected Balb/c mice with the $KPL^{AAV}spCas9^{AAV}$ and compared the tumours 12 weeks post i.t. with $KP^{AAV}SpCas9^{AAV}$ (Figure 3-29).

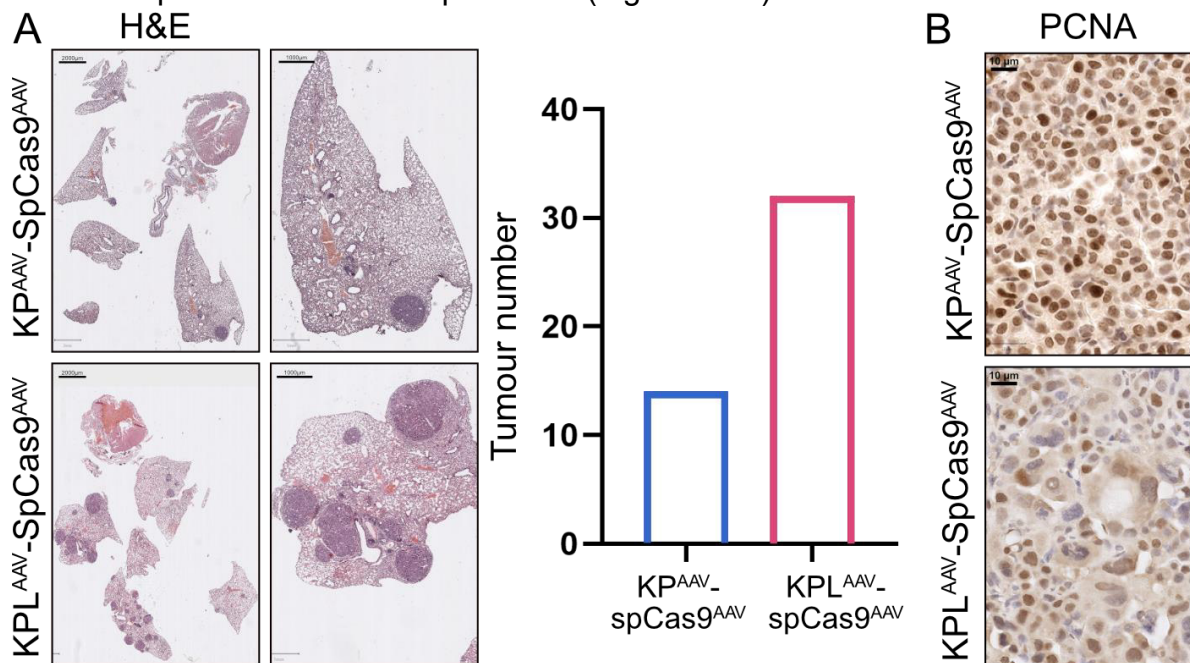


Figure 3-29: Dual viral approach with additional loss of Lkb1 recapitulates the conditional CRISPR model

A Representative H&E images of tumour bearing animals 12 weeks post intratracheal infection with AAV-DJ of Balb/C mice. with $1 * 10^{11} PFU$ encoding for spCas9 and the sgRNAs. (scale bar 2000 μm, 1000 μm) Quantification of absolute tumour numbers in all KP or KPL animals co-infected with an AAV-spCas9. (n =5)

B Representative IHC analysis of PCNA from tumour bearing animals 12 weeks post intratracheal infection. (scale bar 10 μm)

Results

Loss of STK11/LKB1, in combination with mutations of Trp53 and of KRas, resulted in larger tumours, when compared to KP (Figure 3-29A). Furthermore, an increased tumour incidence was observed as well. Thus, these results reflect the previous experiment in which KPL was mutated in constitutive Cas9-expressing animals (Figure 3-23)

Next, we wanted to assess whether the loss of the tumour suppressor affects tumour proliferation to the same extent as previously described. (Figure 3-24). Here, we could detect a robust expression of the proliferation marker PCNA in the KPL^{AAV}-SpCas9^{AAV}. However, due to the overall low number of tumours in the KP^{AAV}-SpCas9^{AAV} model, a statistical analysis was not applicable. Nonetheless, the larger tumours associated with PCNA levels suggest increased proliferation after loss of STK11/LKB1 compared to KP alone.

Next, we wanted to investigate the efficacy of CRISPR-mediated genome editing of the additional targeted tumour suppressors STK11/LKB1 in the dual viral approach. Therefore, we immunohistochemically stained the FFPE tissue samples of tumour-bearing lungs for the target protein of interest, Stk11, and the downstream target pathway effector Nrf2 (Figure 3-30).

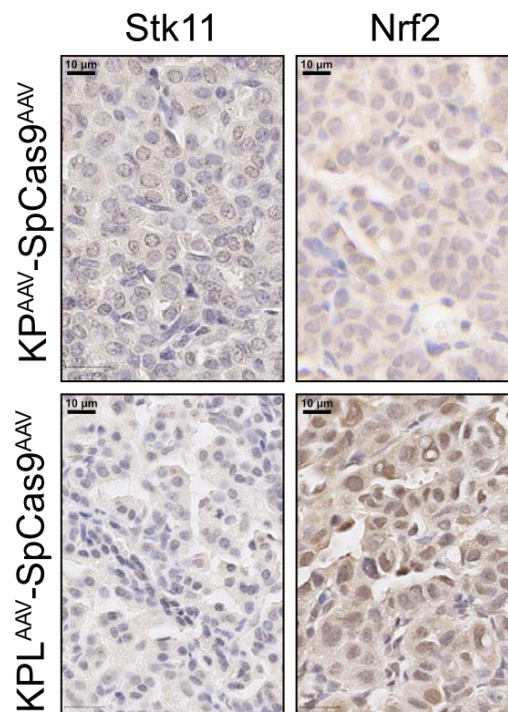


Figure 3-30: Lung tumours had an increased abundance of Nrf2 after loss of Stk11/LKB1 in the dual viral approach

Representative immunohistochemical staining of Stk11/LKB1 and Nrf2 in KP^{AAV}SpCas9^{AAV} and KPL^{AAV}SpCas9^{AAV} (scale bar 20 μm)

Results

Consistent with our previous results (Figure 3-22), we were able to detect the expression of STK11/Lkb1 when we targeted only KP. In this context, only a low amount of Nrf2 was detected in the tumours. The additional loss of STK11/Lkb1, which was confirmed by immunohistochemistry, led to an increase in Nrf2 in the respective tumours. Thus, reproducing the result of the single viral approach (Figure 3-22;23) and confirming the successful alteration of an additional target via the dual viral approach. To finalize the analysis of the dual viral approach, we carried out an immunohistochemical staining to evaluate the marker expression for ADC and SCC in $KP^{AAV}SpCas9^{AAV}$ and $KPL^{AAV}SpCas9^{AAV}$ as well as the abundance of common upregulated oncogenic transcription factors cMYC and cJUN (Figure 3-31).

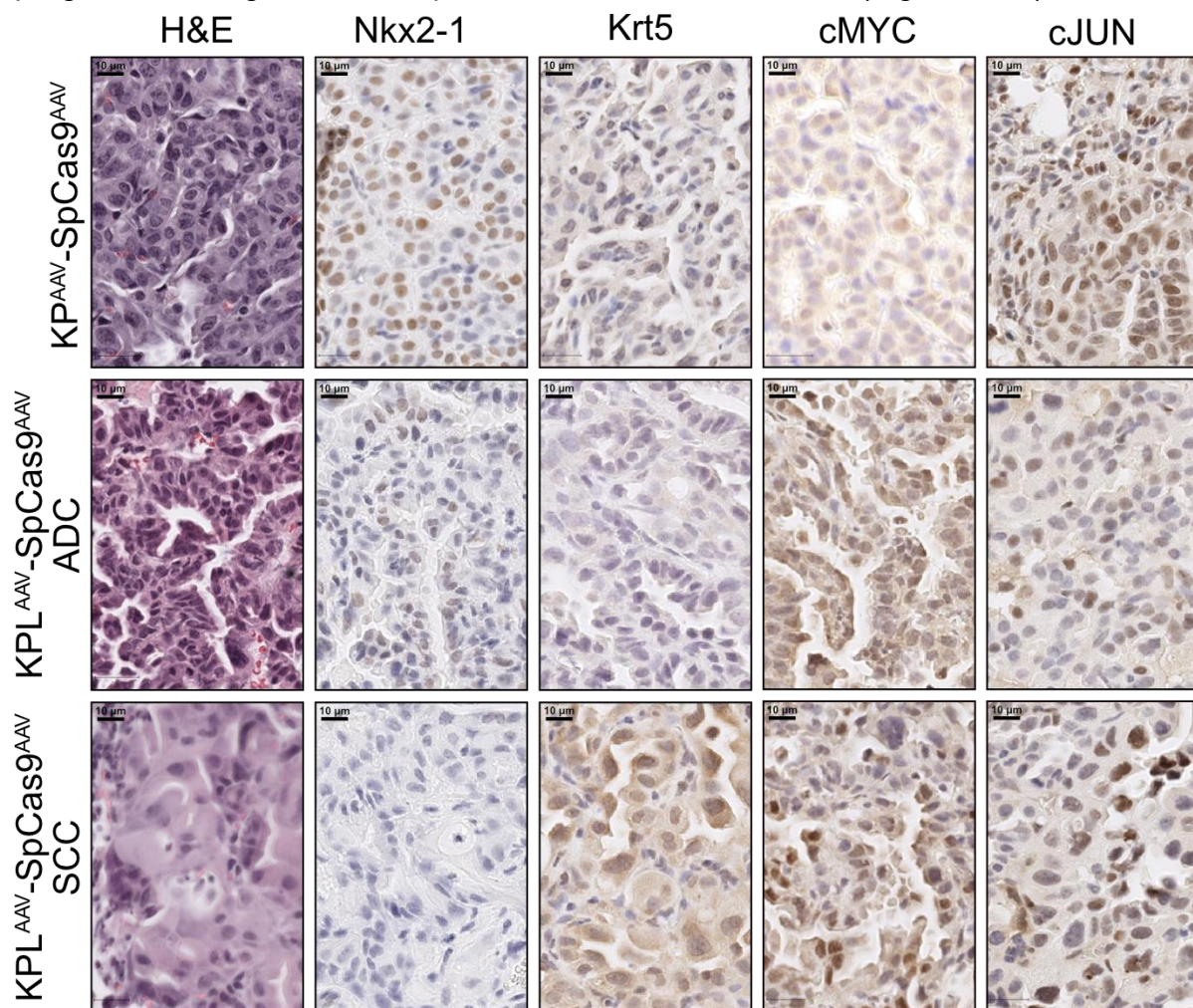


Figure 3-31: Dual AAV-infection induces the formation of ADC and SCC upon loss of Stk11/LKB1

Representative H&E images of tumour bearing animals 12 weeks post intratracheal infection of Balb/C mice with AAV-DJ-KP and KPL as well as AAV-spCas9 ($n \geq 3$ each) (10 μ m)

Representative IHC staining for Nkx2-1/TTF-1 and SCC Krt5 marker expression, and the oncogenes cJUN and cMYC in tumour bearing animals 12 weeks post intratracheal infection. (10 μ m)

Results

Here, too, our earlier findings were confirmed. As described previously, only ADC form in KP, which is confirmed by the presence of Nkx2-1 expression and the absence of Krt5. The development of ADC can also be observed in the KPL cohorts. However, due to the additional loss of Lkb1, SCC can also be detected in the animals, which is confirmed by the expression of Krt5. This is in line with the previous observation we made in our constitutive CRISPR mouse model.

In addition, we found in both, ADC and SCC of $KPL^{AAV}SpCas9^{AAV}$ elevated levels of cMYC and cJUN. The increase in these oncogenes is comparable to the KPL^{CRISPR} model, demonstrating the abilities of a dual infection system and the resulting flexibility for further downstream applications.

Finally, the tumours were examined for the presence of SpCas9. Cas9 was detected in the constitutively expressing $Rosa26^{Sor-CAGG-Cas9-IRES-GFP}$ mice, but all tumours in the dual viral approach were devoid of SpCas9. This indicates the loss of the extrachromosomal viral genome (Figure 3-32).

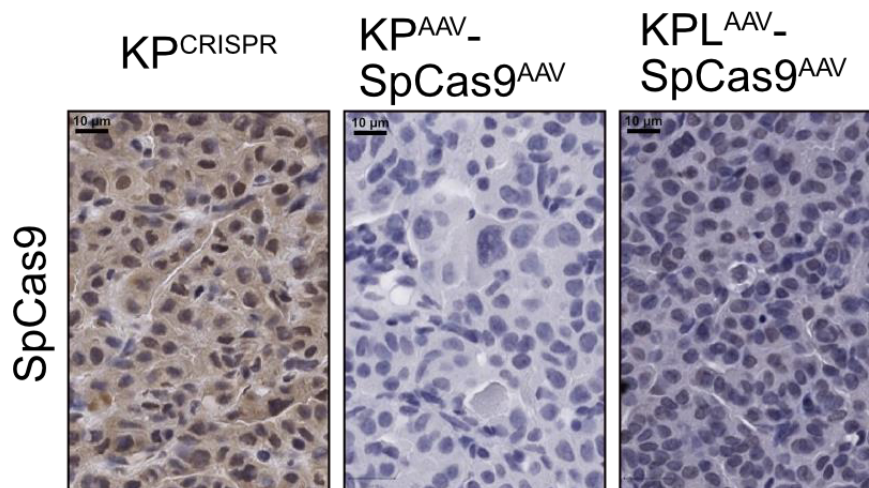
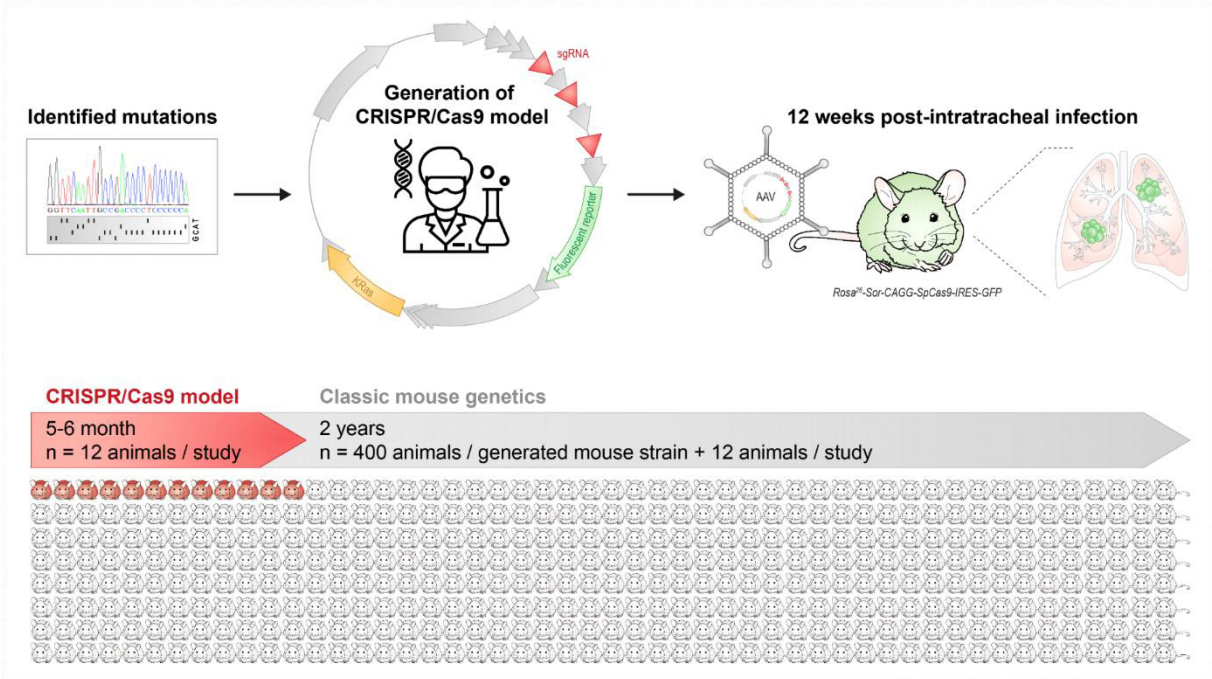


Figure 3-32: Lung tumours in the dual viral approach have no stable expression of spCas9 12 weeks post infection

Representative IHC images of spCas9 in $KP^{AAV}SpCas9^{AAV}$ and $KPL^{AAV}SpCas9^{AAV}$ and $KPCRISPR}$ (scale bar 20 µm)

Results

Taken all of the results together, we could demonstrate that the implementation of CRISPR/Cas9 mediated genome editing induces lung tumour formation in animals in a rapid and reliable fashion. The modular system enables us to quickly recapitulate patient relevant mutations with a defined genetic background. Furthermore, with the dual viral approach, tumour onset is irrespective of the mouse strain. This will reduce the total number of animals needed for *in vivo* studies, as costly breeding for the introduction of relevant mutations will become less necessary (Figure 3-33).



SCIGRAPHIX Scientific Illustrations
 Dr. Sandy Pernitzsch
scigraphix@gmail.com

Figure 3-33: Schematic summary of the advantage of a CRISPR/Cas9 mediated NSCLC mouse model

Discussion

4 Discussion

Research on Non-small cell lung cancer (NSCLC) in mouse models has been instrumental in understanding the disease's biology, testing novel therapies, and exploring mechanisms of drug resistance. Mouse models, particularly genetically engineered mouse models, have played a critical role in advancing NSCLC research. These mice are genetically engineered to develop specific genetic alterations commonly found in human NSCLC, such as activating mutations in KRAS or alterations in tumour suppressor genes like TP53.

For nearly two decades the primary NSCLC mouse model was and is Trp53^{fl/fl} KRas^{lsI-G12D/wt} developed by Tuveson, Jacks and Berns [Jackson et al. 2005, Talmadge et al. 2007, DuPage et al. 2009]. Although it recapitulates a large proportion of ADC and SCC patients, this conditional model is limited in representing the genetic complexity of NSCLC. With the advent of CRISPR/Cas9, reflecting this complexity in the genetic landscape of NSCLC has been simplified. [Sanchez-Rivera et al. 2014, Wang et al. 2014].

4.1 CRISPR/Cas9-mediated editing induces formation of NSCLC morphologically and molecularly indistinguishable from the classical model

In this work, we sought to address the question of whether CRISPR/Cas9-mediated tumour induction is comparable to conditional Cre-mediated loss of TP53 and activation of KRAS^{G12D} expression. Therefore, we compared primary lung tumours induced by both systems at the macroscopic and molecular level.

First, we asked ourselves what type of application would be most reliable and easy to handle in order to successfully administer the virus. To prevent tumour formation outside the lungs, intratracheal installation is the first choice. This was introduced in 2009 as non-invasive procedure that can be performed quickly and reliably under light anaesthesia [DuPage et al. 2009]. This form of viral delivery was also used in the classical model and in the first application of CRISPR-mediated lung tumour induction by Platt et al. [Jackson et al. 2005, DuPage et al. 2009, Platt et al. 2014] Therefore, not only for ease of application, but also to maintain comparability, this was an obvious choice for us.

Discussion

To directly compare primary lung tumours induced either by Cre-mediated activation of KRAS^{G12D} expression and complete loss of both TP53 alleles, or by CRISPR/Cas9-mediated endogenous knock-in of KRAS^{G12D} and introduction of loss-of-function mutations in TP53, animals were infected with AAV-DJ.

The comparison of tumour burden revealed no significant differences in tumour area % normalised to total lung tissue (Figure 3-5). This indicates that both methods have a highly similar capability of tumour induction. Although there was no significant difference, some KP^{GEMM} animals developed larger tumours, occupying about twice the lung area as the KP^{CRISPR} animals at the same time point. A possible explanation might lie in the complete loss of TP53 and the expression of the dominant KRAS^{G12D} immediately after successful recombination. This observation is consistent with published data where complete loss of TP53 accelerates the progression of KRAS-driven lung cancer, especially early on. Jackson et al. were able to show that a TP53 null situation leads to increased tumour burden and faster proliferation in the first 6 weeks in Cre-mediated loss in mice. [Jackson et al. 2005, Zheng et al. 2007]

In addition, the CRISPR-induced double-strand breaks must be repaired by homologous recombination strictly using the supplied repair donor template to successfully implement the KRAS^{G12D} mutation in the KP^{CRISPR} model. HR is limited to S and G2 phase in cells, limiting the efficacy of targeted genome editing and potentially delaying tumour onset [Ira et al. 2004]. Further studies have demonstrated, that a HDR efficacy below 1 % to up to 16 % is achievable, depending on organ, HDR donor size and age of animals [Platt et al. 2014, Behr et al. 2021] In comparison, AAV delivered Cre-Recombinase showed effective recombination in 20 % up to 63 % of cells [Abdallah et al. 2018]. This highlights, that precise genomic alterations facilitated by CRISPR/Cas9 are just at its beginning and still need to be improved.

One possible adjustment would be the size of the HDR and the length of the homologous arms (HA) for directional integration. Here we used a donor template of 800 bp encoding only for the endogenous mutation of KRAS without additional knock in's. Ranawakage et al could show that shorter homologous arms in the repair template can increase the efficacy in a locus dependent fashion [Ranawakage et al. 2020]. If this observation holds true for the KRAS locus remains to be investigated.

Discussion

A second option to increase the efficacy could be a cell cycle dependent expression of Cas9. Limitation of Cas-induced DSBs in G2 or S phase may focus on homologous recombination as the preferred repair mechanism. In cells, a timed delivered Cas9 sgRNA complex could increase the HDR rate up to 38 % [Lin et al. 2014]. A cell cycle dependent Cas activity has been tested in 2020 and was able to increase the genome editing accuracy in cellulo, but has not been yet implemented in mice [Matsumoto et al. 2020].

Despite the differences in Cre mediated and CRISPR/Cas9 mediated tumour initiation, at end point analysis after 12 weeks, the tumour area was not significantly different. This may suggest that the growth advantage of Cas9-mediated mutagenesis is similar to that of Cre recombination. Analysis of the genomic status of our targeted loci (Figure 3-8) in isolated cells from primary tumours revealed loss-of-function mutations and indels in the targeted TP53 region using genomic PCR and Sanger sequencing. Furthermore, we were not able to detect heterozygous TP53 alterations, when sequencing the isolated primary tumour cells. Consistent with this observation, mutant TP53 drives the loss of heterozygosity of the wild-type allele, particularly at early tumour onset [Niederacher et al. 1998, Ghaleb et al. 2019, Ghaleb et al. 2020].

Though, in this thesis, we did not directly analyse the TP53 mutations occurring in primary tumours at the DNA level without culturing them in tissue culture. To better understand which mutations occur *in vivo* and whether Cas9-mediated targeting of TP53 results in truncations or other mutations, direct Sanger sequencing of these tumours is required.

Several publications could show, that mutant TP53 can not only abolish the tumour suppressing functions but can accumulate gain-of-function (GOF) mutations as well. Several 'hot spot' mutations in TP53 are known, e.g., R273H, R248Q, R282H, which are related to GOF. They affect the DNA-binding domain or alter the conformation of TP53. This promotes proliferation, metabolic activity, immune evasion and chemoresistance. [Pfister and Prives 2017, Kim and Lozano 2018, Blagih et al. 2020] The underlying mechanism of Cre recombination prevents the study of this GOF in the chosen model, as TP53 is completely lost. A GEMM carrying this mutation under the control of an LSL cassette or expressing a mutant variant of TP53 would have to be

Discussion

used [Jackson et al. 2005]. However, this would require the existence or breeding of such an animal.

The use of Cas9 could allow the study of GOF mutations in TP53 in a number of ways. On the one hand, sgRNA-mediated mutation by NHEJ can be used to study whether these mutations confer an advantage and accumulate over time. On the other hand, HR-mediated targeted point mutations allow the study of these TP53 variants in a defined genetic background.

Analysis of proliferating cells in the tumours derived from both methods showed no significant difference here either (Figure 3-6). This also underlines how similar the tumours behave and indicates that not the type of initiation plays a role, but rather the underlying mutations. Further supporting this observation is the similarity in tumour stages, that were observed (Figure 3-7).

A highly comparable distribution of all 4 stages were observed in KP^{GEMM} and KP^{CRISPR}. The presence of all stages after twelve weeks may be an indication of current tumour heterogeneity. A potential reason for the early stages could be an insufficient recombination in KP^{GEMM} or Crispr/Cas9-mediated DSB and HDR were not efficient in KP^{CRISPR}. It has been shown that the loss of only a single TP53 copy does not strongly affect the progression of KRAS mutant NSCLC [Jackson et al. 2005]. Furthermore, loss of TP53 alone could show a reduced progression. Wild type KRas has been proposed to have a suppressive function on tumour development [Zhang et al. 2001]. On the other hand, an increase in genomic instability can be assumed due to the loss of TP53 [Zhang et al. 2017]. Thus, more advanced tumours could accumulate additional mutations that further accelerate tumour progression and proliferation, which will subsequently lead to higher staging and larger tumours. In summary, the observed tumour stages are in line with other published studies, where lung tumour formation was driven by mutations in KRAS and TP53 [DuPage et al. 2009, Platt et al. 2014]. The variance in tumour grades could be indicative of a multifocal formation of tumours, suggesting that tumours should be considered individually.

It is noteworthy that despite having stage IV tumours no metastases were found in both models. This observation is in line with previously published studies, where metastasis were found in KRAS^{G12*}/TP53^{mut} lung cancer at later time points, earliest 18-20 weeks post infection [Zheng et al. 2007, DuPage et al. 2009].

Discussion

In order to gain deeper insights in similarities and differences in tumour onset and mutational burden, longer timepoints should be evaluated. Also, a longer period of animal experiments could show how strongly the models behave in terms of metastasis and tumour progression.

Mutations and alterations in the Rat sarcoma family members are common in NSCLC, with Kirsten rat sarcoma (KRAS) accounting for 85 % of all mutations [Soh et al. 2009]. Approximately 30 - 35 % of all NSCLC cases are diagnosed with alterations in KRAS, which will subsequently lead to an activation in the MAPK and PI3K pathways.[Malumbres and Barbacid 2003, Prior et al. 2020]. In this thesis we recapitulate the KRAS^{G12D} mutation with the homologous recombination after CRISPR-mediated DSB. The first lung cancer mouse models, as well as the classic model from 2005 and the CRISPR model from 2014, used this mutation in KRAS. Therefore, this was the only mutation we could use for a direct comparison [Jackson et al. 2001, Jackson et al. 2005, Platt et al. 2014].

We were able to amplify the targeted locus of KRAS in KP^{GEMM} and KP^{CRISPR}. The band intensity for KP^{GEMM} was lower compared to wild type. This could indicate a successful recombination with subsequent LOH which has been described for *KRas*^{G12D/wt} before [Ma et al. 2022]. In the analysed KP^{CRISPR} tumour cell lines, bands comparable to wild type were detected. This could indicate either successful recombination to *KRas*^{G12D}, homologous repair to wild-type *KRas*, or no CRISPR/Cas9 event at all. Therefore, successful point mutation was confirmed by Sanger sequencing (Appendix Figure 6-1). In addition, successful activation of the MAPK due to the mutation of *KRas*^{G12D} was confirmed by an IHC staining of the phosphorylated MAPK1/3 (p-ERK) (Figure 1-2, Figure 3-8 **B**). In both models, significantly elevated levels of p-ERK compared to adjacent non-transformed tissue were observed. This suggests that endogenous mutation in the Cas9-background with the corresponding HDR donor leads to KRAS activation comparable to the Cre system.

As already mentioned above, no in detail analysis of primary tumours were carried out. Similar to the mutational burden in TP53, the efficacy of the endogenous mutation on KRAS should be investigated.

Nevertheless, this analysis shows that targeted endogenous mutation of oncogenes is possible. This allows us to introduce targeted point mutations and to study them in a

Discussion

genetically defined context. In the context of KRAS, with CRISPR/Cas9 hetero- and homozygous mutation in KRAS can be introduced and studied. This is not possible with the classical model, since one wild type allele of KRAS is necessary. The biallelic LSL-cassette would abolish KRAS expression and is embryonically lethal [Ferrer et al. 2018].

As described in the introduction, KRAS^{G12D} is just one of the driving KRAS mutations found in NSCLC patients. This particular point mutation reflects a large subgroup of non-smoking patients, but not the entire clinical situation [Dogan et al. 2012]. Studies have demonstrated the role of different KRAS point mutations and their impact in prognosis and therapeutic interventions. Patients with smoking-induced adenocarcinomas have a higher frequency in KRAS G12C/V mutations. This leads to an increased activation of the NFκB pathway as well as more frequent metastasis to the neighbouring lymphatic system and to the pleura [Ihle et al. 2012, Wu et al. 2021]. By adapting the HDR donor, we may be able to reproduce these mutations very quickly in our model and study them in a defined genetic context.

In the broadest sense, these endogenous genomic alterations could allow us to introduce and analyse other driving point mutations. For example, in squamous cell carcinoma, mutations in KRAS are less common, but activations in PI3K are more commonly diagnosed (Figure 1-2) [Gridelli et al. 2015]. In addition, point mutations in EGFR are more prevalent in patients with an Asian background than KRAS [Cascetta et al. 2022]. CRISPR/cas9 mediated genome editing might be a promising tool to reflect both mentioned situations in NSCLC mouse models as well.

Next, we analysed the KP^{GEMM} and KP^{CRISPR} tumour bearing lungs regarding their marker expression, for the respective NSCLC subtypes: Adenocarcinoma (ADC) and Squamous-cell carcinoma (SCC) (Figure 3-9).

In line with published data, we mainly identified adenocarcinomas in both models. The analysed tumours showed positive expression of the clinically relevant markers Sftpc and Nkx2-1, which are used to histopathologically identify adenocarcinoma. [Jackson et al. 2001, Jackson et al. 2005] Notably, a small proportion of KP^{GEMM} tumours tested positive for the expression of Krt5, a marker for SCC. However, subsequent analysis using a second SCC marker, Sox2, was negative. [Gurda et al. 2015, Ferone et al. 2016] A potential explanation for this observation could be, that, by using an AAV-DJ

Discussion

the tropism for cells was different compared to the previous studies. There, Adenovirus, Lentivirus and AVV-9 were used [DuPage et al. 2009, Platt et al. 2014]. A speculation would be, that the randomized character of the AAV-DJ changed its tropism. Application of luciferase encoding AAV-DJ could show, that this virus predominantly infect AT2 cells, but a small proportion was able to infect endothelial cells as well [Grimm et al. 2008]. These cells express Krt5, and their progenitor cells have been speculated as cell-of-origin for SCC [Langer et al. 2010, Lu et al. 2010, Giangreco et al. 2012].

A second possibility could be a mixed tumour subtype identity. A minor proportion of NSCLC patients have been diagnosed with the biphasic tumour Adenosquamous carcinoma (ASC) with an incidence of 0.4 % up to 4 % depending on how firmly the WHO guidelines on classification are interpreted. [Fitzgibbons and Kern 1985, Ishida et al. 1992, Mordant et al. 2013] This rare tumour has morphological and immunohistological characteristics of adenocarcinoma and squamous cell carcinoma, and overall has a worse prognosis ADC or SCC [Zhu et al. 2018]. However, the mechanism of how this tumour develops is not fully understood. Concurrent alterations in PI3K or EGFR in combination with KRAS^{G12D}, as well as point mutations in TP53, have been detected in sequenced ACS tumour samples and have been suggested to be a possible prerequisite for this tumour subtype. Furthermore, a transdifferentiation of ADC to SCC has been observed in KRAS driven NSCLC [Han et al. 2014, Vassella et al. 2015]. Assuming that the nature of the TP53 point mutation and the accumulation of further alterations in EGFR or PI3K associated with KRAS^{G12D} causes transdifferentiation to ASC, this CRISPR/Cas9 model presented here may be appropriate to study transdifferentiation. The fact that we were not able to detect ASC in the KP^{CRISPR} model is probably only due to the number of animals or the length of the animal experiment. As this tumour entity is very rare, a higher number of animals, a prolongation of tumour growth, but also a targeted induction of the proposed alterations could lead to the development of ASC.

Since we found a high similarity in marker expression in KP^{GEMM} and KP^{CRISPR}, we wanted to investigate whether both tumour models upregulate important oncogenic lung cancer transcription factors, regardless of the method of tumour induction. Due to the dependence of lung tumours on transcription factors such as members of the AP-

Discussion

1 family, cMYC, the WNT signalling pathway and members of the NOTCH family, we hypothesised upregulation in their signalling pathways. In line with publicly available data (Figure 3-10) and previous published studies, commonly dysregulated transcription factors e.g., c-MYC, JUNB, JUND, Notch1, Notch3 and CTNNB1 are significantly higher abundant in both tumour models compared to adjacent non-transformed tissue (Figure 3-11-13). [Nakayama et al. 2014, Xu et al. 2014, Hartl 2016, Sanchez-Vega et al. 2018] However, the AP-1 family members abundance in the tumours is significantly reduced compared to adjacent wild type tissue (Figure 3-11). This observation is unusual, as studies have shown that c-Jun is necessary for RAS-mediated oncogenesis, whereas JUND has a suppressive function in the context of RAS [Pfarr et al. 1994, Johnson et al. 1996]. Nevertheless, a more recent study could demonstrate an opposite effect. In KRAS^{G12D} mutant mice lung adenocarcinoma cJUN has a role pointing more towards a tumour suppressive function rather than oncogenic. Furthermore, for a subgroup of human ADC patients, loss-of-functions in c-Jun can be observed. In contrast, JUND takes over the oncogenic role and drives proliferation and activation of the p38a MAPK pathway. [Ruiz et al. 2021] This observation is recapitulated in a very comparable way in the two tumour models used here.

The observation of similar dysregulated pathways in KP^{GEMM} and KP^{CRISPR} applies not only at the histopathological level but also at the transcriptional level (Figure 3-17). Analysing GSEA and GO-biological processes revealed a high similarity between both models. The successful targeting of KRAS in our CRISPR mediated genome editing is further confirmed in the GSEA. Here we found a similar downregulation of a gene set involved in negative response upon oncogenic KRAS signalling in a comparable manner in both. Furthermore, the downregulation of inflammatory response is in line with the report of immune cold or evasive KRas mutant lung cancer and further implies the successful mutation of KRAS [Caetano et al. 2016, Cullis et al. 2018, van Maldegem and Downward 2020].

Finally, both models showed a significant increase in the upregulation of the MYC pathway and, as an indication of higher proliferation, the upregulation of pathways involved in DNA replication.

In addition to the similarities between KP^{GEMM} and KP^{CRISPR} in GSEA, the GO biological processes confirm the same oncogenic phenotype in both. Upon tumour induction, pathways involved in cell death and regulation of cell cycle are downregulated.

Discussion

Furthermore, the GO processes confirm the immune evasive phenotype since immune response regulation pathways are significantly downregulated in KP^{GEMM} and KP^{CRISPR}. On the other hand, since these tumours are driven by KRAS mutation, the upregulation of the WNT-pathway as well as upregulation in RAS and MAPK pathway can be detected in the GO analysis.

In summary, the histopathological as well as the transcriptional analysis demonstrates, that irrespective of induction method, KP^{GEMM} and KP^{CRISPR} activate the same oncogenic pathways and use similar actions to evade tumour suppressive functions. However, the direct comparison of KP^{GEMM} and KP^{CRISPR} revealed distinct differences on molecular level (Figure 3-16 Figure 3-17). We observed that common key players in the development and progression of NSCLC such as Scgb1a1/CC10, Stk11/Lkb1, Keap1, cJun, cMyc, Notch1, Notch3 or Nkx2-1 did not show any differences when directly comparing KP^{GEMM} and KP^{CRISPR}. However, in KP^{CRISPR} there was a greater upregulation of genes involved in the Wnt pathway, whereas in KP^{GEMM} there was an upregulation of genes involved in EGFR signalling (Figure 3-16B).

Here we propose that this difference may be due to the fact that in the genetic model KRAS is a forced monoallelic mutation. In contrast, the CRISPR-mediated model, allows for homozygous mutations in KRAS.

The increased WNT signalling, could be a result a possible enhanced PI3K activation of the homozygous mutated KRAS^{G12D} in the CRISPR model. The G12D mutation in KRAS has been associated with an increase PI3K activity and thus activation WNT/CTNNB1 signalling by downstream effectors. [Rubinfeld et al. 1996, Ihle et al. 2012] The expression of monoallelic wild type KRAS has been proposed to have a tumour suppressive role [Zhang et al. 2001]. Furthermore, frequent LOH for monoallelic mutant KRAS has been reported for human lung cancer patients [Chiosea et al. 2011, Ma et al. 2022]. The upregulation in EGFR signalling compared to KP^{CRISPR} could be indicative of the accumulation of additional mutations, besides KRAS such as in RAF family member or in EGFR, which could further amplify the signalling pathway and thereby compensate for the wild type KRAS or the monoallelic activation of just one KRAS^{G12D} mutant.

Discussion

In summary, the conducted experiments have demonstrated that both the classical model and CRISPR/Cas9-mediated tumour induction result in comparable tumour formation at the molecular level. Dysregulation of key pathways involved in tumour proliferation, maintenance, immune evasion, and metabolism showed similar changes in both approaches. The only discernible variation was observed in the expression of specific oncogenic signalling pathways due to the restriction of exclusive heterozygous mutation of KRas in the classical model. Overall, our results strongly suggest that CRISPR/Cas9-mediated tumour induction is a viable alternative to the classical model for targeting Trp53 and KRas.

4.2 Modular AAV-vector enables successful targeting of commonly mutated tumour suppressor in mice with simple modifications

With the establishment of a CRISPR/Cas9 mediated mouse model and the successful implementation of genome editing to induce lung tumour formation, we wanted to further advance the genomic complexity. In order to increase the mutational burden in these animals, we added sgRNAs to the AAV-KP vector to increase the repertoire of targets. Characteristic for NSCLC is the tumour heterogeneity and an increased mutational burden, especially in late stages.

Analysis of publicly available datasets and previous studies showed that the most commonly mutated genes include tumour suppressors, the loss of which negatively affects treatment response and patient prognosis. These include APC, KEAP1, STK11/LKB1 and PTEN. (Figure 3-18)[Cancer Genome Atlas Research 2012, Cancer Genome Atlas Research 2014]

The chosen setup of our viral approach (Figure 3-19) enabled us to implement sgRNAs targeting the vicinity of frequently mutated sites of the respective tumour suppressor quickly. In total, design, cloning, and virus production is achievable in less than two weeks. This makes it possible to introduce and establish new sgRNAs *in vitro* very quickly and cost-effectively. In addition, the same virus can then be used for *in vivo* application.

Discussion

Because we wanted to establish a well-defined genetic background for tumour initiation, we want and need to avoid off-target effects in Cas9-mediated genetic manipulation.

Previous studies have identified the possibility of Cas9 binding to unintended sites in the genome, leading thereby to off-target effects. Mismatches of more than three bp in the sgRNA, including the PAM sequence, have been identified as the main cause of unwanted cleavage sites. Therefore, DSBs can occur in the genome at sites other than the targeted loci. In addition, neighbouring loci in the same gene may be affected by mismatches due to sequence homology. [Alkan et al. 2018] Thus, a careful design can reduce potential off-target effects in future experiments. A reduced GC content in the sgRNA can decrease off-target effects. A similar effect can be observed with truncated sgRNAs, where a length of 17 bp showed a higher on target efficacy. [Fu et al. 2014, Wang et al. 2014]

Here we have used two different scoring-based models for the design of the used sgRNAs. The algorithms used to predict off-target effects were developed by the Doench laboratory and the Marenco-Mateos laboratory. [Moreno-Mateos et al. 2015, Doench et al. 2016]. This 'biased' in silico method calculates the putative off-target effects and simultaneously predicts a cleavage probability based on GC content, RNA secondary structures and known epigenetic factors such as DNA methylation [Naeem et al. 2020]. However, the downside is, that the Doench algorithm only performs these calculations based on the human genome GRCh38 [Listgarten et al. 2018]. Thus, off-target effects cannot be 100 % excluded, despite the prediction of zero off-target sites in all used sgRNAs. For future mice experiments additional validations of the designed sgRNAs should be included. Among the possible adjustments, the implementation of mice specific tools to identify and predict off targets should be utilised such as CRISPR-DO [Ma et al. 2016].

To induce tumour formation by targeting a second tumour suppressor, mice were infected with the above-mentioned AAVs and analysed 12 weeks after intratracheal implantation. Cas9-mediated targeting resulted in robust tumour formation in all animals across all genotypes. (Figure 3-20). Immunohistochemical evaluation of our targeting efficacy showed that at end-point over 80 % of all tumours have lost the expression of the targeted tumour suppressor (Figure 3-22). This observation is in line

Discussion

with comparable approaches of sgRNA mediated *in vivo* knock out of tumour suppressors in NSCLS formation [Platt et al. 2014, Romero et al. 2017] Furthermore, the high abundance of tumours without detectable protein abundance at end point analysis indicates a growth advantage of the triple mutant tumour cells. This observation is further confirmed with the increased proliferative state of triple negative tumours, which show a significant increase of PCNA positive cells per tumour (Figure 3-24)

However, the additional loss of the tumour suppressors led to an increased tumour burden only in KPA^{CRISPR} , KPL^{CRISPR} and KPP^{CRISPR} , whereas in KPK^{CRISPR} just an increase in tumour number was observed (Figure 3-20 **A**).

We hypothesised, that the loss of the KEAP1 tumour suppressive function would have a stronger effect on tumour proliferation, when compared to KP mice. Since mutations in KEAP1 or activating alterations in the KEAP1/Nrf2 pathway are associated with resistance to checkpoint inhibition, immune cold tumours, and tumour progression [Romero et al. 2017, Lignitto et al. 2019]

The increased tumour burden in KPK mutant tumours could indicate, that on the one hand the additional loss of KEAP1 does not yield in an increased proliferative state, but might still be beneficial for those tumours, due to its immune evasive function. Furthermore, the increased NRF2 levels that we observed (Figure 3-22) could facilitate a higher tolerance for cellular stress during tumour induction. Thus, leading to an increased overall tumour number in the KPK model. For example, the scavenging of ROS could decrease early apoptotic events upon tumour induction [Wang et al. 2006]. Another possibility could be, a tumour suppressive function of elevated NRF2 levels, especially early on [Sporn and Liby 2012]. In consequence, this could delay the tumour progression in mutant KEAP1 situation.

In line with our observation of smaller KEAP1 mutant lung tumours after twelve weeks is the study of Romero *et.al*. Here they observed an increased tumour burden in $Trp53^{fl/fl};KRas^{lsI-G12D/wt};sgKeap1$ 21 weeks post infection [Romero et al. 2017]. In order now to further interrogate the role of KEAP1 loss in NSCLC, the animal experiments should be prolonged, to recapitulate the results from published studies. Furthermore, KEAP1 mutations are not limited to the chosen target site in this thesis. Loss-of-function and nonsense mutations scattered over the whole length have been identified in patients [Frank et al. 2018]. Thus, the inclusion of HDR mediated point mutants and

Discussion

a larger variance in sgRNA target site could yield in novel insights on the role of Keap1/NRF2 function in NSCLC.

In conclusion, the modular system of AAV in combination with CRISPR/Cas9-mediated genome editing provides a robust and efficient approach for generating rapid in vivo models that faithfully recapitulate patient-relevant NSCLC-driving mutations. This system offers a reliable and relevant surrogate model to investigate treatment options and refine targeted and personalized therapy strategies.

4.3 Dual viral approach allows to reduce and refine animal testing

As mentioned above, intensive research in animal models is time consuming and costly. Generating novel mouse strains and introducing relevant mutations may require extensive breeding. Even under optimal conditions, this can take several months and a significant number of animals.

Here we could demonstrate that the dual viral approach (Figure 3-25) is capable of lung tumour induction with highly similar tumour characteristics in comparison to the constitutive expressing spCas9 animals. Furthermore, effective targeting and genome editing was observed when using two sgRNAs as well as targeting an additional tumour suppressor (Figure 3-27/Figure 3-29).

Despite recapitulating the proliferative state, the activation of the MAPK pathway, as well as demonstrating a similar staging (Figure 3-26/Figure 3-28), it is obvious that the dual viral approach results in a highly decreased amount of tumours when compared to the constitutive expressing model. The main reason for the decreased efficacy in tumour induction is most probably the necessity of a positive double infection of the same cell in order to induce Cas9-mediated tumour onset. Here we achieved a efficacy of 15 % compared to the single viral approach, which is in line with other studies that utilized spCas9 genome editing with a dual virus [Swiech et al. 2015, Yang et al. 2016, Xu et al. 2019]

The adjustments mentioned in 4.1 to increase HDR effectiveness and reduce off-target effects can also be applied here. Although this thesis and other studies show that multiplexing in a dual approach works, albeit not as effectively, the use of a single virus is usually more promising [Swiech et al. 2015]. With 4.2 kb spCas9 is at the limit of an

Discussion

AAV packaging capacity of 4.5 kb. In order to reduce the number of AAVs to one and still provide the necessary sgRNAs, the introduction of smaller and/or engineered Cas variants is imminent. In the recent years novel Cas variants have been refined and thus increased the repertoire of suitable enzymes. Worth mentioning here are Cas12f, which at about 2.1 kb is only half the size of Cas9, and CasMINI at only 1.6 kb. Both have been highly adapted by protein engineering and show high and precise activity in mammalian cells. Due to the significant difference in size, the switch from Cas9 to one of the smaller variants, could give us the high flexibility of CRISPR genome editing without having to rely on a dual viral approach. [Xu et al. 2021, Zhou et al. 2022]

As stated above, the packaging capacity of AAV is limited to 4.5 kb, which limits the possibilities for genetic manipulation. This is especially true for modifications in model systems that do not express spCas9. In previous published mouse containing NSCLC studies, pioneered by the Jacks laboratory, CRISPR/Cas9 mediated editing was implemented in combination with the classic mouse model. [Sanchez-Rivera et al. 2014] In order to successfully induce lung tumour formation a Lentiviral (LV) approach was used. A packaging size of up to 8 kb enables a larger and more complex discussion of genetic alterations or the inclusion of expression systems [Vogt and Simon 1999]. Furthermore, the viral genome is integrated into the host cell. Thus, enabling the generation of stably expressing cell (lines). However, as a downside the host genome integration can yield in unwanted or even disruptive off target effects. [Xu et al. 2019] Furthermore, the origin of LVs are pathogenic viruses and despite a very low risk, the chance of infection of an putative oncogenic LV is not zero. The capacity to work and handle a SII biosafety workplace is not applicable for every laboratory. [Sakuma et al. 2012]

In common with AAVs is the low immunogenic profile of LVs and the capability of infecting dividing and non-dividing cells [Xu et al. 2019]. Compared to the LV, the integration of the AAV genome into the host cell is very low (< 0.05%). [Inagaki et al. 2008, Yang et al. 2008, Yang et al. 2020] Instead, the viral genome is maintained as an episome in the cell. Thus, stable expression of shRNAs or the long-term overexpression is not feasible with AAVs. However, this disadvantage is compensated for by the fact that AAVs are non-pathogenic and do not cause any known diseases in

Discussion

humans. This makes their handling in S1 biosafety possible for a large number of laboratories. [Li and Samulski 2020]

The ease of production at high titres with low biosafety requirements and the ease of manipulation of cis-plasmids make AAV a very versatile tool. In particular, the ability to generate small Cas variants could further expand the repertoire of multiplexed genome modifications.

4.4 Conclusion

The genetic complexity of NSCLC and the heterogeneity of lung cancer, complicates not only clinical intervention but also research on suitable animal models. A tremendous amount of research could be carried out in a genetic engineered mouse model, which could greatly increase the understanding of NSCLC. However, due to its limitations and the length of time it takes to introduce novel genetic changes, we wanted to establish a CRISPR/Cas9-based mouse model that would allow us to interrogate patient-relevant mutations in a timely manner. [Jackson et al. 2005, DuPage et al. 2009, Platt et al. 2014]

The implementation of CRISPR/Cas9 precision genome editing in this work has resulted in a versatile NSCLC mouse model. Comparison at the morphological level with KP^{GEMM} has shown that both models result in almost identical tumours. Using IHC staining and the unbiased quantification by QuPath established here, the commonalities in the deregulated oncogenic pathways of both models could be measured and directly compared.

Next-generation sequencing in the form of RNA sequencing was used to further deepen the comparison and enable a comparison at the molecular level. Again, a high degree of similarity between the two models was demonstrated.

To recapitulate the mutational landscape observed in non-small cell lung cancer patients using CRISPR/Cas9, our first approach was to analyse the frequency of mutations in tumour suppressor genes in both ADC and SCC with publicly available datasets of NSCLC patient data. The targeting of additional commonly mutated tumour suppressors demonstrated the capability of multiplexing with our chosen system. Furthermore, the resulting tumours recapitulated phenotypes observed in patients with comparable driving mutations.

Discussion

Finally, using the dual viral approach, we can induce lung tumours regardless of the genetic make-up of the mouse model chosen.

Taken together, we have demonstrated that CRISPR/Cas9-mediated genome editing can rapidly and reliably induce lung tumours in animals. The modular system allows us to quickly recapitulate patient-relevant mutations in a defined genetic background. In addition, the dual viral approach makes tumour formation independent of the mouse strain. This reduces the total number of animals required for in vivo studies, as costly breeding to introduce relevant mutations is no longer necessary (Figure 3 33).

Bibliography

5 Bibliography

- Abdallah, K., F. Nadeau, F. Bergeron, S. Blouin, V. Blais, K. M. Bradbury, . . . L. Gendron (2018). "**Adeno-associated virus 2/9 delivery of Cre recombinase in mouse primary afferents.**" Scientific Reports 8(1).
- Aitchison, A., C. Hakkaart, R. C. Day, H. R. Morrin, F. A. Frizelle and J. I. Keenan (2020). "**APC Mutations Are Not Confined to Hotspot Regions in Early-Onset Colorectal Cancer.**" Cancers 12(12): 3829.
- Alkan, F., A. Wenzel, C. Anthon, J. H. Havgaard and J. Gorodkin (2018). "**CRISPR-Cas9 off-targeting assessment with nucleic acid duplex energy parameters.**" Genome Biol 19(1): 177.
- AmericanCancerSociety (2019). "**Lung Cancer Early Detection, Diagnosis, and Staging.**" cancer.org 1.800.227.2345.
- Antonia, S. J., A. Villegas, D. Daniel, D. Vicente, S. Murakami, R. Hui, . . . M. Özgüroğlu (2018). "**Overall Survival with Durvalumab after Chemoradiotherapy in Stage III NSCLC.**" New England Journal of Medicine 379(24): 2342-2350.
- Antwi, S. O., E. C. Eckert, C. V. Sabaque, E. R. Leof, K. M. Hawthorne, W. R. Bamlet, . . . G. M. Petersen (2015). "**Exposure to environmental chemicals and heavy metals, and risk of pancreatic cancer.**" Cancer Causes & Control 26(11): 1583-1591.
- Arbour, K. C., E. Jordan, H. R. Kim, J. Dienstag, H. A. Yu, F. Sanchez-Vega, . . . G. J. Riely (2018). "**Effects of Co-occurring Genomic Alterations on Outcomes in Patients with KRAS-Mutant Non-Small Cell Lung Cancer.**" Clin Cancer Res 24(2): 334-340.
- Asao, T., F. Takahashi and K. Takahashi (2019). "**Resistance to molecularly targeted therapy in non-small-cell lung cancer.**" Respir Investig 57(1): 20-26.
- Assoun, S., N. Theou-Anton, M. Nguenang, A. Cazes, C. Danel, B. Abbar, . . . G. Zalcman (2019). "**Association of TP53 mutations with response and longer survival under immune checkpoint inhibitors in advanced non-small-cell lung cancer.**" Lung Cancer 132: 65-71.

Bibliography

- Aubrey, B. J., A. Strasser and G. L. Kelly (2016). "**Tumor-Suppressor Functions of the TP53 Pathway.**" Cold Spring Harbor Perspectives in Medicine 6(5): a026062.
- Baker, S. J., E. R. Fearon, J. M. Nigro, S. R. Hamilton, A. C. Preisinger, J. M. Jessup, . . . B. Vogelstein (1989). "**Chromosome 17 deletions and p53 gene mutations in colorectal carcinomas.**" Science 244(4901): 217-221.
- Barrangou, R., C. Fremaux, H. Deveau, M. Richards, P. Boyaval, S. Moineau, . . . P. Horvath (2007). "**CRISPR provides acquired resistance against viruses in prokaryotes.**" Science 315(5819): 1709-1712.
- Behr, M., J. Zhou, B. Xu and H. Zhang (2021). "**In vivo delivery of CRISPR-Cas9 therapeutics: Progress and challenges.**" Acta Pharm Sin B 11(8): 2150-2171.
- Belton, A., A. Gabrovsky, Y. K. Bae, R. Reeves, C. Jacobuzio-Donahue, D. L. Huso and L. M. S. Resar (2012). "**HMGA1 Induces Intestinal Polyposis in Transgenic Mice and Drives Tumor Progression and Stem Cell Properties in Colon Cancer Cells.**" PLoS ONE 7(1): e30034.
- Best, S. A., D. P. De Souza, A. Kersbergen, A. N. Policheni, S. Dayalan, D. Tull, . . . K. D. Sutherland (2018). "**Synergy between the KEAP1/NRF2 and PI3K Pathways Drives Non-Small-Cell Lung Cancer with an Altered Immune Microenvironment.**" Cell Metab 27(4): 935-943 e934.
- Blagih, J., M. D. Buck and K. H. Vousden (2020). "**p53, cancer and the immune response.**" Journal of Cell Science 133(5): jcs237453.
- Brahmer, J., K. L. Reckamp, P. Baas, L. Crinò, W. E. E. Eberhardt, E. Poddubskaya, . . . D. R. Spigel (2015). "**Nivolumab versus Docetaxel in Advanced Squamous-Cell Non–Small-Cell Lung Cancer.**" New England Journal of Medicine 373(2): 123-135.
- Burger, C., O. S. Gorbatyuk, M. J. Velardo, C. S. Peden, P. Williams, S. Zolotukhin, . . . N. Muzyczka (2004). "**Recombinant AAV viral vectors pseudotyped with viral capsids from serotypes 1, 2, and 5 display differential efficiency and cell tropism after delivery to different regions of the central nervous system.**" Mol Ther 10(2): 302-317.
- Caetano, M. S., H. Zhang, A. M. Cumpian, L. Gong, N. Unver, E. J. Ostrin, . . . S. J. Moghaddam (2016). "**IL6 Blockade Reprograms the Lung Tumor**

Bibliography

- Microenvironment to Limit the Development and Progression of K-ras–Mutant Lung Cancer." Cancer Research 76(11): 3189-3199.**
- Caiola, E., F. Falcetta, S. Giordano, M. Marabese, M. C. Garassino, M. Broggin, . . . L. Brunelli* (2018). **"Co-occurring KRAS mutation/LKB1 loss in non-small cell lung cancer cells results in enhanced metabolic activity susceptible to caloric restriction: an in vitro integrated multilevel approach." Journal of Experimental & Clinical Cancer Research 37(1).**
- Cancer Genome Atlas Research, N.* (2012). **"Comprehensive genomic characterization of squamous cell lung cancers." Nature 489(7417): 519-525.**
- Cancer Genome Atlas Research, N.* (2014). **"Comprehensive molecular profiling of lung adenocarcinoma." Nature 511(7511): 543-550.**
- Carbone, D. P., M. Reck, L. Paz-Ares, B. Creelan, L. Horn, M. Steins, . . . M. A. Socinski* (2017). **"First-Line Nivolumab in Stage IV or Recurrent Non–Small-Cell Lung Cancer." New England Journal of Medicine 376(25): 2415-2426.**
- Cascetta, P., A. Marinello, C. Lazzari, V. Gregorc, D. Planchard, R. Bianco, . . . A. Morabito* (2022). **"KRAS in NSCLC: State of the Art and Future Perspectives." Cancers 14(21): 5430.**
- Chen, Z., C. M. Fillmore, P. S. Hammerman, C. F. Kim and K. K. Wong* (2014). **"Non-small-cell lung cancers: a heterogeneous set of diseases." Nat Rev Cancer 14(8): 535-546.**
- Cheng, Y., T. Zhang and Q. Xu* (2021). **"Therapeutic advances in non-small cell lung cancer: Focus on clinical development of targeted therapy and immunotherapy." MedComm 2(4): 692-729.**
- Cherfils, J. and M. Zeghouf* (2013). **"Regulation of small GTPases by GEFs, GAPs, and GDIs." Physiol Rev 93(1): 269-309.**
- Chiosea, S. I., C. K. Sherer, T. Jelic and S. Dacic* (2011). **"KRAS mutant allele-specific imbalance in lung adenocarcinoma." Mod Pathol 24(12): 1571-1577.**
- Choi, Y. S., Y. M. Shim, S. H. Kim, D. S. Son, H. S. Lee, G. Y. Kim, . . . J. Kim* (2003). **"Prognostic significance of E-cadherin and beta-catenin in**

Bibliography

- resected stage I non-small cell lung cancer." Eur J Cardiothorac Surg 24(3): 441-449.
- Colby, T. V., I. Wistuba and A. Gazdar (1998). "Precursors to Pulmonary Neoplasia." Anatomic Pathology 5(4): 205-215.
- Cullis, J., S. Das and D. Bar-Sagi (2018). "Kras and Tumor Immunity: Friend or Foe?" Cold Spring Harbor Perspectives in Medicine 8(9): a031849.
- Davidson, M. R., A. F. Gazdar and B. E. Clarke (2013). "The pivotal role of pathology in the management of lung cancer." J Thorac Dis 5 Suppl 5(Suppl 5): S463-478.
- Day, C. P., G. Merlino and T. Van Dyke (2015). "Preclinical mouse cancer models: a maze of opportunities and challenges." Cell 163(1): 39-53.
- DeMayo, F. J., M. J. Finegold, T. N. Hansen, L. A. Stanley, B. Smith and D. W. Bullock (1991). "Expression of SV40 T antigen under control of rabbit uteroglobin promoter in transgenic mice." Am J Physiol 261(2 Pt 1): L70-76.
- Dias Carvalho, P., A. L. Machado, F. Martins, R. Seruca and S. Velho (2019). "Targeting the Tumor Microenvironment: An Unexplored Strategy for Mutant KRAS Tumors." Cancers 11(12): 2010.
- Ding, L., G. Getz, D. A. Wheeler, E. R. Mardis, M. D. McLellan, K. Cibulskis, . . . R. K. Wilson (2008). "Somatic mutations affect key pathways in lung adenocarcinoma." Nature 455(7216): 1069-1075.
- Doench, J. G., N. Fusi, M. Sullender, M. Hegde, E. W. Vaimberg, K. F. Donovan, . . . D. E. Root (2016). "Optimized sgRNA design to maximize activity and minimize off-target effects of CRISPR-Cas9." Nature Biotechnology 34(2): 184-191.
- Dogan, S., R. Shen, D. C. Ang, M. L. Johnson, S. P. D'Angelo, P. K. Paik, . . . M. Ladanyi (2012). "Molecular epidemiology of EGFR and KRAS mutations in 3,026 lung adenocarcinomas: higher susceptibility of women to smoking-related KRAS-mutant cancers." Clin Cancer Res 18(22): 6169-6177.
- DuPage, M., A. L. Dooley and T. Jacks (2009). "Conditional mouse lung cancer models using adenoviral or lentiviral delivery of Cre recombinase." Nat Protoc 4(7): 1064-1072.

Bibliography

- Ehrhardt, A., T. Bartels, A. Geick, R. Klocke, D. Paul and R. Halter (2001).*
"Development of pulmonary bronchiolo-alveolar adenocarcinomas in transgenic mice overexpressing murine c- myc and epidermal growth factor in alveolar type II pneumocytes." British Journal of Cancer 84(6): 813-818.
- Engelman, J. A., J. Luo and L. C. Cantley (2006).* **"The evolution of phosphatidylinositol 3-kinases as regulators of growth and metabolism."** Nature Reviews Genetics 7(8): 606-619.
- Ettinger, D. S., D. E. Wood, D. L. Aisner, W. Akerley, J. R. Bauman, A. Bharat, . . . M. Hughes (2021).* **"NCCN Guidelines Insights: Non–Small Cell Lung Cancer, Version 2.2021."** Journal of the National Comprehensive Cancer Network 19(3): 254-266.
- Ferone, G., J.-Y. Song, Kate, R. Bhaskaran, K. Monkhorst, J.-P. Lambooj, . . . A. Berns (2016).* **"SOX2 Is the Determining Oncogenic Switch in Promoting Lung Squamous Cell Carcinoma from Different Cells of Origin."** Cancer Cell 30(4): 519-532.
- Ferrer, I., J. Zugazagoitia, S. Herberth, W. John, L. Paz-Ares and G. Schmid-Bindert (2018).* **"KRAS-Mutant non-small cell lung cancer: From biology to therapy."** Lung Cancer 124: 53-64.
- Fischer, T., O. Hartmann, M. Reissland, C. Prieto-Garcia, K. Klann, N. Pahor, . . . M. E. Diefenbacher (2022).* **"PTEN mutant non-small cell lung cancer require ATM to suppress pro-apoptotic signalling and evade radiotherapy."** Cell & Bioscience 12(1).
- Fitzgibbons, P. L. and W. H. Kern (1985).* **"Adenosquamous carcinoma of the lung: a clinical and pathologic study of seven cases."** Hum Pathol 16(5): 463-466.
- Frank, R., M. Scheffler, S. Merkelbach-Bruse, M. A. Ihle, A. Kron, M. Rauer, . . . J. Wolf (2018).* **"Clinical and Pathological Characteristics of KEAP1- and NFE2L2-Mutated Non-Small Cell Lung Carcinoma (NSCLC)."** Clin Cancer Res 24(13): 3087-3096.
- Fu, Y., J. D. Sander, D. Reyon, V. M. Cascio and J. K. Joung (2014).* **"Improving CRISPR-Cas nuclease specificity using truncated guide RNAs."** Nat Biotechnol 32(3): 279-284.

Bibliography

- Gabay, M., Y. Li and D. W. Felsher (2014). "**MYC Activation Is a Hallmark of Cancer Initiation and Maintenance.**" Cold Spring Harbor Perspectives in Medicine 4(6): a014241-a014241.
- Galan-Cobo, A., P. Sitthideatphaiboon, X. Qu, A. Poteete, M. A. Pisegna, P. Tong, . . . J. V. Heymach (2019). "**LKB1 and KEAP1/NRF2 Pathways Cooperatively Promote Metabolic Reprogramming with Enhanced Glutamine Dependence in *KRAS*-Mutant Lung Adenocarcinoma.**" Cancer Research 79(13): 3251-3267.
- Galan-Cobo, A., P. Sitthideatphaiboon, X. Qu, A. Poteete, M. A. Pisegna, P. Tong, . . . J. V. Heymach (2019). "**LKB1 and KEAP1/NRF2 Pathways Cooperatively Promote Metabolic Reprogramming with Enhanced Glutamine Dependence in *KRAS*-Mutant Lung Adenocarcinoma.**" Cancer Res 79(13): 3251-3267.
- Ganti, A. K., A. B. Klein, I. Cotarla, B. Seal and E. Chou (2021). "**Update of Incidence, Prevalence, Survival, and Initial Treatment in Patients With Non-Small Cell Lung Cancer in the US.**" JAMA Oncology 7(12): 1824.
- Geick, A., P. Redecker, A. Ehrhardt, R. Klocke, D. Paul and R. Halter (2001). "**Uteroglobin promoter-targeted c-MYC expression in transgenic mice cause hyperplasia of Clara cells and malignant transformation of T-lymphoblasts and tubular epithelial cells.**" Transgenic Res 10(6): 501-511.
- Ghaleb, A., M. Padellan and N. Marchenko (2020). "**Mutant p53 drives the loss of heterozygosity by the upregulation of Nek2 in breast cancer cells.**" Breast Cancer Research 22(1).
- Ghaleb, A., A. Yallowitz and N. Marchenko (2019). "**Irradiation induces p53 loss of heterozygosity in breast cancer expressing mutant p53.**" Communications Biology 2(1).
- Giangreco, A., L. Lu, C. Vickers, V. H. Teixeira, K. R. Groot, C. R. Butler, . . . S. M. Janes (2012). " **β -Catenin determines upper airway progenitor cell fate and preinvasive squamous lung cancer progression by modulating epithelial-mesenchymal transition.**" The Journal of Pathology 226(4): 575-587.

Bibliography

- Gkoutakos, A., G. Sartori, I. Falcone, G. Piro, L. Ciuffreda, C. Carbone, . . . S. Pilotto (2019). "PTEN in Lung Cancer: Dealing with the Problem, Building on New Knowledge and Turning the Game Around." Cancers 11(8): 1141.
- Goulding, R. E., M. Chenoweth, G. C. Carter, M. E. Boye, K. M. Sheffield, W. J. John, . . . E. Druyts (2020). "KRAS mutation as a prognostic factor and predictive factor in advanced/metastatic non-small cell lung cancer: A systematic literature review and meta-analysis." Cancer Treat Res Commun 24: 100200.
- Gridelli, C., A. Rossi, D. P. Carbone, J. Guarize, N. Karachaliou, T. Mok, . . . R. Rosell (2015). "Non-small-cell lung cancer." NATURE REVIEWS | DISEASE PRIMERS 1.
- Grimm, D., J. S. Lee, L. Wang, T. Desai, B. Akache, T. A. Storm and M. A. Kay (2008). "In Vitro and In Vivo Gene Therapy Vector Evolution via Multispecies Interbreeding and Retargeting of Adeno-Associated Viruses." Journal of Virology 82(12): 5887-5911.
- Gu, M., T. Xu and P. Chang (2021). "KRAS/LKB1 and KRAS/TP53 co-mutations create divergent immune signatures in lung adenocarcinomas." Ther Adv Med Oncol 13: 17588359211006950.
- Guo, S., L. Tan, W. Pu, J. Wu, K. Xu, J. Wu, . . . J. Wang (2014). "Quantitative assessment of the diagnostic role of APC promoter methylation in non-small cell lung cancer." Clinical Epigenetics 6(1): 5.
- Gurda, G. T., L. Zhang, Y. Wang, L. Chen, S. Geddes, W. C. Cho, . . . Q. K. Li (2015). "Utility of five commonly used immunohistochemical markers TTF-1, Napsin A, CK7, CK5/6 and P63 in primary and metastatic adenocarcinoma and squamous cell carcinoma of the lung: a retrospective study of 246 fine needle aspiration cases." Clinical and Translational Medicine 4(1).
- Han, X., F. Li, Z. Fang, Y. Gao, F. Li, R. Fang, . . . H. Ji (2014). "Transdifferentiation of lung adenocarcinoma in mice with Lkb1 deficiency to squamous cell carcinoma." Nat Commun 5: 3261.
- Hartl, M. (2016). "The Quest for Targets Executing MYC-Dependent Cell Transformation." Front Oncol 6: 132.

Bibliography

- Hassanpour, S. H. and M. Dehghani (2017). **"Review of cancer from perspective of molecular."** Journal of Cancer Research and Practice 4(4): 127-129.
- Heng, W. S., R. Gosens and F. A. E. Kruyt (2019). **"Lung cancer stem cells: origin, features, maintenance mechanisms and therapeutic targeting."** Biochemical Pharmacology 160: 121-133.
- Henschke, C. I., D. I. McCauley, D. F. Yankelevitz, D. P. Naidich, G. McGuinness, O. S. Miettinen, . . . J. P. Smith (1999). **"Early Lung Cancer Action Project: overall design and findings from baseline screening."** Lancet 354(9173): 99-105.
- Hommura, F., K. Furuuchi, K. Yamazaki, S. Ogura, I. Kinoshita, M. Shimizu, . . . H. Dosaka-Akita (2002). **"Increased expression of β -catenin predicts better prognosis in nonsmall cell lung carcinomas."** Cancer 94(3): 752-758.
- Hu, X., H. Xu, Q. Xue, R. Wen, W. Jiao and K. Tian (2021). **"The role of ERBB4 mutations in the prognosis of advanced non-small cell lung cancer treated with immune checkpoint inhibitors."** Molecular Medicine 27(1).
- Huang (2010). **"Intratumoral Wnt1 expression affects survivin gene expression in non-small cell lung cancer."** International Journal of Oncology 37(3).
- Ihle, N. T., L. A. Byers, E. S. Kim, P. Saintigny, J. J. Lee, G. R. Blumenschein, . . . G. Powis (2012). **"Effect of KRAS oncogene substitutions on protein behavior: implications for signaling and clinical outcome."** J Natl Cancer Inst 104(3): 228-239.
- Ikeda, S. (1998). **"Axin, a negative regulator of the Wnt signaling pathway, forms a complex with GSK-3 β and β -catenin and promotes GSK-3 β - dependent phosphorylation of β -catenin."** The EMBO Journal 17(5): 1371-1384.
- Inagaki, K., C. Piao, N. M. Kotchey, X. Wu and H. Nakai (2008). **"Frequency and spectrum of genomic integration of recombinant adeno-associated virus serotype 8 vector in neonatal mouse liver."** J Virol 82(19): 9513-9524.
- Inoue, K., E. Fry, D. Maglic and S. Zhu (2013). Genetically Engineered Mouse Models for Human Lung Cancer, InTech.
- Ira, G., A. Pellicoli, A. Balijja, X. Wang, S. Fiorani, W. Carotenuto, . . . M. Foiani (2004). **"DNA end resection, homologous recombination and DNA**

Bibliography

- damage checkpoint activation require CDK1." Nature 431(7011): 1011-1017.
- Ireson, C. R., M. S. Alavijeh, A. M. Palmer, E. R. Fowler and H. J. Jones (2019). "The role of mouse tumour models in the discovery and development of anticancer drugs." Br J Cancer 121(2): 101-108.
- Ishida, T., S. Kaneko, H. Yokoyama, T. Inoue, K. Sugio and K. Sugimachi (1992). "Adenosquamous carcinoma of the lung. Clinicopathologic and immunohistochemical features." Am J Clin Pathol 97(5): 678-685.
- Jacks, T., A. Fazeli, E. M. Schmitt, R. T. Bronson, M. A. Goodell and R. A. Weinberg (1992). "Effects of an Rb mutation in the mouse." Nature 359(6393): 295-300.
- Jackson, E. L., K. P. Olive, D. A. Tuveson, R. Bronson, D. Crowley, M. Brown and T. Jacks (2005). "The differential effects of mutant p53 alleles on advanced murine lung cancer." Cancer Res 65(22): 10280-10288.
- Jackson, E. L., N. Willis, K. Mercer, R. T. Bronson, D. Crowley, R. Montoya, . . . D. A. Tuveson (2001). "Analysis of lung tumor initiation and progression using conditional expression of oncogenic K-ras." Genes Dev 15(24): 3243-3248.
- Janker, F., W. Weder, J.-H. Jang and W. Jungraithmayr (2018). "Preclinical, non-genetic models of lung adenocarcinoma: a comparative survey." Oncotarget 9(55): 30527-30538.
- Ji, H., M. R. Ramsey, D. N. Hayes, C. Fan, K. McNamara, P. Kozlowski, . . . K.-K. Wong (2007). "LKB1 modulates lung cancer differentiation and metastasis." Nature 448(7155): 807-810.
- Ji, M., H. Guan, C. Gao, B. Shi and P. Hou (2011). "Highly frequent promoter methylation and PIK3CA amplification in non-small cell lung cancer (NSCLC)." BMC Cancer 11(1): 147.
- Johnson, L., K. Mercer, D. Greenbaum, R. T. Bronson, D. Crowley, D. A. Tuveson and T. Jacks (2001). "Somatic activation of the K-ras oncogene causes early onset lung cancer in mice." Nature 410(6832): 1111-1116.
- Johnson, R., B. Spiegelman, D. Hanahan and R. Wisdom (1996). "Cellular Transformation and Malignancy Induced by ras Require c-jun." Molecular and Cellular Biology 16(8): 4504-4511.

Bibliography

- Karachaliou, N., C. Mayo, C. Costa, I. Magri, A. Gimenez-Capitan, M. A. Molina-Vila and R. Rosell (2013). "**KRAS mutations in lung cancer.**" Clin Lung Cancer 14(3): 205-214.
- Kaufman, J. M., J. M. Amann, K. Park, R. R. Arasada, H. Li, Y. Shyr and D. P. Carbone (2014). "**LKB1 Loss induces characteristic patterns of gene expression in human tumors associated with NRF2 activation and attenuation of PI3K-AKT.**" J Thorac Oncol 9(6): 794-804.
- Kelland, L. R. (2004). "**Of mice and men: values and liabilities of the athymic nude mouse model in anticancer drug development.**" Eur J Cancer 40(6): 827-836.
- Kim, C. F. B., E. L. Jackson, A. E. Woolfenden, S. Lawrence, I. Babar, S. Vogel, . . . T. Jacks (2005). "**Identification of Bronchioalveolar Stem Cells in Normal Lung and Lung Cancer.**" Cell 121(6): 823-835.
- Kim, M. P. and G. Lozano (2018). "**Mutant p53 partners in crime.**" Cell Death & Differentiation 25(1): 161-168.
- Kim, S. and J.-S. Kim (2011). "**Targeted genome engineering via zinc finger nucleases.**" Plant Biotechnology Reports 5(1): 9-17.
- Kinzler, K. W., M. C. Nilbert, L. K. Su, B. Vogelstein, T. M. Bryan, D. B. Levy, . . . et al. (1991). "**Identification of FAP locus genes from chromosome 5q21.**" Science 253(5020): 661-665.
- Kou, F., H. Sun, L. Wu, B. Li, B. Zhang, X. Wang and L. Yang (2020). "**TOP2A Promotes Lung Adenocarcinoma Cells' Malignant Progression and Predicts Poor Prognosis in Lung Adenocarcinoma.**" Journal of Cancer 11(9): 2496-2508.
- Kumar V, A. Abbas A and J. R. . (2013). Basic Pathology. Philadelphia, PA: , Elsevier/Saunders, .
- Kurotani, R., N. Kumaki, X. Naizhen, J. M. Ward, R. I. Linnoila and S. Kimura (2011). "**Secretoglobin 3A2/uteroglobin-related protein 1 is a novel marker for pulmonary carcinoma in mice and humans.**" Lung Cancer 71(1): 42-48.
- Kwong, L. N. and W. F. Dove (2009). APC and Its Modifiers in Colon Cancer, Springer New York: 85-106.
- Lane, D. P. (1992). "**p53, guardian of the genome.**" Nature 358(6381): 15-16.

Bibliography

- Lane, D. P. and L. V. Crawford (1979). "T antigen is bound to a host protein in SY40-transformed cells." Nature 278(5701): 261-263.
- Langer, C. J., B. Besse, A. Gualberto, E. Brambilla and J.-C. Soria (2010). "The Evolving Role of Histology in the Management of Advanced Non–Small-Cell Lung Cancer." Journal of Clinical Oncology 28(36): 5311-5320.
- Lau, S. K., M. J. Desrochers and D. J. Luthringer (2002). "Expression of Thyroid Transcription Factor-1, Cytokeratin 7, and Cytokeratin 20 in Bronchioloalveolar Carcinomas: an Immunohistochemical Evaluation of 67 Cases." Modern Pathology 15(5): 538-542.
- Lawrence, M. S., P. Stojanov, C. H. Mermel, J. T. Robinson, L. A. Garraway, T. R. Golub, . . . G. Getz (2014). "Discovery and saturation analysis of cancer genes across 21 tumour types." Nature 505(7484): 495-501.
- Lee, S. H. (2019). "Chemotherapy for Lung Cancer in the Era of Personalized Medicine." Tuberculosis and Respiratory Diseases 82(3): 179.
- Lei, L., W. X. Wang, Z. Y. Yu, X. B. Liang, W. W. Pan, H. F. Chen, . . . M. Y. Fang (2020). "A Real-World Study in Advanced Non-Small Cell Lung Cancer with KRAS Mutations." Transl Oncol 13(2): 329-335.
- Li, C. and R. J. Samulski (2020). "Engineering adeno-associated virus vectors for gene therapy." Nature Reviews Genetics 21(4): 255-272.
- Liaw, D., D. J. Marsh, J. Li, P. L. M. Dahia, S. I. Wang, Z. Zheng, . . . R. Parsons (1997). "Germline mutations of the PTEN gene in Cowden disease, an inherited breast and thyroid cancer syndrome." Nature Genetics 16(1): 64-67.
- Licciulli, S., J. L. Avila, L. Hanlon, S. Troutman, M. Cesaroni, S. Kota, . . . J. L. Kissil (2013). "Notch1 is required for Kras-induced lung adenocarcinoma and controls tumor cell survival via p53." Cancer Res 73(19): 5974-5984.
- Lignitto, L., S. E. Leboeuf, H. Homer, S. Jiang, M. Askenazi, T. R. Karakousi, . . . M. Pagano (2019). "Nrf2 Activation Promotes Lung Cancer Metastasis by Inhibiting the Degradation of Bach1." Cell 178(2): 316-329.e318.
- Lim, Z. F. and P. C. Ma (2019). "Emerging insights of tumor heterogeneity and drug resistance mechanisms in lung cancer targeted therapy." J Hematol Oncol 12(1): 134.

Bibliography

- Lin, S., B. T. Staahl, R. K. Alla and J. A. Doudna (2014). "Enhanced homology-directed human genome engineering by controlled timing of CRISPR/Cas9 delivery." Elife 3: e04766.
- Linzer, D. I. H. and A. J. Levine (1979). "Characterization of a 54K Dalton Cellular SV40 Tumor Antigen Present in SV40-Transformed Cells and Uninfected Embryonal Carcinoma Cells " Cell 17: 43-52.
- Listgarten, J., M. Weinstein, B. P. Kleinstiver, A. A. Sousa, J. K. Joung, J. Crawford, . . . N. Fusi (2018). "Prediction of off-target activities for the end-to-end design of CRISPR guide RNAs." Nature Biomedical Engineering 2(1): 38-47.
- Liu, K., M. Zheng, R. Lu, J. Du, Q. Zhao, Z. Li, . . . S. Zhang (2020). "The role of CDC25C in cell cycle regulation and clinical cancer therapy: a systematic review." Cancer Cell International 20(1).
- Lu, Y., C. Futtner, J. R. Rock, X. Xu, W. Whitworth, B. L. M. Hogan and M. W. Onaitis (2010). "Evidence That SOX2 Overexpression Is Oncogenic in the Lung." PLoS ONE 5(6): e11022.
- M. Bibikova, K. Beumer, J. K. Trautman and D. Carroll (2003). "Enhancing Gene Targeting with Designed Zinc Finger Nucleases." Science 300: 764.
- M. Bibikova, M. Golic, K. G. Golic† and a. D. Carroll (2002). "Targeted Chromosomal Cleavage and Mutagenesis in Drosophila." Genetics 161(3): 1169-1175.
- Ma, J., J. Koster, Q. Qin, S. Hu, W. Li, C. Chen, . . . X. S. Liu (2016). "CRISPR-DO for genome-wide CRISPR design and optimization." Bioinformatics 32(21): 3336-3338.
- Ma, Q. (2013). "Role of nrf2 in oxidative stress and toxicity." Annu Rev Pharmacol Toxicol 53: 401-426.
- Ma, Y., S. Ling, Y. Li, M. Hu, B. Kong, P. Huang and H. Liu (2022). "Loss of Heterozygosity for KrasG12D Promotes Malignant Phenotype of Pancreatic Ductal Adenocarcinoma by Activating HIF-2 α -c-Myc-Regulated Glutamine Metabolism." International Journal of Molecular Sciences 23(12): 6697.
- Malkoski, S. P., T. G. Cleaver, J. J. Thompson, W. P. Sutton, S. M. Haeger, K. J. Rodriguez, . . . X.-J. Wang (2014). "Role of PTEN in basal cell derived lung carcinogenesis." Molecular Carcinogenesis 53(10): 841-846.

Bibliography

- Malumbres, M. and M. Barbacid* (2003). "**RAS oncogenes: the first 30 years.**" Nature Reviews Cancer 3(6): 459-465.
- Mansoori, B., A. Mohammadi, H. J. Ditzel, P. H. G. Duijf, V. Khaze, M. F. Gjerstorff and B. Baradaran* (2021). "**HMGA2 as a Critical Regulator in Cancer Development.**" Genes 12(2): 269.
- Mao, C., L. X. Qiu, R. Y. Liao, F. B. Du, H. Ding, W. C. Yang, . . . Q. Chen* (2010). "**KRAS mutations and resistance to EGFR-TKIs treatment in patients with non-small cell lung cancer: a meta-analysis of 22 studies.**" Lung Cancer 69(3): 272-278.
- Marsit, C. J., S. Zheng, K. Aldape, P. W. Hinds, H. H. Nelson, J. K. Wiencke and K. T. Kelsey* (2005). "**PTEN expression in non-small-cell lung cancer: evaluating its relation to tumor characteristics, allelic loss, and epigenetic alteration.**" Hum Pathol 36(7): 768-776.
- Matsumoto, D., H. Tamamura and W. Nomura* (2020). "**A cell cycle-dependent CRISPR-Cas9 activation system based on an anti-CRISPR protein shows improved genome editing accuracy.**" Communications Biology 3(1).
- Mengoli, M. C., F. R. Longo, F. Fraggetta, A. Cavazza, A. Dubini, G. Ali, . . . P. Graziano* (2018). "**The 2015 World Health Organization Classification of lung tumors: new entities since the 2004 Classification.**" Pathologica 110(1): 39-67.
- Meuwissen, R. and A. Berns* (2005). "**Mouse models for human lung cancer.**" Genes & Development 19(6): 643-664.
- Mogi, A. and H. Kuwano* (2011). "**TP53 mutations in nonsmall cell lung cancer.**" J Biomed Biotechnol 2011: 583929.
- Moldaver, D., M. Hurry, W. K. Evans, P. K. Cheema, R. Sangha, R. Burkes, . . . D. Grima* (2020). "**Development, validation and results from the impact of treatment evolution in non-small cell lung cancer (iTEN) model.**" Lung Cancer 139: 185-194.
- Mordant, P., B. Grand, A. Cazes, C. Foucault, A. Dujon, F. Le Pimpec Barthes and M. Riquet* (2013). "**Adenosquamous carcinoma of the lung: surgical management, pathologic characteristics, and prognostic implications.**" Ann Thorac Surg 95(4): 1189-1195.

Bibliography

- Moreno-Mateos, M. A., C. E. Vejnar, J.-D. Beaudoin, J. P. Fernandez, E. K. Mis, M. K. Khokha and A. J. Giraldez (2015). "**CRISPRscan: designing highly efficient sgRNAs for CRISPR-Cas9 targeting in vivo.**" Nature Methods 12(10): 982-988.
- Morris GF.; Hoyle GW.; Athas GB, L. W., Xu J, Morris CB, Friedman M. (1998). "**Lung-specific expression in mice of a dominant negative mutant form of the p53 tumor suppressor protein.**" J La State Med Soc 5.
- Mosely, S. I., J. E. Prime, R. C. Sainson, J. O. Koopmann, D. Y. Wang, D. M. Greenawalt, . . . R. W. Wilkinson (2017). "**Rational Selection of Syngeneic Preclinical Tumor Models for Immunotherapeutic Drug Discovery.**" Cancer Immunol Res 5(1): 29-41.
- Mou, H., Z. Kennedy, D. G. Anderson, H. Yin and W. Xue (2015). "**Precision cancer mouse models through genome editing with CRISPR-Cas9.**" Genome Medicine 7(1).
- Mullard, A. (2021). "**Amgen overcomes historically undruggable target, with FDA nod for first KRAS inhibitor.**" Nat Rev Drug Discov 20(7): 496.
- Naeem, M., S. Majeed, M. Z. Hoque and I. Ahmad (2020). "**Latest Developed Strategies to Minimize the Off-Target Effects in CRISPR-Cas-Mediated Genome Editing.**" Cells 9(7).
- Nakashima, T., D. Liu, J. Nakano, S. Ishikawa, H. Yokomise, M. Ueno, . . . C.-L. Huang (2008). "**Wnt1 overexpression associated with tumor proliferation and a poor prognosis in non-small cell lung cancer patients.**" Oncology Reports.
- Nakayama, S., N. Sng, J. Carretero, R. Welner, Y. Hayashi, M. Yamamoto, . . . S. S. Kobayashi (2014). "**beta-catenin contributes to lung tumor development induced by EGFR mutations.**" Cancer Res 74(20): 5891-5902.
- Niederacher, D., H. X. An, S. Camrath, S. I. Dominik, U. J. Göhring, A. Oertel, . . . M. W. Beckmann (1998). "**Loss of heterozygosity of BRCA1, TP53 and TCRD markers analysed in sporadic endometrial cancer.**" European Journal of Cancer 34(11): 1770-1776.
- Ohgaki, H., J. M. Kros, Y. Okamoto, A. Gaspert, H. Huang and M. O. Kurrer (2004). "**APC mutations are infrequent but present in human lung cancer.**" Cancer Lett 207(2): 197-203.

Bibliography

- Okudela, K., M. Suzuki, S. Kageyama, T. Bunai, K. Nagura, H. Igarashi, . . . H. Sugimura (2007). "**PIK3CA mutation and amplification in human lung cancer.**" Pathology International 57(10): 664-671.
- Pacheco-Pinedo, E. C., A. C. Durham, K. M. Stewart, A. M. Goss, M. M. Lu, F. J. Demayo and E. E. Morrissey (2011). "**Wnt/ β -catenin signaling accelerates mouse lung tumorigenesis by imposing an embryonic distal progenitor phenotype on lung epithelium.**" Journal of Clinical Investigation 121(5): 1935-1945.
- Pacheco-Pinedo, E. C. and E. E. Morrissey (2011). "**Wnt and Kras signaling-dark siblings in lung cancer.**" Oncotarget 2(7): 569-574.
- Paez, J. G., P. A. Jänne, J. C. Lee, S. Tracy, H. Greulich, S. Gabriel, . . . M. Meyerson (2004). "**EGFR Mutations in Lung Cancer: Correlation with Clinical Response to Gefitinib Therapy.**" Science 304(5676): 1497-1500.
- Parkin, D. M. (2006). "**The global health burden of infection-associated cancers in the year 2002.**" International Journal of Cancer 118(12): 3030-3044.
- Perez-Ramirez, C., M. Canadas-Garre, M. A. Molina, M. J. Faus-Dader and M. A. Calleja-Hernandez (2015). "**PTEN and PI3K/AKT in non-small-cell lung cancer.**" Pharmacogenomics 16(16): 1843-1862.
- Pfarr, C. M., F. Mehta, G. Spyrou, D. Lallemand, S. Carillo and M. Yaniv (1994). "**Mouse JunD negatively regulates fibroblast growth and antagonizes transformation by ras.**" Cell 76(4): 747-760.
- Pfister, N. T. and C. Prives (2017). "**Transcriptional Regulation by Wild-Type and Cancer-Related Mutant Forms of p53.**" Cold Spring Harbor Perspectives in Medicine 7(2): a026054.
- Pignon, J.-P., H. Tribodet, G. V. Scagliotti, J.-Y. Douillard, F. A. Shepherd, R. J. Stephens, . . . T. Le Chevalier (2008). "**Lung Adjuvant Cisplatin Evaluation: A Pooled Analysis by the LACE Collaborative Group.**" Journal of Clinical Oncology 26(21): 3552-3559.
- Platt, S. Chen, Y. Zhou, Michael, L. Swiech, Hannah, . . . F. Zhang (2014). "**CRISPR-Cas9 Knockin Mice for Genome Editing and Cancer Modeling.**" Cell 159(2): 440-455.

Bibliography

- Platt, R. J., S. Chen, Y. Zhou, M. J. Yim, L. Swiech, H. R. Kempton, . . . F. Zhang (2014). "**CRISPR-Cas9 knockin mice for genome editing and cancer modeling.**" Cell 159(2): 440-455.
- Poon, S., J. R. McPherson, P. Tan, B. Teh and S. G. Rozen (2014). "**Mutation signatures of carcinogen exposure: genome-wide detection and new opportunities for cancer prevention.**" Genome Medicine 6(3): 24.
- Pottier, C., M. Fresnais, M. Gilon, G. Jerusalem, R. Longuespee and N. E. Sounni (2020). "**Tyrosine Kinase Inhibitors in Cancer: Breakthrough and Challenges of Targeted Therapy.**" Cancers (Basel) 12(3).
- Prior, I. A., F. E. Hood and J. L. Hartley (2020). "**The Frequency of Ras Mutations in Cancer.**" Cancer Research 80(14): 2969-2974.
- Rallis, K. S., T. H. Lai Yau and M. Sideris (2021). "**Chemoradiotherapy in Cancer Treatment: Rationale and Clinical Applications.**" Anticancer Research 41(1): 1-7.
- Ramalingam, S. and C. Belani (2008). "**Systemic chemotherapy for advanced non-small cell lung cancer: recent advances and future directions.**" Oncologist 13 Suppl 1: 5-13.
- Ranawakage, D. C., K. Okada, K. Sugio, Y. Kawaguchi, Y. Kuninobu-Bonkohara, T. Takada and Y. Kamachi (2020). "**Efficient CRISPR-Cas9-Mediated Knock-In of Composite Tags in Zebrafish Using Long ssDNA as a Donor.**" Front Cell Dev Biol 8: 598634.
- Rawlins, E. L., T. Okubo, Y. Xue, D. M. Brass, R. L. Auten, H. Hasegawa, . . . B. L. M. Hogan (2009). "**The Role of Scgb1a1+ Clara Cells in the Long-Term Maintenance and Repair of Lung Airway, but Not Alveolar, Epithelium.**" Cell Stem Cell 4(6): 525-534.
- Reck, M., D. Rodríguez-Abreu, A. G. Robinson, R. Hui, T. Csőszi, A. Fülöp, . . . J. R. Brahmer (2021). "**Five-Year Outcomes With Pembrolizumab Versus Chemotherapy for Metastatic Non–Small-Cell Lung Cancer With PD-L1 Tumor Proportion Score \geq 50%.**" Journal of Clinical Oncology 39(21): 2339-2349.
- Reita, D., L. Pabst, E. Pencreach, E. Guérin, L. Dano, V. Rimelen, . . . M. Beau-Faller (2022). "**Direct Targeting KRAS Mutation in Non-Small Cell Lung Cancer: Focus on Resistance.**" Cancers 14(5): 1321.

Bibliography

- Research, C. G. A. (2012). **"Comprehensive genomic characterization of squamous cell lung cancers."** Nature 489(7417): 519-525.
- Riely, G. J., W. Pao, D. Pham, A. R. Li, N. Rizvi, E. S. Venkatraman, . . . V. A. Miller (2006). **"Clinical course of patients with non-small cell lung cancer and epidermal growth factor receptor exon 19 and exon 21 mutations treated with gefitinib or erlotinib."** Clin Cancer Res 12(3 Pt 1): 839-844.
- Rizvi, N. A., J. Mazières, D. Planchard, T. E. Stinchcombe, G. K. Dy, S. J. Antonia, . . . S. S. Ramalingam (2015). **"Activity and safety of nivolumab, an anti-PD-1 immune checkpoint inhibitor, for patients with advanced, refractory squamous non-small-cell lung cancer (CheckMate 063): a phase 2, single-arm trial."** The Lancet Oncology 16(3): 257-265.
- Rodak, O., M. D. Peris-Díaz, M. Olbromski, M. Podhorska-Okółów and P. Dzięgiel (2021). **"Current Landscape of Non-Small Cell Lung Cancer: Epidemiology, Histological Classification, Targeted Therapies, and Immunotherapy."** Cancers 13(18): 4705.
- Rojo, A. I., P. Rada, M. Mendiola, A. Ortega-Molina, K. Wojdyla, A. Rogowska-Wrzesinska, . . . A. Cuadrado (2014). **"The PTEN/NRF2 axis promotes human carcinogenesis."** Antioxid Redox Signal 21(18): 2498-2514.
- Romero, R., V. I. Sayin, S. M. Davidson, M. R. Bauer, S. X. Singh, S. E. Leboeuf, . . . T. Papagiannakopoulos (2017). **"Keap1 loss promotes Kras-driven lung cancer and results in dependence on glutaminolysis."** Nature Medicine 23(11): 1362-1368.
- Rubinfeld, B., I. Albert, E. Porfiri, C. Fiol, S. Munemitsu and P. Polakis (1996). **"Binding of GSK3beta to the APC-beta-catenin complex and regulation of complex assembly."** Science 272(5264): 1023-1026.
- Ruiz, E. J., M. E. Diefenbacher, J. K. Nelson, R. Sancho, F. Pucci, A. Chakraborty, . . . A. Behrens (2019). **"LUBAC determines chemotherapy resistance in squamous cell lung cancer."** J Exp Med 216(2): 450-465.
- Ruiz, E. J., L. Lan, M. E. Diefenbacher, E. M. Riising, C. Da Costa, A. Chakraborty, . . . A. Behrens (2021). **"JunD, not c-Jun, is the AP-1 transcription factor required for Ras-induced lung cancer."** JCI Insight 6(13).

Bibliography

- Rygaard, J. and C. O. Povlsen (1969). "Heterotransplantation of a human malignant tumour to "Nude" mice." Acta Pathol Microbiol Scand 77(4): 758-760.
- Sakuma, T., M. A. Barry and Y. Ikeda (2012). "Lentiviral vectors: basic to translational." Biochem J 443(3): 603-618.
- Sanchez-Rivera, F. J., T. Papagiannakopoulos, R. Romero, T. Tammela, M. R. Bauer, A. Bhutkar, . . . T. Jacks (2014). "Rapid modelling of cooperating genetic events in cancer through somatic genome editing." Nature 516(7531): 428-431.
- Sanchez-Vega, F., M. Mina, J. Armenia, W. K. Chatila, A. Luna, K. C. La, . . . N. Schultz (2018). "Oncogenic Signaling Pathways in The Cancer Genome Atlas." Cell 173(2): 321-337 e310.
- Sandmüller A, H. R., Gómez-La-Hoz E, Gröne HJ, Suske G, Paul D, Beato M. (1994). "The uteroglobin promoter targets expression of the SV40 T antigen to a variety of secretory epithelial cells in transgenic mice." Oncogene.
- Scheffler, M., M. Bos, M. Gardizi, K. König, S. Michels, J. Fassunke, . . . J. Wolf (2015). "PIK3CA mutations in non-small cell lung cancer (NSCLC): genetic heterogeneity, prognostic impact and incidence of prior malignancies." Oncotarget 6(2): 1315-1326.
- Schiller, J. H., D. Harrington, C. P. Belani, C. Langer, A. Sandler, J. Krook, . . . D. H. Johnson (2002). "Comparison of Four Chemotherapy Regimens for Advanced Non-Small-Cell Lung Cancer." New England Journal of Medicine 346(2): 92-98.
- Sezer, A., S. Kilickap, M. Gumus, I. Bondarenko, M. Ozguroglu, M. Gogishvili, . . . P. Rietschel (2021). "Cemiplimab monotherapy for first-line treatment of advanced non-small-cell lung cancer with PD-L1 of at least 50%: a multicentre, open-label, global, phase 3, randomised, controlled trial." Lancet 397(10274): 592-604.
- Shackelford, D. B. and R. J. Shaw (2009). "The LKB1-AMPK pathway: metabolism and growth control in tumour suppression." Nature Reviews Cancer 9(8): 563-575.

Bibliography

- Shah, S. N., L. Cope, W. Poh, A. Belton, S. Roy, C. C. Talbot, . . . L. M. S. Resar (2013). "**HMGA1: A Master Regulator of Tumor Progression in Triple-Negative Breast Cancer Cells.**" PLoS ONE 8(5): e63419.
- Shapiro, M., G. Akiri, C. Chin, J. P. Wisnivesky, M. B. Beasley, T. S. Weiser, . . . S. A. Aaronson (2013). "**Wnt Pathway Activation Predicts Increased Risk of Tumor Recurrence in Patients With Stage I Nonsmall Cell Lung Cancer.**" Annals of Surgery 257(3): 548-554.
- Shen, M., R. Qi, J. Ren, D. Lv and H. Yang (2021). "**Characterization With KRAS Mutant Is a Critical Determinant in Immunotherapy and Other Multiple Therapies for Non-Small Cell Lung Cancer.**" Front Oncol 11: 780655.
- Siegel, R. L., K. D. Miller, H. E. Fuchs and A. Jemal (2022). "**Cancer statistics, 2022.**" CA: A Cancer Journal for Clinicians 72(1): 7-33.
- Simanshu, D. K., D. V. Nissley and F. McCormick (2017). "**RAS Proteins and Their Regulators in Human Disease.**" Cell 170(1): 17-33.
- Sitthideatphaiboon, P., A. Galan-Cobo, M. V. Negrao, X. Qu, A. Poteete, F. Zhang, . . . J. V. Heymach (2021). "**STK11/LKB1 Mutations in NSCLC Are Associated with KEAP1/NRF2-Dependent Radiotherapy Resistance Targetable by Glutaminase Inhibition.**" Clin Cancer Res 27(6): 1720-1733.
- Skoulidis, F., L. A. Byers, L. Diao, V. A. Papadimitrakopoulou, P. Tong, J. Izzo, . . . J. V. Heymach (2015). "**Co-occurring Genomic Alterations Define Major Subsets of *KRAS*-Mutant Lung Adenocarcinoma with Distinct Biology, Immune Profiles, and Therapeutic Vulnerabilities.**" Cancer Discovery 5(8): 860-877.
- Soh, J., N. Okumura, W. W. Lockwood, H. Yamamoto, H. Shigematsu, W. Zhang, . . . A. F. Gazdar (2009). "**Oncogene Mutations, Copy Number Gains and Mutant Allele Specific Imbalance (MASI) Frequently Occur Together in Tumor Cells.**" PLoS ONE 4(10): e7464.
- Soussi, T. (2005). "**The p53 pathway and human cancer.**" Br J Surg 92(11): 1331-1332.
- Spagnuolo, A., P. Maione and C. Gridelli (2022). "**The treatment of advanced non-small cell lung cancer harboring KRAS mutation: a new class of drugs for an old target—a narrative review.**" Translational Lung Cancer Research 11(6): 1199-1216.

Bibliography

- Spiro, S. G. and G. A. Silvestri* (2005). "One hundred years of lung cancer." Am J Respir Crit Care Med 172(5): 523-529.
- Sporn, M. B. and K. T. Liby* (2012). "NRF2 and cancer: the good, the bad and the importance of context." Nature Reviews Cancer 12(8): 564-571.
- Stiles, B. L.* (2009). "Phosphatase and tensin homologue deleted on chromosome 10: Extending its PTENacles." The International Journal of Biochemistry & Cell Biology 41(4): 757-761.
- Stokoe, D., S. G. Macdonald, K. Cadwallader, M. Symons and J. F. Hancock* (1994). "Activation of Raf as a result of recruitment to the plasma membrane." Science 264(5164): 1463-1467.
- Sung, H., J. Ferlay, R. L. Siegel, M. Laversanne, I. Soerjomataram, A. Jemal and F. Bray* (2021). "Global Cancer Statistics 2020: GLOBOCAN Estimates of Incidence and Mortality Worldwide for 36 Cancers in 185 Countries." CA: A Cancer Journal for Clinicians 71(3): 209-249.
- Swiech, L., M. Heidenreich, A. Banerjee, N. Habib, Y. Li, J. Trombetta, . . . F. Zhang* (2015). "In vivo interrogation of gene function in the mammalian brain using CRISPR-Cas9." Nature Biotechnology 33(1): 102-106.
- Talmadge, J. E., R. K. Singh, I. J. Fidler and A. Raz* (2007). "Murine models to evaluate novel and conventional therapeutic strategies for cancer." Am J Pathol 170(3): 793-804.
- Tan, A. C.* (2020). "Targeting the PI3K/Akt/mTOR pathway in non-small cell lung cancer (NSCLC)." Thoracic Cancer 11(3): 511-518.
- Thomsen, M. K.* (2022). "Application of CRISPR for In Vivo Mouse Cancer Studies." Cancers 14(20): 5014.
- Tian, Y., Q. Liu, S. Yu, Q. Chu, Y. Chen, K. Wu and L. Wang* (2020). "NRF2-Driven KEAP1 Transcription in Human Lung Cancer." Mol Cancer Res 18(10): 1465-1476.
- Travis, W. D., E. Brambilla, A. P. Burke, A. Marx and A. G. Nicholson* (2015). "Introduction to The 2015 World Health Organization Classification of Tumors of the Lung, Pleura, Thymus, and Heart." J Thorac Oncol 10(9): 1240-1242.
- Travis, W. D., E. Brambilla, A. G. Nicholson, Y. Yatabe, J. H. M. Austin, M. B. Beasley, . . . I. Wistuba* (2015). "The 2015 World Health Organization

Bibliography

- Classification of Lung Tumors." Journal of Thoracic Oncology 10(9): 1243-1260.**
- Travis, W. D., E. Brambilla, A. G. Nicholson, Y. Yatabe, J. H. M. Austin, M. B. Beasley, . . . W. H. O. Panel (2015). **"The 2015 World Health Organization Classification of Lung Tumors: Impact of Genetic, Clinical and Radiologic Advances Since the 2004 Classification."** J Thorac Oncol 10(9): 1243-1260.
- Travis, W. D., E. Brambilla, M. Noguchi, A. G. Nicholson, K. R. Geisinger, Y. Yatabe, . . . D. Yankelewitz (2011). **"International Association for the Study of Lung Cancer/American Thoracic Society/European Respiratory Society International Multidisciplinary Classification of Lung Adenocarcinoma."** Journal of Thoracic Oncology 6(2): 244-285.
- van Maldegem, F. and J. Downward (2020). **"Mutant KRAS at the Heart of Tumor Immune Evasion."** Immunity 52(1): 14-16.
- Vassella, E., S. Langsch, M. S. Dettmer, C. Schlup, M. Neuenschwander, M. Frattini, . . . S. C. Schäfer (2015). **"Molecular profiling of lung adenosquamous carcinoma: hybrid or genuine type?"** Oncotarget 6(27): 23905-23916.
- Vaughan, A. E., C. L. Halbert, S. K. Wootton and A. D. Miller (2012). **"Lung cancer in mice induced by the jaagsiekte sheep retrovirus envelope protein is not maintained by rare cancer stem cells, but tumorigenicity does correlate with Wnt pathway activation."** Mol Cancer Res 10(1): 86-95.
- Ventura, J. J., S. Tenbaum, E. Perdiguero, M. Huth, C. Guerra, M. Barbacid, . . . A. R. Nebreda (2007). **"p38 α MAP kinase is essential in lung stem and progenitor cell proliferation and differentiation."** Nature Genetics 39(6): 750-758.
- Vinod, S. K. and E. Hau (2020). **"Radiotherapy treatment for lung cancer: Current status and future directions."** Respirology 25(S2): 61-71.
- Vogt, V. M. and M. N. Simon (1999). **"Mass Determination of Rous Sarcoma Virus Virions by Scanning Transmission Electron Microscopy."** Journal of Virology 73(8): 7050-7055.
- Wang, R., L. Wang, Y. Li, H. Hu, L. Shen, X. Shen, . . . H. Chen (2014). **"FGFR1/3 tyrosine kinase fusions define a unique molecular subtype of non-small cell lung cancer."** Clin Cancer Res 20(15): 4107-4114.

Bibliography

- Wang, X. J., J. D. Hayes and C. R. Wolf (2006). "**Generation of a stable antioxidant response element-driven reporter gene cell line and its use to show redox-dependent activation of nrf2 by cancer chemotherapeutic agents.**" Cancer Res 66(22): 10983-10994.
- Wang, Y., X. Cheng, Q. Shan, Y. Zhang, J. Liu, C. Gao and J.-L. Qiu (2014). "**Simultaneous editing of three homoeoalleles in hexaploid bread wheat confers heritable resistance to powdery mildew.**" Nature Biotechnology 32(9): 947-951.
- Whitman, M., D. R. Kaplan, B. Schaffhausen, L. Cantley and T. M. Roberts (1985). "**Association of phosphatidylinositol kinase activity with polyoma middle-T competent for transformation.**" Nature 315(6016): 239-242.
- Wikenheiser KA, C. J., Linnoila RI, Stahlman MT, Whitsett JA. (1992). "**Simian virus 40 large T antigen directed by transcriptional elements of the human surfactant protein C gene produces pulmonary adenocarcinomas in transgenic mice.**" Cancer Research 19: 5342-5352.
- Wu, M. Y., E. W. Zhang, M. R. Strickland, D. P. Mendoza, L. Lipkin, J. K. Lennerz, . . . S. R. Digumarthy (2021). "**Clinical and Imaging Features of Non-Small Cell Lung Cancer with G12C KRAS Mutation.**" Cancers 13(14): 3572.
- Xu, C., Christine, S. Koyama, H. Wu, Y. Zhao, Z. Chen, . . . K.-K. Wong (2014). "**Loss of Lkb1 and Pten Leads to Lung Squamous Cell Carcinoma with Elevated PD-L1 Expression.**" Cancer Cell 25(5): 590-604.
- Xu, C. L., M. Z. C. Ruan, V. B. Mahajan and S. H. Tsang (2019). "**Viral Delivery Systems for CRISPR.**" Viruses 11(1): 28.
- Xu, X., A. Chemparathy, L. Zeng, H. R. Kempton, S. Shang, M. Nakamura and L. S. Qi (2021). "**Engineered miniature CRISPR-Cas system for mammalian genome regulation and editing.**" Mol Cell 81(20): 4333-4345 e4334.
- Xu, X., L. Huang, C. Futtner, B. Schwab, R. R. Rampersad, Y. Lu, . . . M. W. Onaitis (2014). "**The cell of origin and subtype of K-Ras-induced lung tumors are modified by Notch and Sox2.**" Genes Dev 28(17): 1929-1939.
- Xu, X., J. R. Rock, Y. Lu, C. Futtner, B. Schwab, J. Guinney, . . . M. W. Onaitis (2012). "**Evidence for type II cells as cells of origin of K-Ras-induced distal lung adenocarcinoma.**" Proceedings of the National Academy of Sciences 109(13): 4910-4915.

Bibliography

- Yang, J. J., Q. Zhou, H. H. Yan, X. C. Zhang, H. J. Chen, H. Y. Tu, . . . Y. L. Wu (2017). "A phase III randomised controlled trial of erlotinib vs gefitinib in advanced non-small cell lung cancer with EGFR mutations." British Journal of Cancer 116(5): 568-574.
- Yang, S.-H., P.-H. Cheng, R. T. Sullivan, J. W. Thomas and A. W. S. Chan (2008). "Lentiviral integration preferences in transgenic mice." genesis 46(12): 711-718.
- Yang, Y., L. Wang, P. Bell, D. McMenamin, Z. He, J. White, . . . J. M. Wilson (2016). "A dual AAV system enables the Cas9-mediated correction of a metabolic liver disease in newborn mice." Nature Biotechnology 34(3): 334-338.
- Yang, Y. M., Y. Jang, S. H. Lee, B. Kang and S. M. Lim (2020). "AXL/MET dual inhibitor, CB469, has activity in non-small cell lung cancer with acquired resistance to EGFR TKI with AXL or MET activation." Lung Cancer 146: 70-77.
- Zappa, C. and S. A. Mousa (2016). "Non-small cell lung cancer: current treatment and future advances." Translational Lung Cancer Research 5(3): 288-300.
- Zhang, M., G. Zhuang, X. Sun, Y. Shen, W. Wang, Q. Li and W. Di (2017). "TP53 mutation-mediated genomic instability induces the evolution of chemoresistance and recurrence in epithelial ovarian cancer." Diagnostic Pathology 12(1).
- Zhang, Z., Y. Wang, H. G. Vikis, L. Johnson, G. Liu, J. Li, . . . M. You (2001). "Wildtype Kras2 can inhibit lung carcinogenesis in mice." Nature Genetics 29(1): 25-33.
- Zheng, S., A. K. El-Naggar, E. S. Kim, J. M. Kurie and G. Lozano (2007). "A genetic mouse model for metastatic lung cancer with gender differences in survival." Oncogene 26(48): 6896-6904.
- Zhou, B. P., Y. Liao, W. Xia, Y. Zou, B. Spohn and M.-C. Hung (2001). "HER-2/neu induces p53 ubiquitination via Akt-mediated MDM2 phosphorylation." Nature Cell Biology 3(11): 973-982.
- Zhou, J., P. Chen, H. Wang, H. Liu, Y. Li, Y. Zhang, . . . L. Yin (2022). "Cas12a variants designed for lower genome-wide off-target effect through stringent PAM recognition." Mol Ther 30(1): 244-255.

Bibliography

Zhu, L., L. Jiang, J. Yang, W. Gu and J. He (2018). "Clinical characteristics and prognosis of patients with lung adenosquamous carcinoma after surgical resection: results from two institutes." Journal of Thoracic Disease 10(4): 2397-2402.

Zou, B., X. L. Zhou, S. Q. Lai and J. C. Liu (2018). "Notch signaling and non-small cell lung cancer (Review)." Oncology Letters.

Appendix

6 Appendix

6.1 Supplementary Figure

G12

Kras locus 5' GTG GTG GTT GGA GCT GGT GGC GTA GGC AAG AGC 3'

wt GTG GTG GTT GGA GCT GGT GGC GTA GGC AAG AGC

G12D

KP^{Crispr} 1 GTG GTC GTG GGC ACC GAC GGA GGG AGC AAG AGC

KP^{Crispr} 2 GTG GTC GTG GGC GCC GAC GGC GTG GGC ACG AGC

sgRNA Tp53

Tp53 locus 5' AAG TAC ATG TGT AAT AGC TCC TGC ATG GGG GGC ATG 3'

wt AAG TAC ATG TGT AAT AGC TCC TGC ATG GGG GGC ATG

KP^{Crispr} 1 AAG TAC ATG TGT AAT AGC TCC - - - ATG TGG GGC ATG

KP^{Crispr} 2 Deletion in Intron 6

Figure 6-1: Exemplary loci of sanger sequenced TP53 and KRAS sgRNA target sides compared to wildtype

Appendix

6.2 List of abbreviations

AAH	atypical adenomatous hyperplasia
AAV	Adeno-associated virus
ADC	Adenocarcinoma
AIS	Adenocarcinoma in situ
AKT	Protein kinase B
AMPK	'5 adenosine monophosphate-activated protein kinase
APC	Adenomatous Polyposis Coli
ASC	Adenosquamous carcinoma
AT2	alveolar stem cells
ATP	Adenosine triphosphate
BASC	bronchioalveolar stem cells
BSA	Bovine serum albumin
CC10	Club Cell Secretory Protein
CRISPR	Clustered Regularly Interspaced Short Palindromic Repeats
DMSO	Dimethyl sulfoxide
DNA	Deoxyribonucleic acid
DSB	Double strand break
DTT	Dithiothreitol
EDTA	Ethylenediaminetetraacetic acid
EGF	epidermal growth factor
EGFR	EGF receptor
EGFR-TKIs	EGFR tyrosine kinase inhibitors
EtOH	Ethanol
FAP	familial adenomatous polyposis
FC	Fold change
FFPE	formalin-fixed paraffin-embedded
GDP	guanosine diphosphate
GEMM	genetically engineered mouse model
GOF	Gain of function
GO-term	gene ontology biological process
gRNA	Guide RNA
GSEA	Gene-set enrichment analysis

Appendix

GSK3	Glycogen synthase kinase 3
GTP	guanosine triphosphate
H&E	Hematoxylin and Eosin
HA	Homologous arm
HDR	Homologous repair donor
HER2	human epidermal growth factor receptor 2
HMG	High Mobility Group
IF	immunofluorescent
IHC	Immunohistochemistry
IP	Intraperitoneal
IRES	Internal ribosome entry site
IT	intratracheal
KEAP1	Kelch-like ECH-associated protein 1
KM	Kaplan-Meier
KP	KRas/TP53
KRAS	Kirsten rat sarcoma virus
KRT	Cytokeratin
LCC	Large cell carcinoma
LCNEC	large cell neuroendocrine cancer
LKB1	Liver-Kinase B1
LOH	Loss of heterozygosity
LSL	Lox-stop-lox
MAPK	mitogen-activated protein kinase
MASI	mutant allele-specific imbalance
MDM2	Mouse double minute 2 homolog
MIA	minimally invasive adenocarcinoma
mTOR	mammalian target of rapamycin
NBF	Natural buffered formalin
NGS	Next-Generation Sequencing
NHEJ	non-homologous end joining
NICD	Notch-1 intracellular domain
NRF2	nuclear factor erythroid 2-related factor 2
NSCLC	Non-small cell lung cancer

Appendix

OD	Optical density
OS	Overall survival
PBS	Phosphate-buffered saline
PCNA	Proliferating cell nuclear antigen
PCR	Polymerase chain reaction
PD-L1	programmed cell death–ligand 1
PFS	progression-free survival
PI3K	phosphatidylinositol-3-kinase
POI	Protein of interest
PTEN	Phosphatase and tensin homolog
RB	Retinoblastoma
RNA	Ribonucleic acid
ROS	Reactive oxygen species
SCC	Squamous cell carcinoma
SCLC	small cell lung carcinoma
SDS	Sodiumdodecylsulfat-
SDS-PAGE	SDS-Polyacrylamide gel electrophoresis
SEMM	somatic engineered mouse models
shRNA	short hairpin RNA
SOX2	SRY-box 2
SPC	surfactant protein C
STK11	Serin-Threonine Kinase 11
SV40	Simian virus large T-antigen
TCGA	The cancer genome atlas
TME	Tumour microenvironment
TP53	Tumor protein P53
TTF1	Thyroid transcription factor 1
WB	Western blot
WHO	World Health Organisation
WNT	Wingless and Int-1
WT	wildtype

Appendix

6.3 List of Figures

Figure 1-1: A diagram of a lung with the regions for SCC and ADC.....	- 3 -
Figure 1-2: Most common genetic alterations in Adenocarcinoma and Squamous Cell Carcinoma	- 6 -
Figure 1-3: A simplified overview of the impact of commonly altered genes in NSCLC	- 8 -
Figure 1-4: A simplified overview of current therapeutic strategies and their targeted pathways in NSCLC.....	- 14 -
Figure 3-1: TP53 and KRAS are frequently altered in NSCLC subtypes	- 54 -
Figure 3-2: Deregulated oncogenic driver in ADC and SCC	- 55 -
Figure 3-3: Schematic of the intratracheal tumor induction	- 57 -
Figure 3-4: Intratracheal administration of AAV-DJ yields the highest efficacy.....	- 58 -
Figure 3-5: Type of tumour induction in KRas/Trp53-driven NSCLC shows no significant difference in tumour burden	- 59 -
Figure 3-6: Quantification of PCNA indicates no significant difference in proliferation	- 60 -
Figure 3-7: KP ^{GEMM} and KP ^{CRISPR} presented comparable distributions of all stages	- 61 -
Figure 3-8: Analysing genomic DNA and the MAPK-pathway confirms successful targeting of Trp53 and KRas in KP ^{CRISPR}	- 62 -
Figure 3-9: Marker expression in KP ^{GEMM} and KP ^{CRISPR} indicates an adeno-squamous phenotype	- 64 -
Figure 3-10: Oncogenic transcription factors commonly upregulated in NSCLC	- 65 -
Figure 3-11: Ap-1 family member JUNB and JUND are significantly increased in KP ^{GEMM} and KP ^{CRISPR} tumours ..	- 66 -
Figure 3-12: NICD and NOTCH3 are significantly more abundant in KP ^{GEMM} and KP ^{CRISPR} compared to non-transformed tissue	- 67 -
Figure 3-13: CTNNB1 and cMYC are significantly upregulated in KP ^{GEMM} and KP ^{CRISPR} tumours	- 68 -
Figure 3-14: KP ^{GEMM} and KP ^{CRISPR} show highly similar transcriptomic profiles.....	- 70 -
Figure 3-15: KP ^{GEMM} and KP ^{CRISPR} demonstrate a similar up- and down-regulation of cancer related genes ..	- 71 -
Figure 3-16: Direct comparison of KP ^{GEMM} and KP ^{CRISPR} highlights difference in oncogenic pathways.....	- 72 -
Figure 3-17: Gene set enrichment and GO term analysis show the same comparatively deregulated tumour pathways in KP ^{GEMM} and KP ^{CRISPR}	- 74 -
Figure 3-18: APC, KEAP1, STK11/LKB1 and PTEN are frequently altered and thus negatively impact patient survival	- 77 -
Figure 3-19: Schematic for the AAV approach to rapidly model common loss of function mutations	- 79 -
Figure 3-20: Modular AAV-vector enables successful targeting of commonly mutated tumour suppressor in mice and induces lung cancer formation	- 81 -
Figure 3-21: Additional loss of STK11/Lkb1 and PTEN decreases animal survival.....	- 82 -
Figure 3-22: CRISPR/Cas9 mediated genome editing as a high targeting efficacy in mice on those tumour suppressors.....	- 83 -
Figure 3-23: Successful targeting of APC, KEAP1, LKB1 and PTEN lead to an increased abundance of downstream pathway member	- 84 -

Appendix

Figure 3-24: Loss of tumour suppressor increased proliferation of tumours compared to KP ^{CRISPR}	- 85 -
Figure 3-25: Dual viral approach to induce lung tumour formation irrespective of the mouse strain	- 87 -
Figure 3-26: KP ^{CRISPR} and KP ^{AAV} -spCas9 ^{AAV} presented comparable distributions of all stages.....	- 88 -
Figure 3-27: Double viral approach led to formation of adenocarcinomas comparable to KP ^{CRISPR}	- 89 -
Figure 3-28: Activation of the MAPK-pathway in KP ^{AAV} SpCas9 ^{AAV} to the same extent as in KP ^{CRISPR}	- 90 -
Figure 3-29: Dual viral approach with additional loss of Lkb1 recapitulates the conditional CRISPR model	- 91 -
Figure 3-30: Lung tumours had an increased abundance of Nrf2 after loss of Stk11/LKB1 in the dual viral approach.....	- 92 -
Figure 3-31: Dual AAV-infection induces the formation of ADC and SCC upon loss of Stk11/LKB1.....	- 93 -
Figure 3-32: Lung tumours in the dual viral approach have no stable expression of spCas9 12 weeks post infection.....	- 94 -
Figure 3-33: Schematic summary of the advantage of a CRISPR/Cas9 mediated NSCLC mouse model	- 95 -
Figure 6-1: Exemplary loci of sanger sequenced TP53 and KRAS sgRNA target sides compared to wildtype-	136

-

Acknowledgments

7 Acknowledgments

My biggest thanks go to the “Chef”, Dr. Markus Diefenbacher. Thank you not only for the opportunity to work with you on this project, but especially for your support and for giving me the freedom to learn what I'm good at and the time to get better at it. I really appreciate all the scientific discussions, all the ideas and input I got from you. I have really learned a lot from you.

I would like to thank Prof. Dr. Martin Eilers for his patience, the fruitful scientific discussions and the all the help we got from with his experience and his support in the small groups.

Prof. Dr. Stefan Müller and Prof. Dr. Emma Rawlins I would like to acknowledge for being members of my thesis committee and their help with this project.

In particular, I would also like to thank Prof. Dr Alex Buchberger, Julia Seubert and the GRK2243. The scientific impressions and experiences I was able to gain through retreats, seminars, but also through the student coffees will be very helpful for the future. I would also like to thank the GRK for making so many conferences possible for me.

I would like to express my gratitude to the Graduate School of Life Science for the provided courses and their support.

To all the current and former members of the Diefenbacher Lab Cristian, Fabi, Niki, Thomas, and Angela, I want to express my gratitude and appreciation of going this long way together with you. Especially to my partner in crime Michi I want to say thank you for all the time spent together. For all the moments we have driven Markus insane, the coffee breaks, the “Lidl-Tours” but as well for your helpful input in my project for your bioinformatics work and for the discussion we had. Additionally, I want to thank Carmina for not only reading and correcting this work, but as well for the amazing albeit short, time in the lab. Thanks to both of you for becoming really good friends.

Furthermore, I want to thank the members, former and current, of the Department of Biochemistry and Molecular Biology. Working together with all of you has always been

Acknowledgments

very helpful, encouraging, and supportive. It is a great working atmosphere knowing, you can get help from everyone when in need. A special thanks goes to the “Mensa-People”: Daniel, Lorenz, Basti, Leonie, Amel, Mareike, the second Daniel, Steffi, Sinah and Katrin. I will really miss the time we spent together during work, but also especially outside the lab.

I want to thank Dr. Carsten Ade and Dr. Apoorva Baluapuri for helping me with the RNA-sequencing and the bioinformatics.

Finally, I want to thank my mum and dad and my brother. Thanks for your support, for listening, for making all this possible, for the motivation and for believing in me.

Last but not least, I would like to thank my wife Carina. For always being by my side, for always motivating me when I needed it and especially for picking me up when things didn't go well.

Thanks to all of you. Without your help, this would not have been possible.

Publications

8 Publications

Hartmann, O., M. Reissland, C. R. Maier, T. Fischer, C. Prieto-Garcia, A. Baluapuri, J. Schwarz, W. Schmitz, M. Garrido-Rodriguez, N. Pahor, C. C. Davies, F. Bassermann, A. Orian, E. Wolf, A. Schulze, M. A. Calzado, M. T. Rosenfeldt and M. E. Diefenbacher (2021). "Implementation of CRISPR/Cas9 Genome Editing to Generate Murine Lung Cancer Models That Depict the Mutational Landscape of Human Disease." Front Cell Dev Biol **9**: 641618.

Hartmann O., Maier, C. R., C. Prieto-Garcia, K. M. Al-Shami, L. Schlicker, F. C. E. Vogel, S. Haid, K. Klann, V. Buck, C. Münch, W. Schmitz, E. Einig, B. Krenz, M. A. Calzado, M. Eilers, N. Popov, M. T. Rosenfeldt, M. E. Diefenbacher and A. Schulze (2023). "USP28 controls SREBP2 and the mevalonate pathway to drive tumour growth in squamous cancer." Cell Death & Differentiation **30**(7): 1710-1725.

Fischer, T., **Hartmann O.**, M. Reissland, C. Prieto-Garcia, K. Klann, N. Pahor, C. Schülein-Völk, A. Baluapuri, B. Polat, A. Abazari, E. Gerhard-Hartmann, H.-G. Kopp, F. Essmann, M. Rosenfeldt, C. Münch, M. Flentje and M. E. Diefenbacher (2022). "PTEN mutant non-small cell lung cancer require ATM to suppress pro-apoptotic signalling and evade radiotherapy." Cell & Bioscience **12**

Prieto-Garcia, C., **Hartmann O.**, M. Reissland, F. Braun, T. Fischer, S. Walz, C. Schulein-Volk, U. Eilers, C. P. Ade, M. A. Calzado, A. Orian, H. M. Maric, C. Munch, M. Rosenfeldt, M. Eilers and M. E. Diefenbacher (2020). "Maintaining protein stability of Np63 via USP28 is required by squamous cancer cells." EMBO Mol Med **12**(4): e11101.

Prieto-Garcia, C., **Hartmann O.**, M. Reissland, T. Fischer, C. R. Maier, M. Rosenfeldt, C. Schülein-Völk, K. Klann, R. Kalb, I. Dikic, C. Münch and M. E. Diefenbacher (2022). "Inhibition of USP28 overcomes Cisplatin-resistance of squamous tumors by suppression of the Fanconi anemia pathway." Cell Death & Differentiation **29**(3): 568-584.

Publications

Prieto-Garcia, C., **Hartmann O.**, M. Reissland, F. Braun, S. Bozkurt, N. Pahor, C. Fuss, A. Schirbel, C. Schülein-Völk, A. Buchberger, M. A. Calzado Canale, M. Rosenfeldt, I. Dikić, C. Münch and M. E. Diefenbacher (2022). "USP28 enables oncogenic transformation of respiratory cells, and its inhibition potentiates molecular therapy targeting mutant EGFR, BRAF and PI3K." Molecular Oncology.

Novak, R., Y. A. Ahmad, M. Timaner, E. Bitman-Lotan, A. Oknin-Vaisman, R. Horwitz, **Hartmann O.**, M. Reissland, V. Buck, M. Rosenfeldt, D. Nikomarov, M. E. Diefenbacher, Y. Shaked and A. Orian (2022). "RNF4~RGMB~BMP6 axis required for osteogenic differentiation and cancer cell survival." Cell Death & Disease **13**(9)

Reissland M, Tauch S, Prieto-Garcia C, **Hartmann O.**, Sugino T, Schulte C, Schülein-Völk C, Ade C, Cossa G, Rosenfeldt M, Wiegering A, Potente M, Eilers M, Maric H, Li V, Maurice M, Dikić I, Orian M, Gallant M & Diefenbacher ME: β -Catenin regulation by USP10 is essential for intestinal stem cell homeostasis and tumour progression. (in preparation)

Affidavit

9 Affidavit

I hereby confirm that my thesis entitled “**Development of somatic modified mouse models of Non-Small cell lung cancer**” is the result of my own work. I did not receive any help or support from commercial consultants. All Sources and/or materials applied are listed and specified in the thesis.

Furthermore, I confirm that this thesis has not yet been submitted as part of another examination process neither in identical nor in similar form.

Place, Date

Signature

Hiermit erkläre ich an Eides statt, die Dissertation „**Entwicklung von somatisch veränderten Mausmodellen für nicht-kleinzelligen Lungenkrebs**“ eigenständig, d.h. insbesondere selbstständig und ohne Hilfe eines kommerziellen Promotionsberaters angefertigt und keine anderen als die von mir angegebenen Quellen und Hilfsmittel verwendet zu haben.

Ich erkläre weiterhin, dass die Disseratation weder in gleicher noch in ähnlicher Form bereits im Rahmen eines anderen Prüfungsverfahrens eingereicht worden ist.

Ort, Datum

Unterschrift